EFFECTS OF VERTICAL EXCITATION ON SEISMIC PERFORMANCE OF HIGHWAY BRIDGES AND HOLD-DOWN DEVICE REQUIREMENTS

A THESIS SUBMITTED TO
THE GRADUATE SCHOOL OF NATURAL AND APPLIED SCIENCES
OF
MIDDLE EAST TECHNICAL UNIVERSITY

BY

KEMAL ARMAN DOMANİÇ

IN PARTIAL FULFILLMENT OF THE REQUIREMENTS
FOR
THE DEGREE OF MASTER OF SCIENCE
IN
CIVIL ENGINEERING

JANUARY 2008

Approval of the thesis:

EFFECTS OF VERTICAL EXCITATION ON SEISMIC PERFORMANCE OF HIGHWAY BRIDGES AND HOLD-DOWN DEVICE REQUIREMENTS

submitted by **KEMAL ARMAN DOMANİÇ** in partial fulfillment of the requirements for the degree of **Master of Science in Civil Engineering Department, Middle East Technical University** by,

Prof. Dr. Canan Özgen ____________________
Dean, Graduate School of **Natural and Applied Sciences**

Prof. Dr. Güney Özcebe ____________________
Head of Department, **Civil Engineering**

Assist. Prof. Dr. Alp Caner ____________________
Supervisor, **Civil Engineering Dept., METU**

Examining Committee Members:

Prof. Dr. Polat Gülkan ____________________
Civil Engineering Dept., METU

Assist. Prof. Dr. Alp Caner ____________________
Civil Engineering Dept., METU

Assoc. Prof. Dr. Cem Topkaya ____________________
Civil Engineering Dept., METU

Inst. Dr. Ayşegül Askan ____________________
Civil Engineering Dept., METU

Yeşim Esat (Civil Engineer, M.S.) ____________________
Vice General Director,
Division of Bridge Survey and Design,
General Directorate of Highways

I hereby declare that all information in this document has been obtained and presented in accordance with academic rules and ethical conduct. I also declare that, as required by these rules and conduct, I have fully cited and referenced all material and results that are not original to this work.

Name, Last name : **KEMAL ARMAN DOMANİÇ**

Signature :

ABSTRACT

EFFECTS OF VERTICAL EXCITATION ON SEISMIC PERFORMANCE OF HIGHWAY BRIDGES AND HOLD-DOWN DEVICE REQUIREMENT

Domaniç, Kemal Arman
M.S., Department of Civil Engineering
Supervisor: Assist. Prof. Dr. Alp Caner

January 2008, 152 pages

Most bridge specifications ignore the contribution of vertical motion in earthquake analyses. However, vertical excitation can develop significant damage, especially at bearing locations as indeed was the case in the recent 1999 İzmit Earthquake. These observations, combined with recent developments in the same direction, supplied the motivation to investigate the effects of vertical component of strong ground motion on standard highway bridges in this study. Reliability checks of hold-down device requirements per AASHTO Bridge Specifications have been conducted in this context. Six spectrum compatible accelerograms were generated and time history analyses were performed to observe the uplift at bearings. Selected case studies included precast pre-stressed I-girders with concrete slab, composite steel I-girders, post-tensioned concrete box section, and composite double steel box section. According to AASHTO specifications, hold-down devices were required in two cases, for which actual forces obtained from time history analyses have been compared with those suggested per AASHTO. The only non-linearity introduced to the analyses was at the bearing level. A discussion of effects on substructure response as well as compressive bearing forces resulting from vertical excitation is also included. The results of the study confirmed that the provisions of AASHTO governing hold-down devices are essential and reasonably accurate. On the other hand, they might be interpreted as well to be suggesting that vertical ground motion components could also be included in the load combinations supplied by AASHTO, especially to be able to estimate pier axial forces and cap beam moments accurately under combined vertical and horizontal excitations.

Keywords: Uplift at bearings, hold-down device, vertical excitation, spectrum compatible accelerogram, dynamic analysis

ÖZ

DÜŞEY DEPREM HAREKETİNİN KARAYOLU KÖPRÜLERİNİN DEPREM PERFORMANSI ÜZERİNDEKİ ETKİLERİ VE DÜŞEY KİLİTLEME AYGITI GEREKSİNİMİ

Domaniç, Kemal Arman
Yüksek Lisans, İnşaat Mühendisliği Bölümü
Tez Yöneticisi: Yar. Doç. Dr. Alp Caner

Ocak 2008, 152 sayfa

Çoğu köprü tasarım şartnamesi, deprem analizlerinde düşey bileşenin etkisini göz önüne almamaktadır. Fakat 1999 İzmit Depreminin de gösterdiği üzere, düşey deprem hareketi özellikle mesnet bölgelerinde yoğunlaşan ciddi hasarlar yaratabilmektedir. Bu gözlemler, yakın tarihteki araştırmalar ile birlikte, düşey deprem yükünün standart karayolu köprüleri üzerindeki etkilerini konu alan bu çalışmaya ilham kaynağı olmuştur. Bu bağlamda AASHTO Köprü Şartnamesinin düşey kilitleme aygıtları ile ilgili tasarım kriterlerinin güvenilirliği araştırılmıştır. Altı adet tasarım spektrumuna uygun deprem ivme kaydı üretilip, zaman tanım alanında gerçekleştirilen dinamik analizler vasıtası ile mesnet bölgelerindeki yukarı kalkma olgusu araştırılmıştır. Seçilen köprü tipleri öndöküm öngermeli beton kirişli, komposit çelik kirişli, ardgermeli beton kutu kesitli ve komposit çelik kutu kesitli üstyapıları kapsamaktadır. AASHTO kıstaslarına göre iki köprüde düşey kilitleme aygıtı gereksinimi ortaya çıkmıştır. Zaman tanım alanı sonuçları ile AASHTO tasarım yükleri karşılaştırılmıştır. Analizlerde doğrusal olmayan şartlar sadece mesnetlerde gözönüne alınmıştır. Düşey deprem hareketinin altyapı tesirleri ve mesnet basınç kuvvetleri üzerindeki etkileri de irdelenmiştir. Sonuçlar, AASHTO tarafından düşey kilitleme aygıtları konusunda sağlanan kıstasların gerekli ve yeterli hassasiyette olduğunu göstermiştir. Öte yandan bu çalışma, düşey deprem bileşeninin AASHTO yük kombinasyonlarına ilave edilmesinin, özellikle başlık kirişi momentlerini ve ayak eksenel kuvvetlerini bileşik deprem yüklemesi altında doğru tahmin edebilmek açısından faydalı olabileceğini ortaya koymuştur.

Anahtar kelimeler: Mesnetlerde düşey hareket, düşey kilitleme aygıtı, düşey deprem, spektrum uyumlu ivme kaydı, dinamik analiz

ACKNOWLEDGEMENTS

The author wishes to express his deepest gratitude and sincere appreciation to Assist. Prof. Dr. Alp Caner for his guidance, advice and encouragement throughout the research.

The author would also like to thank to his mother F. Serpil Domaniç, his father Yüksel Domaniç and his brother Nevzat Onur Domaniç for their invaluable support. Similarly he wishes to express his gratitude to his friends Zeynep Atalay, Berksan Apaydın, Meriç Selamoğlu, Özge Göbelez, Emrah Özkaya, Ayşegül Akay, Tunç Koç and all workmates for their motivation and tolerance during this study.

Finally, the author would like to express his sincere appreciation to the originator of “RSCA” software, Marko Thiele for his valuable cooperation and kind attitude during this thesis.

TABLE OF CONTENTS

CHAPTER 1

INTRODUCTION

Recent developments in computer technology have made it possible for engineers to simulate the effects of strong ground motions in more detailed and realistic ways. The well known *Time-History Analysis* method serves this purpose, as one can apply time dependent excitations in any direction and combination to the structure. More and more sophisticated models incorporating considerable degrees of material and geometrical nonlinearities are allowed in carrying out these dynamical analyses, the outputs of which are time dependent responses of the system.

Yet, time and storage space required for such an analysis can be still excessive in most cases, especially if the structure to be analyzed is of a very high degree of freedom (DOF) with considerable nonlinearity. Additionally, such an application requires collection of appropriate strong ground motion records. As a remedy for these difficulties, *Response Spectrum Analysis* is recommended by almost all of current guidelines and specifications, making it into a most preferred method in engineering practice.

On the other hand, when analyzing bridge structures with this method, the vertical component of ground motion is omitted in most of the cases, thus taking into account only the horizontal contribution of the shaking. This is also the suggested approach in specifications [2, 3] which find widespread use in Turkey.

However, site investigations after İzmit Earthquake (August 17, 1999) showed that significant bearing displacements and unseating of girders occurred in various bridges, probably due to uplift of superstructure enforced by combined horizontal and vertical excitation (Figure 1.1) [5, 20, 28, 29, 35].

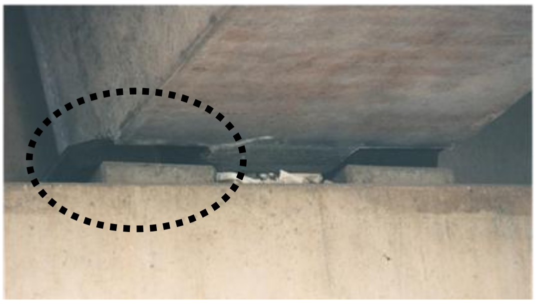

(a) Transverse movement of bearing

(b) Unseating of girder

(c) Unseating of girder

(d) Extensive bearing damage

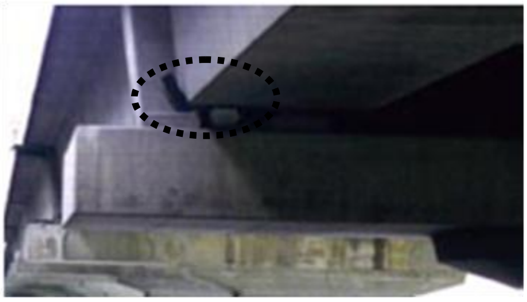

(e) Dislodging of bearing

Figure 1.1: Various damages at bearing locations observed in Sakarya Viaduct after 1999 İzmit Earthquake [5, 20, 28, 29, 35]

One of the conclusions from these investigations was that a bearing, shown in Figure 1.1 (d), was unseated and had even fallen to ground during the same earthquake.

Insufficiency of support lengths and the resulting unseating of girders were also observed after 1994 Northridge, 1995 Kobe and 1999 Chi-Chi Earthquakes [13, 17, 23, 35]. Findings in [24] also verified these observations, underlining that bearing damages can play major roles in unseating failures. It is also noted that, additional collapse mechanisms may occur due to effects of vertical excitation on axial, shear and flexural responses [10, 30].

Moreover, recent studies emphasized that vertical ground motions may have considerable effects on major responses, such as amplification and even reversal of deck moments [18], as well as significant alteration of pier axial forces in bridges close to the fault within a distance of 10-20 km [11].

All these observations and findings question the importance of both vertical strong ground motion component and hold-down devices (vertical restrainers), which prevents the uplift of superstructure during earthquake.

Therefore, and possibly as a complement to the widespread approach of response spectrum analysis, the objective of this study is to investigate the effects of vertical excitation on most common types of highway bridges. In this context, examination of the current rules set by Association of State Highway and Transportation Officials (AASHTO) Bridge Specifications related to the design of hold-down devices is among main considerations of this study.

To achieve this, four bridge models have been investigated using a general structural analyses program, “LARSA 4D V7.0”, where the necessity of designing the hold-down devices according to the provisions of AASHTO showed up in two cases. Selected case studies included common superstructure types used in standard highway bridges; pre-stressed I-girders with concrete slab, composite steel I-girders, concrete box section, and composite double steel box section.

Six earthquake records, each consisting of three spectrum compatible orthogonal excitations (two in horizontal and one in vertical directions), were generated using a modified version of freeware program “RSCA” and applied to the structures via linear and nonlinear time-history analyses.

The results of time-history analyses have been compared with those of response spectrum computations and five different peak value combinations, of which three includes responses due to vertical excitation as well. A discussion of compressive axial forces in bearings, substructure responses and girder seat width requirements is also included.

CHAPTER 2

SPECTRUM COMPATIBLE ACCELEROGRAMS

In this chapter, brief information will be provided about the process of constructing spectrum compatible time-history records, which was an essential tool to carry out this study. To achieve a better understanding of the subject, a review which covers fundamental concepts of earthquake engineering is provided in following sections.

2.1 RESPONSE SPECTRUM CONCEPT

First introduced in 1932 by M.A. Biot, response spectrum is now a central concept in earthquake engineering. It summarizes the maximum responses of all possible linear SDOF systems to a particular component of ground motion. A plot of the peak value of a response quantity as a function of natural vibration period T_n of the system, or a related parameter such as circular frequency ω_n or cyclic frequency f_n, is called the response spectrum for that quantity [14]. The most used type to represent a strong ground motion component is the pseudo acceleration response spectrum. To understand this concept better, it will be helpful to recall the basics of structural dynamics.

The equation of motion for any single degree of freedom (SDOF) system (Figure 2.1) subjected to an earthquake excitation can be expressed as [14];

$$m\ddot{u} + c\dot{u} + ku = -m\ddot{u}_g(t) \tag{2.1}$$

where m is mass, c is viscous damping coefficient and k is stiffness of the system.

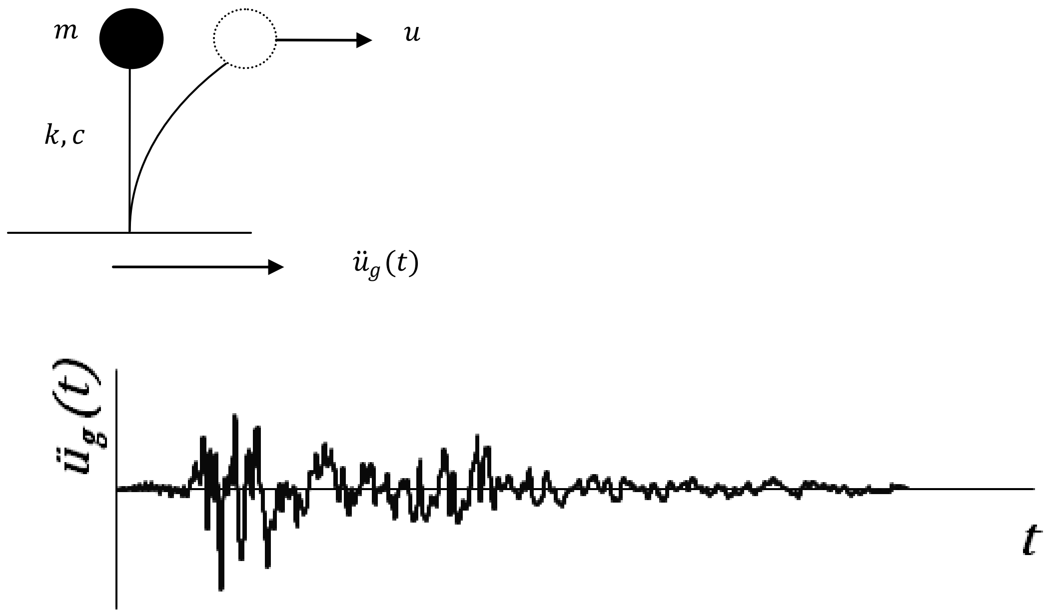

Figure 2.1: SDOF system subjected to earthquake excitation

Introducing the concept of *equivalent static force*, f_S, at any time instant *t*, the external static force that will produce the same deformation *u* determined by dynamic analysis can be expressed as;

$$f_S(t) = ku(t) \tag{2.2}$$

From dynamics, circular frequency, ω_n, is defined as;

$$\omega_n = \sqrt{\frac{k}{m}} \tag{2.3}$$

Thus *the equivalent static force*, f_S, can be expressed in an alternative way;

$$f_S(t) = mA(t) \tag{2.4}$$

Where $A(t)$ is defined as *pseudo-static acceleration* of the system at any time instant t;

$$A(t) = {\omega_n}^2 u(t) \tag{2.5}$$

The *pseudo-static acceleration response spectrum* is basically the plot of *peak pseudo-static acceleration,A,* as a function of natural vibration period, T_n or natural vibration frequency, f_n of the SDOF system [14], where;

$$T = 1/f_n = 2\pi\sqrt{\frac{m}{k}} \tag{2.6}$$

Figure 2.2 illustrates this concept.

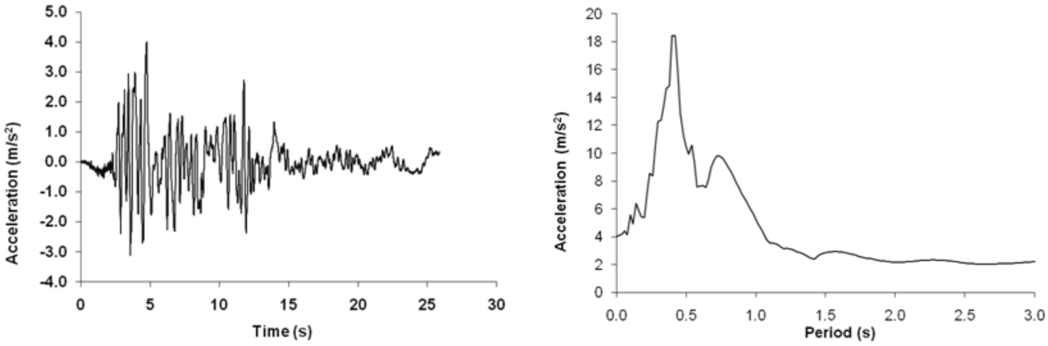

(a) (b)

Figure 2.2: (a) accelerogram; (b) resultant pseudo-static acceleration spectrum

There are several numerical methods to solve Equation (2.1) for a SDOF system, where ground acceleration varies arbitrarily with time. In this thesis, *central difference method* was used to compute pseudo-acceleration response spectra of earthquake records. All of the expressions given below exist in the relevant reference [14].

Taking constant time steps through solution;

$$\dot{u}_i = \frac{u_{i+1} - u_{i-1}}{2\Delta t} \tag{2.7}$$

$$\ddot{u}_i = \frac{u_{i+1} - 2u_i + u_{i-1}}{(\Delta t)^2} \tag{2.8}$$

These are the central difference expressions for velocity and acceleration. Substituting these terms into Equation (2.1), equation of motion becomes;

$$m\frac{u_{i+1}-2u_i+u_{i-1}}{(\Delta t)^2}+c\frac{u_{i+1}-u_{i-1}}{2\Delta t}+ku_i=-m\ddot{u}_g(t_i) \tag{2.9}$$

Assuming u_i and u_{i-1} are known;

$$\left[\frac{m}{(\Delta t)^2}+\frac{c}{2\Delta t}\right].u_{i+1}=-m\ddot{u}_g(t_i)-\left[\frac{m}{(\Delta t)^2}-\frac{c}{2\Delta t}\right].u_{i-1}-\left[k-\frac{2m}{(\Delta t)^2}\right]u_i \tag{2.10}$$

Rearranging Equation (2.10);

$$\hat{k}.u_{i+1}=\hat{p}_i \tag{2.11}$$

where;

$$\hat{k}=\frac{m}{(\Delta t)^2}+\frac{c}{2\Delta t} \tag{2.12}$$

$$\hat{p}_i=-m\ddot{u}_g(t_i)-\left[\frac{m}{(\Delta t)^2}-\frac{c}{2\Delta t}\right]u_{i-1}-\left[k-\frac{2m}{(\Delta t)^2}\right]u_i \tag{2.13}$$

This process is an *explicit method*, because the solution of u_{i+1} at time $i+1$ is determined from the equilibrium condition at instant i using Equation (2.11).

To begin with, one must know the initial conditions, u_0 and u_{-1}. Using central difference expressions in Equation (2.7) and Equation (2.8), these terms are calculated as;

$$\dot{u}_0=\frac{u_1-u_{-1}}{2\Delta t} \tag{2.14}$$

$$\ddot{u}_0=\frac{u_1-2u_0+u_{-1}}{(\Delta t)^2} \tag{2.15}$$

Solving Equation (2.14) for u_1, and substituting into Equation (2.15) gives;

$$u_{-1} = u_0 - \Delta t(\dot{u}_0) + \frac{(\Delta t)^2}{2}\ddot{u}_0 \tag{2.16}$$

Once initial conditions u_0, $\dot{u}_0$ and $\ddot{u}_0$ are known, displacements u_i can be obtained for successive time steps. For a system just subjected to strong ground motion, initial displacement and velocity are zero, whereas initial acceleration is equal to that of applied excitation.

Care must be to satisfy the stability condition;

$$\frac{\Delta t}{T_n} < \frac{1}{\pi}$$

Otherwise meaningless values will be obtained due to numerical round-off. Thus this method is a *conditionally stable* one.

2.2 DESIGN RESPONSE SPECTRUM CONCEPT

As briefly discussed in Section 2.1, the information supplied by response spectrum reflects the characteristics of the individual excitation. However, design or seismic evaluation of structures must be carried out in a comprehensive and systematic approach, which should consider the effects of future earthquakes [14]. To serve for this purpose, codes and specifications provide engineers with simple site specific tools to represent the effects of probable future strong ground motions, using the data obtained from the past records. This is the philosophy behind the concept of *design response spectrum*. To summarize, the design response spectrum is based on statistical analysis of the response spectra for the ensemble of ground motions [14, 16]. The process of its construction is a highly complicated and comprehensive matter, which is out of the scope of this thesis work. Although the provisions of certain guidelines and specifications about this subject will be reviewed in Section 3.1, the one used in this study is presented in Figure 2.3 [2, 3].

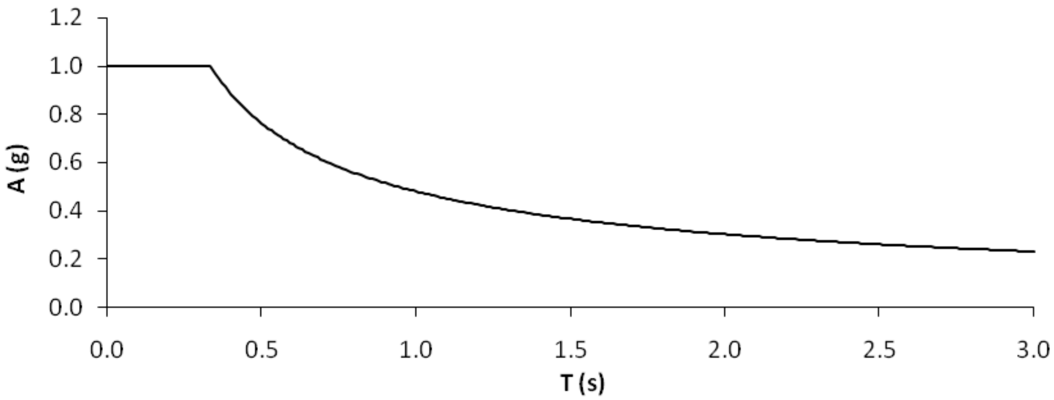

Figure 2.3: Typical design acceleration response spectrum

2.3 SPECTRUM COMPATIBLE RECORDS WITHIN "RSCA" SOFTWARE

The methods that will be presented and used through this thesis work are relatively simple but effective ones. Since a detailed study on this subject is also a branch of seismology as well as structural engineering, it will be appropriate to emphasize that the techniques explained and used here were chosen only to serve the practical needs of engineering.

After a literature review about this subject, the author would like to direct reader to the relevant references [15, 21]. Although some comprehensive softwares are available for generation of spectrum compatible accelerograms, such as "SIMQKE" (shareware, M.I.T.), "SPECTIME" (commercial, ANCO Engineers, Inc.) and "SYNTH" (commercial, Naumoski), a simple but freeware program called "RSCA", released under GNU public license by Thiele, M., was used in this study. Lucid code structure of the software made it possible to utilize some modifications that will also include the design parameters of engineering practice applied in Turkey.

In this section, algorithms used through "RSCA" software will be reviewed briefly. Although almost all of the material here is taken from [32], reference [15] may be referred as well for more information.

2.3.1 ORIGIN OF THE SOFTWARE AND MODIFICATIONS

"RSCA" software was written by Thiele, M. in 2002 using the Compaq Visual FORTRAN Compiler 6.5 in Microsoft Developer Environment 6.0. In the field of practical civil engineering, this freeware program is undoubtedly a valuable tool to generate modified and synthetic spectrum compatible accelerograms. Yet the program was operating with minor bugs, error handling routines were not present as stated in [32] due to short time limit of the original project. Additionally, the usability seemed to be complicated for the average end user because it included splinted routines that are many in number. The software is handled on internet by GNU public license, thus making it a freeware program open to the use of any engineer and developer. The author of this thesis work had some minor improvements on the calculation routines and user interface of the software, to achieve better usability as well as to obtain more precise results for his needs. Those and modifications made to the software are listed as;

1) **Duhamel integral routine existing in the acceleration response spectrum calculation scheme is replaced by a central difference algorithm.**

The original calculation scheme of pseudo acceleration response spectrum consisted of a Duhamel integral algorithm written by M. Durán. The code had some minor bugs which result in oscillations in the resultant response spectrum. This routine was replaced by a central difference algorithm. Brief information on this method can be found in Section 2.1, but for more [14, 15] may be referred. Modified code had improved the compatibility of resultant accelerograms in low periods by approximately 10% (Figure 2.4).

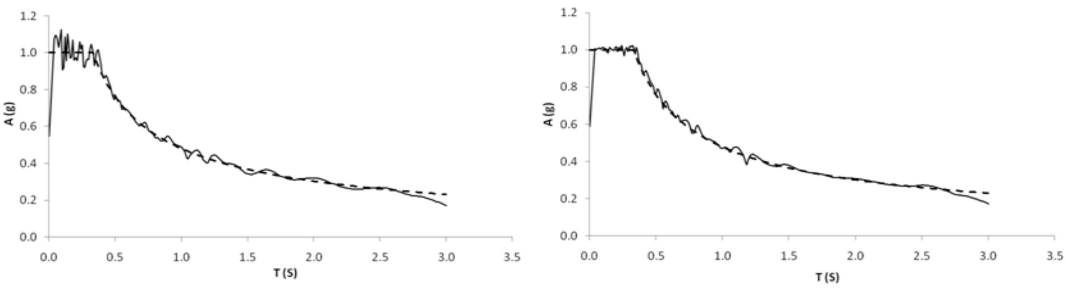

(a) Original Version (b) Modified Version

Figure 2.4: Results of original and modified codes after identical manipulations.

2) **Minor bug in target response spectrum loading routine was fixed. Chilean Earthquake Code module was replaced by AASHTO and 1998 Turkish Earthquake Design Code design response spectra.**

A minor bug had been causing incorrect evaluation of target response spectrum. Pseudo acceleration value $T_n = 0$ was reaching to infinity when custom target spectrum file was loaded, causing numerical stability while computing spectrum compatible accelerograms. Error was eliminated by supplying PGA value at $Tn = 0$. Additionally, "Chilean Earthquake Code" design spectrum module was replaced by introducing provisions of AASHTO [2, 3] and 1998 Turkish Earthquake Design Code to extend the usability of the program in possible future cases.

3) **Error handling routines were written.**

Error handling routines were not included in the original version of the software, resulting in abrupt termination due to request of an inconvenient action, e.g. trying to scale an accelerogram that was not yet loaded, or requesting a filtering action in case of a null target response spectrum. Error handling loops were implemented into the code to protect user from unexpected errors as well as to provide brief instructions about the operation sequence.

4) **User interface is simplified.**

Original version of the program had contained many separate routines on the dialog box. This advanced design could lead to difficulties and confusions for the user, so all relevant routines were packed up and the dialog box is simplified to a version composed of one command button for scaling of existing accelerograms, and two others for generating synthetic accelerograms. Modified interface is shown in Figure 2.5.

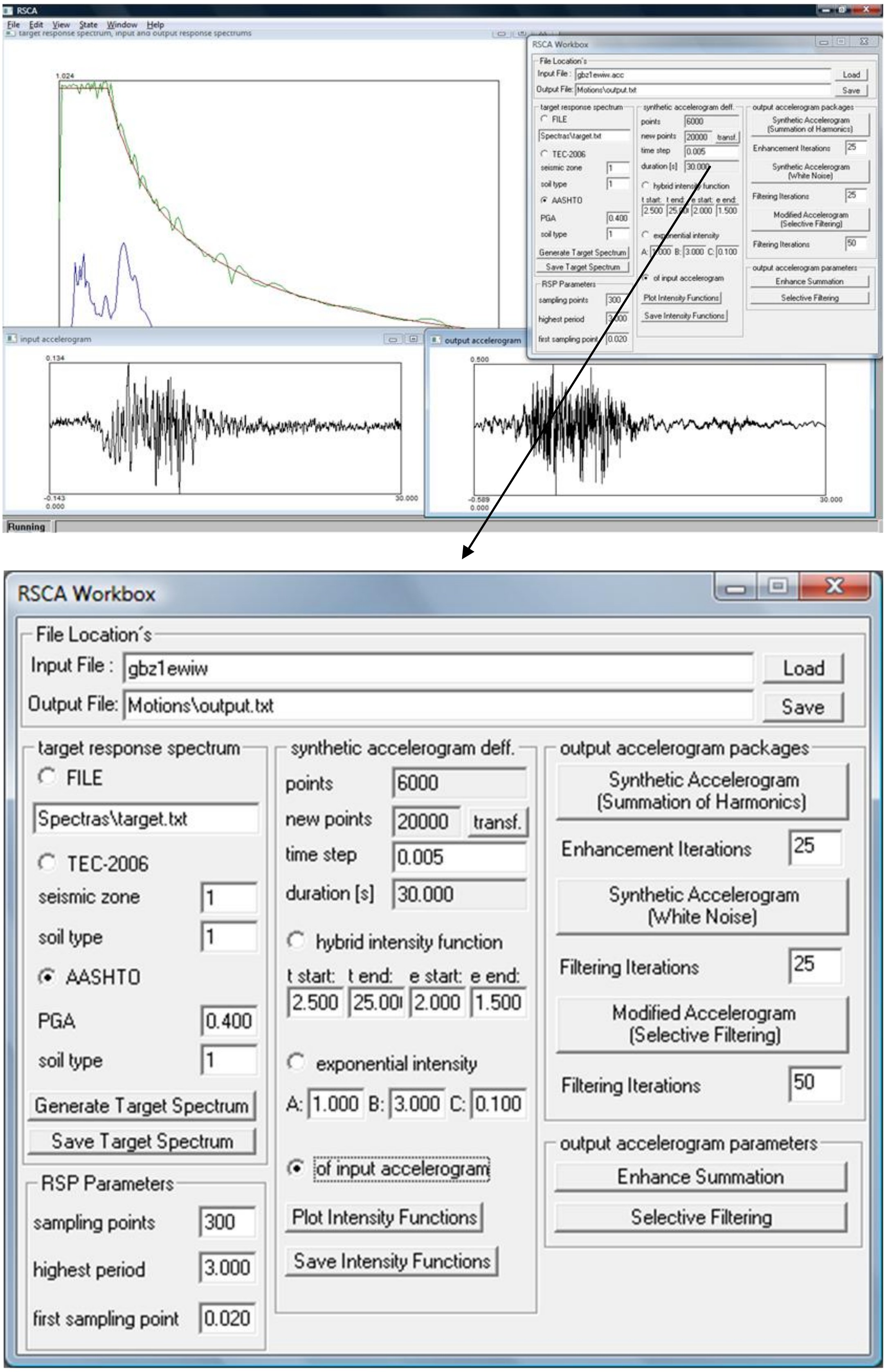

Figure 2.5: Input, output accelerograms and dialog windows of modified “RSCA” software

2.3.2 SCALING OF EXISTING ACCELEROGRAMS

Within “RSCA” software, the scheme of obtaining a spectrum compatible accelerogram involves three distinct steps [32];

1) Scalar multiplication of the acceleration amplitudes
2) An overall frequency content manipulation
3) Filtering of the unwanted responses

Scalar multiplication of the acceleration amplitudes: The response spectrum is nothing more than the plot of peak responses due to an earthquake excitation as a function of the natural vibration period of any linear SDOF system. Thus, multiplying the ordinates of an existing accelerogram will yield a response spectrum that is factored by the same value. This will result in a ground motion record having a spectrum of which pseudo acceleration values are closer to those of target spectrum, as illustrated in Figure 2.6.

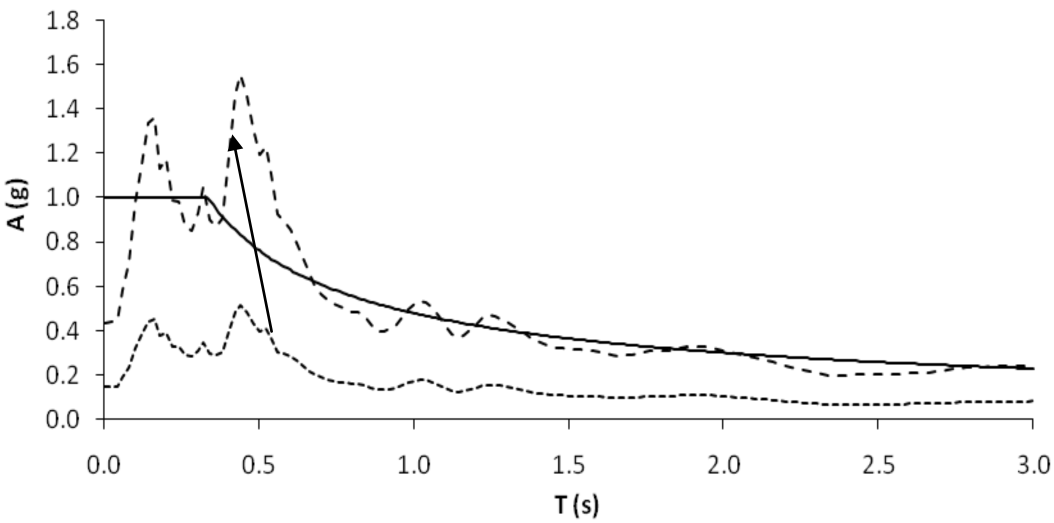

Figure 2.6: Result of multiplication process

Manipulation of frequency content: The purpose of this operation is to shift the peak response periods of input response spectrum to approximately match those of target response spectrum. This task can be easily accomplished by simply altering the time intervals of existing input accelerogram.

The ratio of resultant shift operation is of the same order with the change of time interval of input accelerogram [32]. For instance, a change of time interval from 0.01 to 0.005 results in a shift of response spectrum to the right by 50% (Figure 2.7). However, this procedure was not used in this study in order to preserve original time step of the record.

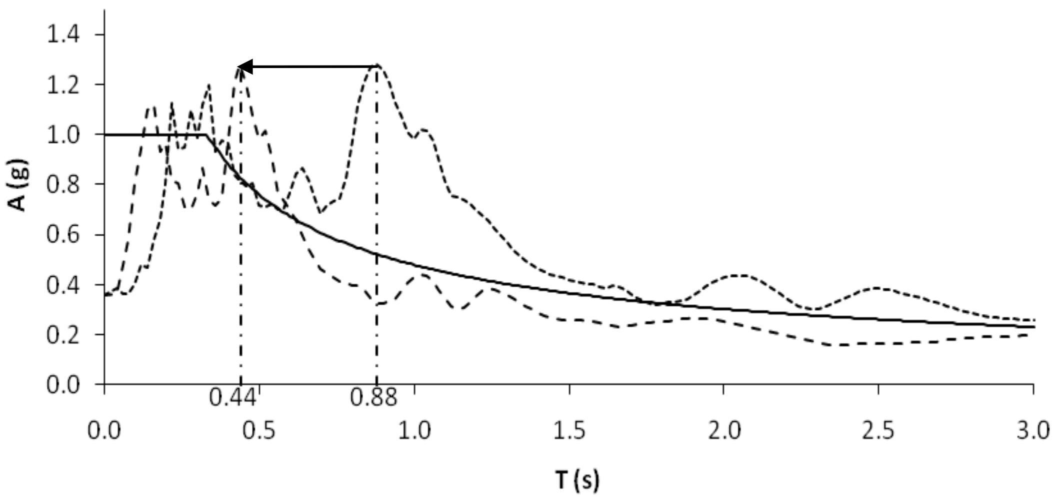

Figure 2.7: Result of the shifting process

Response Filtering: Perhaps the most complex operation involved in this compound scaling scheme is filtering the frequency content of existing accelerogram. It is possible to modify the earthquake excitation so that higher and/or lower response portions of the response spectrum may be altered to fit the target response spectrum. Basically, this can be achieved in an efficient way by changing the amplitudes of desired frequencies, after performing a FFT (fast Fourier transformation) of the existing accelerogram. It can be assumed that; an alteration of the amplitude of a special frequency will affect the response of the linear SDOF system having the same natural vibration frequency by much greater degree than the other ones [32]. The results of this operation are illustrated in Figure 2.8.

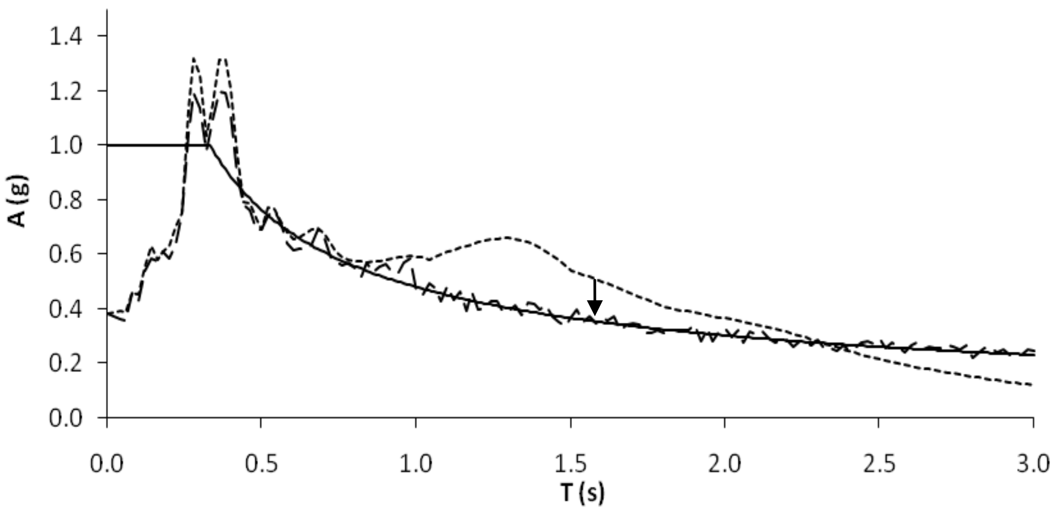

Figure 2.8: Result of selective filtering process

2.3.3 GENERATION OF SYNTHETIC ACCELEROGRAMS

Two methods are available within the aforementioned "RSCA" software. Besides their simplicity, these methods are also the frequently used ones to generate spectrum compatible accelerograms. These are called;

4) Synthesis through sums of harmonics functions
5) Filtering of white noise

Synthesis through sums of harmonics functions: The accelerogram is derived through the following summation [32];

$$\ddot{v}(t) = I(t) \sum_{i=1}^{n} A_i \sin(\omega_i t + \emptyset_i) \tag{2.17}$$

where $\emptyset_i$, ω_i, A_i are the phase, frequency, amplitude and $I(t)$ is the function of intensity and duration of the earthquake excitation. Different types of intensity functions are shown in Figure 2.9.

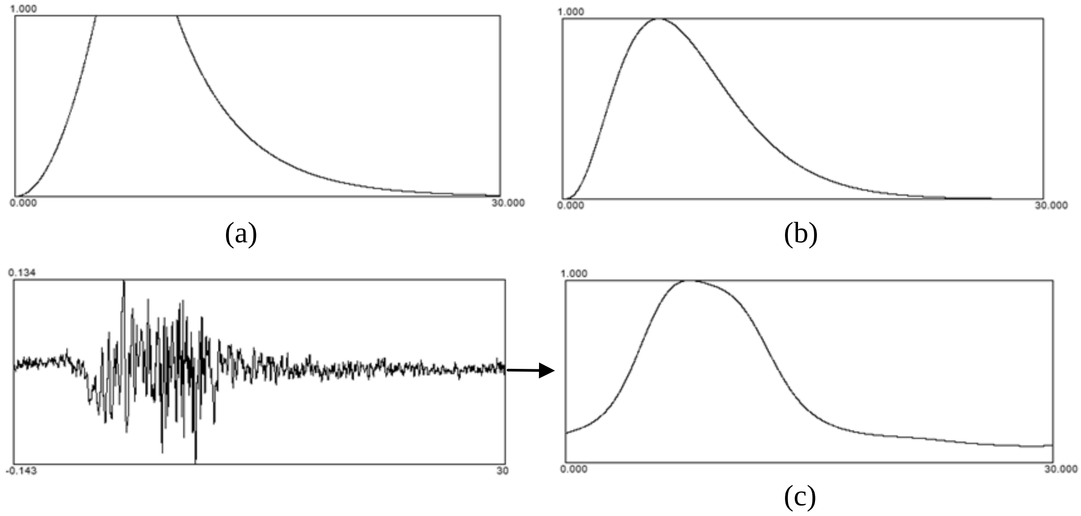

Figure 2.9: Different types of intensity functions in RSCA, (a) hybrid, (b) exponential, (c) intensity function of an accelerogram

Intensity function is basically a smoothed curve of absolute amplitudes of the earthquake accelerogram. One may prefer any suitable intensity function, to orient the shape of resultant accelerogram for meeting the requirements. It is evident that, every target response spectrum may not have a realizable accelerogram. So the final intensity function of the resultant accelerogram greatly depends on the shape of target response spectrum in some cases. References [15, 32] may be referred for more information about the subject.

Filtering of white noise: The hypothesis from which this method originates is that; source of ground motion is a random sequence of impulses generated at some distance and propagated to the observation point through the base medium [32]. Choosing an intensity function that will simulate the characteristics of real accelerograms, the scaling scheme is applied to generated white-noise, and spectrum compatible synthetic accelerogram is obtained.

CHAPTER 3

ANALYSIS GUIDELINE

In this chapter, the layout of this study and concerned rules set by certain specifications will be explained. In Turkey, AASHTO Standard Bridge Specifications [2] is currently being used as a guideline for design of highway bridges, thus its content will be emphasized.

3.1 SEISMIC PROVISIONS OF CODES

Reliability of hold-down device requirement per AASHTO Bridge Specifications is the main concern of this study. In this sense, time-history and response spectrum analyses were performed, making determination of earthquake characteristics of great importance. Following sections covers information about this subject.

3.1.1 SEISMIC PERFORMANCE CATEGORIES

AASHTO Bridge Specifications classifies bridges into four groups according to *Acceleration Coefficient* and *Importance Classification (IC)* [2].

Acceleration Coefficient	**Importance Classification (IC)**	
	I	**II**
$A \leq 0.09$	A	A
$0.09 < A \leq 0.19$	B	B
$0.19 < A \leq 0.29$	C	C
$0.29 < A$	D	C

Table 3.1: Seismic performance category (SPC)

Here, acceleration coefficient is supplied by contour maps of United States, Alaska, Hawaii and Puerto Rico given by AASHTO. However, in Turkey, a map of earthquake regions is used for this purpose (Figure 3.1). A detailed version can be found in reference [19].

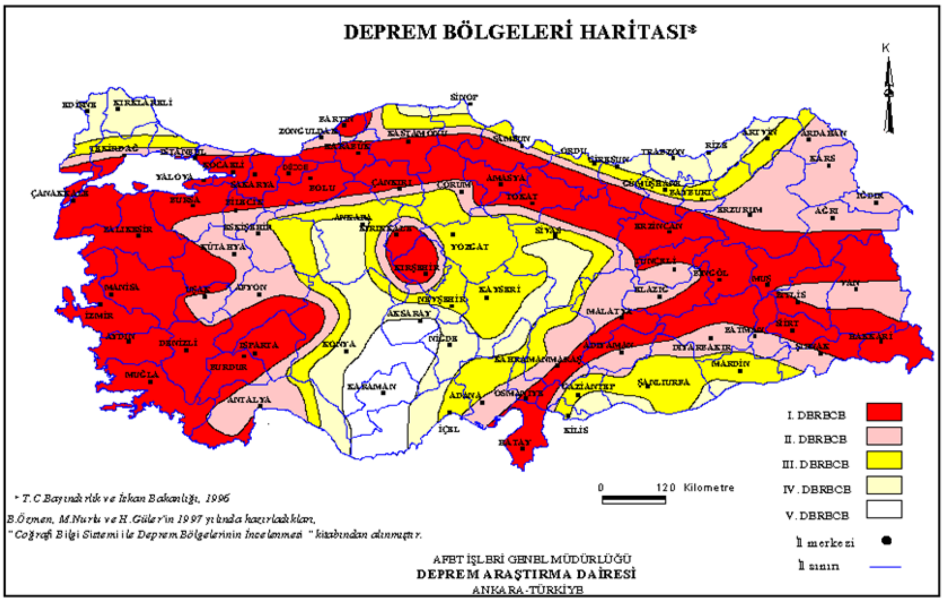

Figure 3.1: Map of seismic zones of Turkey (1996)

Acceleration coefficient is determined according to these regions. That is; A is equal to 0.40, 0.30, 0.20 and 0.10 for regions labeled as 1, 2, 3 and 4. Consideration of earthquake event is not mandatory for structures to be built in region 5 [26].

AASHTO Bridge Specifications states that, important classification (IC) is equal to I and II for essential and other bridges respectively [2]. Minimum analysis and design requirements per AASHTO are governed by this seismic performance category obtained according to A and IC, using Table 3.1 [2].

3.1.2 SITE CLASSIFICATION

According to AASHTO Bridge Specifications, effects of site conditions are taken into account by the *Site Coefficient (S)* based on the profile of medium. A brief explanation is supplied here [2, 3];

SOIL PROFILE I: Rock of any characteristics, or stiff soils where depth is less than 60 m.
SOIL PROFILE II: Stiff clay or cohesionless conditions where depth exceeds 60 m.
SOIL PROFILE III: Soft to medium-stiff clays and sands where layer depth exceeds 9 m.
SOIL PROFILE IV: Soft clays or silts where layer depth exceeds 12 m.

Site coefficient (S) is then determined from Table 3.2.

	Soil Profile Type			
	I	**II**	**III**	**IV**
S	1.0	1.2	1.5	2.0

Table 3.2: Site Coefficient (S)

3.1.3 HORIZONTAL DESIGN RESPONSE SPECTRUM

The term that compensates design response spectrum of horizontal strong ground motion is *Elastic Seismic Response Coefficient* (C_s) in AASHTO Bridge Specifications. It is calculated by the formula [2, 3];

$$C_s = \frac{1.2 * A * S}{T^{2/3}} \tag{3.1}$$

where;

A = Acceleration coefficient
S = Soil site coefficient
T = Period

and C_s need not exceed $2.5A$. For soil profiles III or IV where $A \geq 0.30$, $C_s \leq 2.0A$.

A plot of elastic seismic coefficient C_s vs period T forms design response spectrum for horizontal earthquake motion. Return period of this design earthquake motion is approximately 475 years, which corresponds to 10% probability of exceedance in 50 years.

3.1.4 VERTICAL DESIGN SPECTRUM

Currently, bridge specifications and guidelines do not include any provisions to construct vertical design spectrum. However, recent studies and commentary parts of these codes contains some discussions of the concept.

Commentary sections of AASHTO Bridge Specifications provide the ratio of 2/3, for construction of vertical design spectrum by multiplying the ordinates of the spectrum for horizontal motion [2, 3]. Likewise, it stated in Applied Technology Council Recommendations (ATC-32) that, a vertical design response spectrum having ordinates of 2/3 of horizontal one shall be used if better site specific information is not available [7]. New York State Department of Transportation (NYCDOT) [27] considers the same approach also. Commentary part of American Petroleum Institute (API) Recommended Practice suggests the ratio of 1/2 [4].

California Department of Transportation (CALTRANS) Seismic Design Criteria does not contain any elaborate approach. It is expressed that for ordinary bridges where rock peak acceleration is equal to 0.6 g or greater, an equivalent static vertical load shall be applied to the superstructure to estimate the effects of vertical acceleration [12].

Recent studies pointed out that, horizontal/vertical peak acceleration ratio for a structure under strong ground motion greatly depends on two specific parameters; distance to fault and fundamental period of the system. According to the findings, the common ratio of 2/3 tends to underestimate the actual ratio in lower periods ($T \leq 0.2 - 0.3\ sec$) especially at near fault, however being usually conservative for longer periods [9, 11]. Although many attenuation relationships offer equations to develop empirical site-specific vertical response spectra, an approximate procedure for distance-dependent one is supplied in [8].

3.1.5 COMBINATION OF ORTHOGONAL EXCITATIONS

AASHTO Bridge Specifications provides no information about simultaneous application of neither orthogonal horizontal nor vertical excitations. Rather it prefers to suggest two different combinations of maximum separate horizontal responses to account for directional uncertainty of strong ground motions and simultaneous occurrences of directional components [2, 3].

Same load combinations are also supplied by CALTRANS Seismic Design Criteria and ATC-6 Seismic Design Guide Lines, and are as follows [2, 3, 6];

Load combination 1: 1.0X + 0.3Y
Load Combination 2: 0.3X + 1.0Y

where X is the maximum specific response due to longitudinal excitation and Y is the same for transverse component.

However, ATC-32 Seismic Design Criteria suggest the following combinations of maximum responses, including the effects of vertical excitation as well [7].

Load combination 1: 0.4X + 1.0Y + 0.4Z
Load Combination 2: 1.0X + 0.4Y + 0.4Z
Load Combination 3: 0.4X + 0.4Y + 1.0Z

NYCDOT suggest the same, with a factor of 0.3 instead of 0.4 [27].

Moreover, SRSS of orthogonal peak responses was noted to produce most accurate results in a recent study [11]. Two other methods were given in [16], but will not be reviewed here.

On the other hand, AASHTO Guide Specifications for Seismic Isolation Design supplies some information about simultaneous application of horizontal earthquake motions. According to that; ensemble horizontal SRSS spectrum of horizontal components is scaled so that acceleration values does not fall below 1.3 times the design spectrum in the interval between periods T_1 to T_2, which are 0.5 times of fundamental period of vibration of structure in the direction under consideration, and 1.5 times of the same [1].

3.1.6 HOLD-DOWN DEVICE REQUIREMENTS

It is stated in AASHTO Standard Specifications and ATC-6 that; for bridges having seismic performance category (SPC) C and D, hold-down devices shall be provided at all supports or hinges in continuous structures, where the vertical seismic force due to the longitudinal horizontal seismic component opposes and exceeds 50% but is less than 100% of the dead load reaction.

In this case, the minimum net upward force ld-down device shall be 10% of the dead load downward force that would be exerted if the span were simply supported. If the vertical seismic force (Q) due to the longitudinal horizontal seismic load opposes and exceeds 100 percent of the dead load reaction (DR), the net upwards force for the hold-down device shall be 1.2(Q-DR) but it shall not be less than that specified before [2, 6]. AASHTO LRFD Specifications includes identical provisions, only replacing condition of having SPC C and D by *seismic zones* 2, 3 and 4 [3].

Occurrence of uplift can also result in damage or stability loss. But it also a fact that vertical motion restrainers are usually not considered to be feasible unless other bearing retrofits are being performed [33]. Thus disadvantages of sacrificing these devices were also investigated in this study.

3.1.7 MINIMUM SUPPORT LENGTH REQUIREMENT

According to AASHTO, bridges classified as seismic performance category (SPC) C or D, minimum support length N shall satisfy [2, 3];

$$N = (305 + 2.5L + 10H)(1 + 0.000125S^2) \text{ (mm)} \tag{3.2}$$

where,

$L =$ length of bridge deck to the adjacent expansion joint or end of bridge deck (m).
$S =$ angle of skew of support measured from a line normal to the span (degrees).
$H =$ for abutments, average height of columns supporting L length of bridge deck;
for columns and/or piers, own height (m).

Concept of minimum support length is visualized on Figure 3.2.

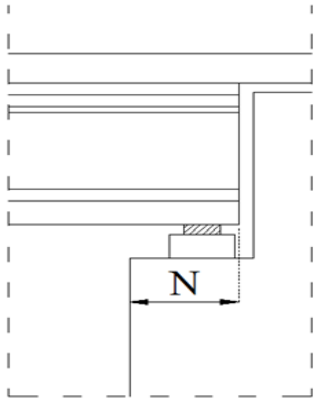

Figure 3.2: Minimum support length

3.2 ANALYSIS METHODS

This section contains only brief explanation about structural analysis methods used through this study, as detailed information about these can be found on any standard text book. Definitions and equations used in this section are exclusively taken from [14].

3.2.1 MODAL ANALYSIS

Modal analysis is a fundamental tool to perform response spectrum analysis, as well as to interpret the earthquake response of a structure.

As any set of N independent vectors can be used as a basis of representing any other of order N, and due to well known orthogonality condition of mode shapes of a structure, once they are calculated, displacement vector u of a linear MDOF system can be expressed in terms of these as;

$$u = \sum_{r=1}^{N} \emptyset_r q_r(t) \tag{3.3}$$

where $\emptyset_r$ and $q_r(t)$ represents displacement vector of natural mode shapes and modal coordinates respectively.

Equation of motion is rewritten for a multi degree of freedom (MDOF) system as;

$$\mathbf{m}\ddot{u} + \mathbf{c}\dot{u} + \mathbf{k}u = -\mathbf{m}\ddot{u}_g(t) \tag{3.4}$$

Since it is possible to express displacement vector u of a linear MDOF system in terms of modal contributions, equation of motion can be expressed as;

$$\sum_{r=1}^{N} \mathbf{m}\emptyset_r \ddot{q}_r(t) + \sum_{r=1}^{N} \mathbf{c}\emptyset_r \dot{q}_r(t) + \sum_{r=1}^{N} \mathbf{k}\emptyset_r q_r(t) = \mathbf{p}(t) \tag{3.5}$$

where $p(t)$ represents external force $-m\ddot{u}_g(t)$. Premultiplying each term by ${\emptyset_r}^T$, this equation can be expressed for each mode n as;

$$M_n \ddot{q}_r(t) + \sum_{r=1}^{N} C_{nr} \dot{q}_r(t) + K_n q_r(t) = P_n(t) \tag{3.6}$$

where;

$$M_n = {\emptyset_n}^T \mathbf{m} \emptyset_n$$
$$C_{nr} = {\emptyset_n}^T \mathbf{c} \emptyset_r$$
$$K_n = {\emptyset_n}^T \mathbf{k} \emptyset_n$$
$$P_n = {\emptyset_\mathrm{n}}^T \mathbf{p}(t) \tag{3.7}$$

Note that mass and stiffness terms (M_n and K_n) are uncoupled scalar quantities for each mode n. This is due to the orthogonality condition of modes. Damping term in Equation (3.6) will be uncoupled only if the system has classical damping. Under that condition, C_{nr} will be equal to zero for $n \neq r$. Thus Equation (3.6) will become;

$$M_n \ddot{q}_r(t) + C_n \dot{q}_r(t) + K_n q_r(t) = P_n(t) \tag{3.8}$$

which means that equation of motion of a MDOF system will be reduced to n number of uncoupled equations for SDOF systems in modal coordinates. This is basic idea behind the method of response spectrum analysis, which will be described in the next section.

3.2.2 RESPONSE SPECTRUM ANALYSIS

As defined above, response of a linear MDOF system as a function of time can be calculated for each mode by solving Equation (3.6).

Superposing these results, exact response history solution of the same structure can be obtained. Then the desired maximum response can be extracted, as design procedure is usually governed by the critical value. The superposition of modal responses is performed introducing and using various modal contribution factors, which are lengthy in description, so will not be reviewed here.

Response spectrum analysis method is an approximation of those maximum responses, by obtaining each one from prescribed response spectrum for relevant mode and then combining in a special manner, rather than solving Equation (3.6) for each mode.

This turns out to be a quite practical method, as one does not have to collect or generate time-history records. Instead, a derived design response spectrum shall be used.

However, solution is not exact in this method, as response histories, and thus occurrence time of peak responses of each mode cannot be known without solving Equation (3.6) for each mode. Special combinations methods are used for this purpose, of which the preferred ones are well known SRSS and CQC rules in most of the cases.

As mentioned earlier in this text, simplicity of this method ensures its prevalence.

3.2.3 TIME HISTORY ANALYSIS

Time history method is direct solution of equation of motion. Different approaches may be utilized according to the properties and idealization of structure.

If linear response is required, a superposition of modal responses may be used. As explained in Section 3.2.1, this method requires a classical damping matrix to be provided.

In case of a nonlinear structure, or a linear system having a non-classical damping matrix, application of numerical methods is inevitable. Various alternatives exist to carry out the calculations, of which details are explained in [14, 15].

3.3 FLOWCHART AND LEGEND

This section covers the steps performed through the study. Initially, analysis models were prepared for each bridge. Following completion of structural idealizations, earthquake characteristics were determined using related provisions described earlier. Then spectrum compatible accelerograms were produced. To begin with the calculations, response spectrum analyses were determined to acquire member forces and to check hold-down design requirements for each bridge per AASHTO. Then one-directional linear time history analyses were carried out to validate both Rayleigh damping coefficients and generated spectrum compatible strong ground motion records. Multi directional linear time history analyses were performed also to supply additional comparisons and explanations in certain cases. If hold-down design requirement was triggered for a case, nonlinear time-history analyses were performed to verify the location bearings that are subjected to uplift, which were determined according to AASHTO provisions. Then making a preliminary hold-down device design per AASHTO design forces, actual device forces obtained from an additional set of nonlinear time-history analyses were compared with those. Finally, a set of linear time-history and response spectrum solutions, to be called *lower-bound analyses* through this text, were performed to investigate the stability condition of the bridges where application hold-down devices was mandatory but not carried out. Details of all those nonlinear analysis models will be explained in Section 4.2.3.

Deviations between results of time-history analyses and response spectrum load combinations were presented and interpreted. Discussion of cap beam moments, pier axial forces and moments as well as compressive bearing forces was also included. Those were directly obtained from analyses results, in other words; they are not divided by any reduction factors.

Global directions were denoted by;

X: Longitudinal Direction
Y: Transverse Direction
Z: Vertical Direction

Abutments and pier axes were denoted by relevant letters, A and P respectively, followed by ID number ascending in X direction.

Bearings were labeled such that all ID's are sorted in ascending order first according to X, and then Y coordinates. Legend is presented in Figure 3.3 for Bridge 1.

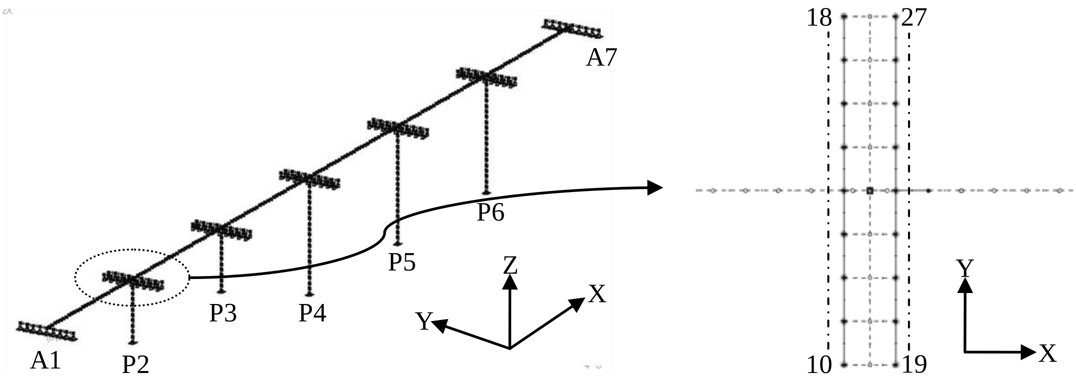

Figure 3.3: Demonstration of legends on Bridge 1

Analyses cases are tabulated in Table 3.3.

Table 3.3: Summary of Analyses Cases

ID	Type	Direction
Dead (D)	Static	Dead
1	Response Spectrum	X
2	Response Spectrum	Y
3	Response Spectrum	Z
4	Linear Time History	X
5	Linear Time History	Y
6	Linear Time History	Z
7	Linear Time History	Dead+X+Y+Z
8	Nonlinear Time History (non-retrofitted)	Dead+X+Y+Z
9	Nonlinear Time History (retrofitted)	Dead+X+Y+Z
10	Nonlinear Time History (lower bound)	Dead+X+Y+Z
11	Response Spectrum (lower bound)	X
12	Response Spectrum (lower bound)	Y
13	Response Spectrum (lower bound)	Z

Used peak response combinations are tabulated in Table 3.4. Effects of vertical excitations were also included in the latest group, to examine the possibility of increasing accuracy of AAHTO load combinations.

Table 3.4: Summary of Load Combinations

ID	Combination of Maximum Responses
C1	1.0X+0.3Z
C2	0.3X+1.0Z
C3	1.0X+0.3Y+0.3Z
C4	0.3X+1.0Y+0.3Z
C5	0.3X+0.3Y+1.0Z

Load combinations are classified as;

Group 1: Maximum of C1 and C2
Group 2: Maximum of C3, C4 and C5

Group 1 will also be expressed as "AASHTO load combinations" in charts and discussions.

AASHTO Standard Specifications [2] also suggest the use a load factor of 0.75, to reduce dead loads when checking maximum pier moments. Although this reduction is omitted for bridges having SPC B, C and D in the same specifications, there is also a practice of extending this approach for all bridges. These load combinations were also included in comparison of pier axial forces, under the name of "Reduced AASHTO Load Combinations".

Abbreviations RSP, LTH and NLTH will be used to denote response spectrum, linear time-history and nonlinear time-history analyses respectively. CASE ID's will be employed to point out relevant analyses or load combinations through the study (e.g. RSP-1, LTH-7, NLTH-8, Load Combination C1, or simply 1, 7, 8, C1 etc.).

Unless otherwise stated, all force, moment, displacement and vibration period outputs will be presented in units of "kN", "kN.m", "mm" and "sec" respectively through whole text. To avoid congestion, definitions of units will not be repeated in tables.

In tables, “T.” and “C.” will be used to represent tensile and compressive directions respectively due to same reason.

Bearing results will be displayed for half of them only, due to the complete symmetry of all models about X direction. Absolute maximum responses obtained for two symmetric bearings will be presented by that having smaller ID. (e.g. As bearings 10 and 18 constitute a symmetric pair, absolute maximum of their responses will be assigned to 10 in result tables).

Earthquake records that were used in the study are tabulated in Table 3.5.

Table 3.5: Summary of Generated Records

ID	**Origin**	**Type**
1	Gebze (İzmit EQ, 1999, Mw = 7.4), 7.74 km	Modified
2	Duzce (Bolu EQ, 1999, Mw = 7.2), 8.30 km	Modified
3	Duzce (İzmit EQ, 1999, Mw = 7.4), 17.06 km	Modified
4	Gebze (İzmit EQ, 1999, Mw = 7.4), 7.74 km	Synthetic
5	Duzce (Bolu EQ, 1999, Mw = 7.2), 8.30 km	Synthetic
6	Duzce (İzmit EQ, 1999, Mw = 7.4), 17.06 km	Synthetic

Explanations regarding selection of these records will be included in Section 4.1.2.

Flowchart of explained investigation scheme is presented on Figure 3.4.

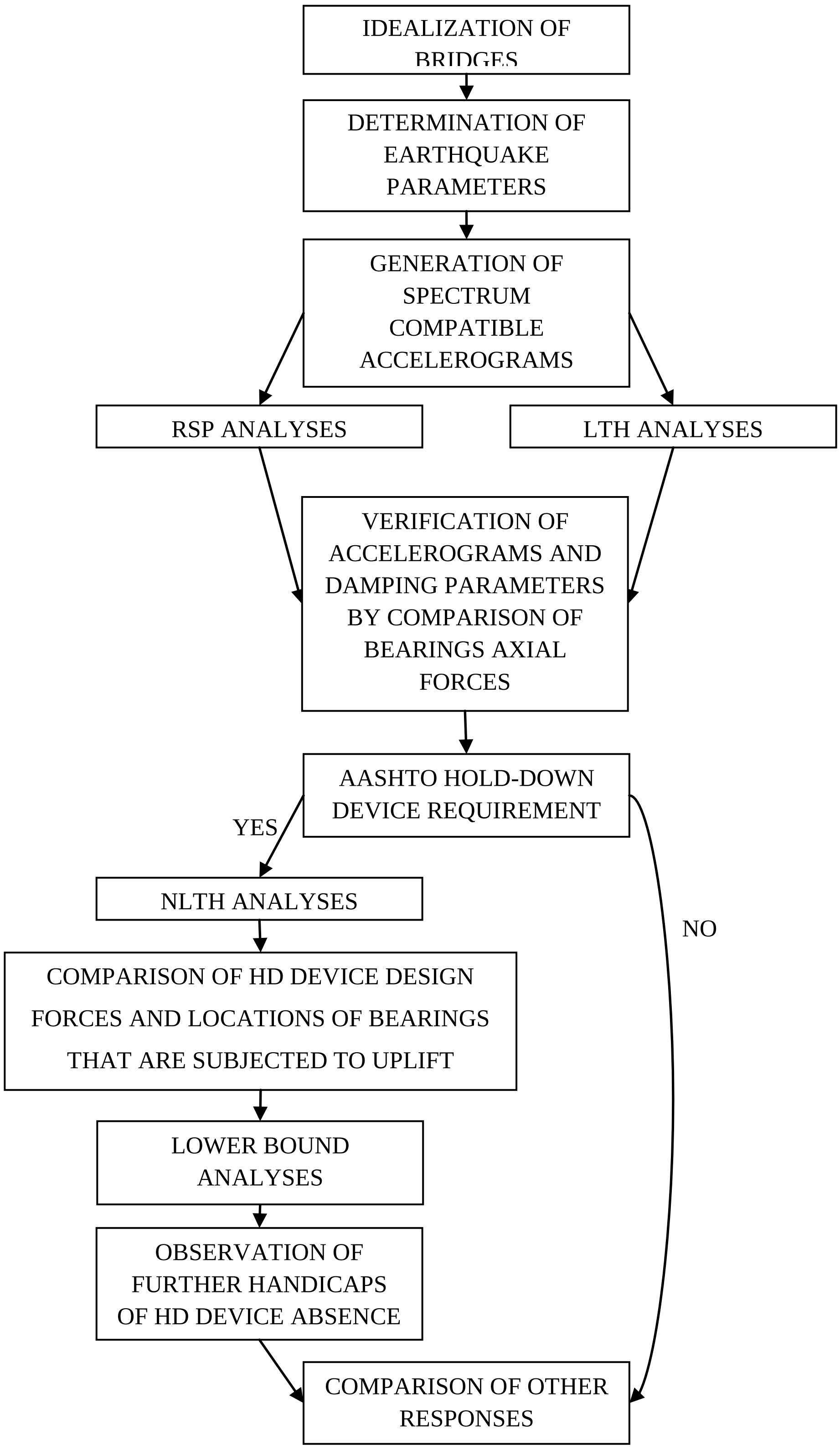

Figure 3.4: Flowchart of the study

CHAPTER 4

CASE STUDIES

4.1 EARTHQUAKE CHARACTERISTICS

In Turkey, earthquake is generally the primary concern in the design of highway bridges. In this respect, the extreme hazard level described by AASHTO is considered.

4.1.1 DESIGN RESPONSE SPECTRUM

For all case studies, soil profile is assumed to be of type I (rock site) to eliminate the complexity of soil-structure interaction. Seismic acceleration coefficient was selected to be 0.4, to impose extreme design earthquake intensity. Design response spectrum of horizontal earthquake motion was calculated using Equation (3.1) and presented on Figure 4.1.

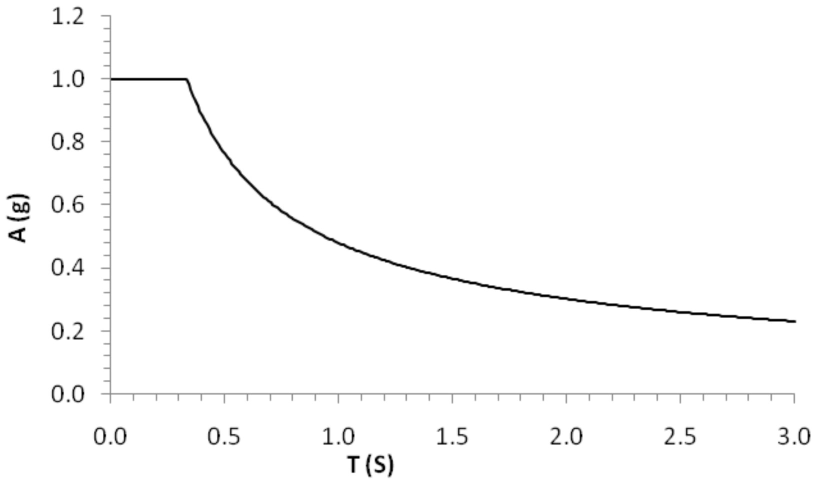

Figure 4.1: Horizontal design response spectrum used in case studies

Vertical response spectrum was constructed by multiplying the ordinates of the one for the horizontal motion by 2/3, which is the typical ratio, considered in design of standard highway bridges as suggested by current specifications (Section 3.1.3). The same ratio was also used in similar studies [10, 27].

Seismic performance category (SPC) was determined as D for all bridges using Table 3.1.

4.1.2 COMPATIBLE TIME-HISTORY RECORDS

Two sets of spectrum compatible time-history records were generated.

First set was obtained by modifying existing histories, resulting in three accelerograms per orthogonal direction.

For this purpose, three records were obtained from [25]. Two of them were recorded during 17 August Kocaeli Earthquake, and the other belongs to 12 November 1999 Bolu-Düzce Earthquake.

Due to the modification process, frequency content and peak ground accelerations (PGA) were altered significantly. Only intensity functions were approximately preserved during modification. Thus properties such as distances to fault zone and PGA values were not the primary factors that govern this selection.

The main concern was to provide a small time interval between digitized values, thus making it possible to calculate resultant response spectrum at smaller period intervals, without occurrence of numerical instability using central-difference procedure explained in Section 2.1. As each of these records provided an interval of 0.005 sec as well as with different intensity functions, they supplied the accuracy and variation that is intended to be included in this study. Accelerograms before and after modification are shown in Figure 4.2, Figure 4.3 and Figure 4.4 for records 1, 2 and 3, respectively.

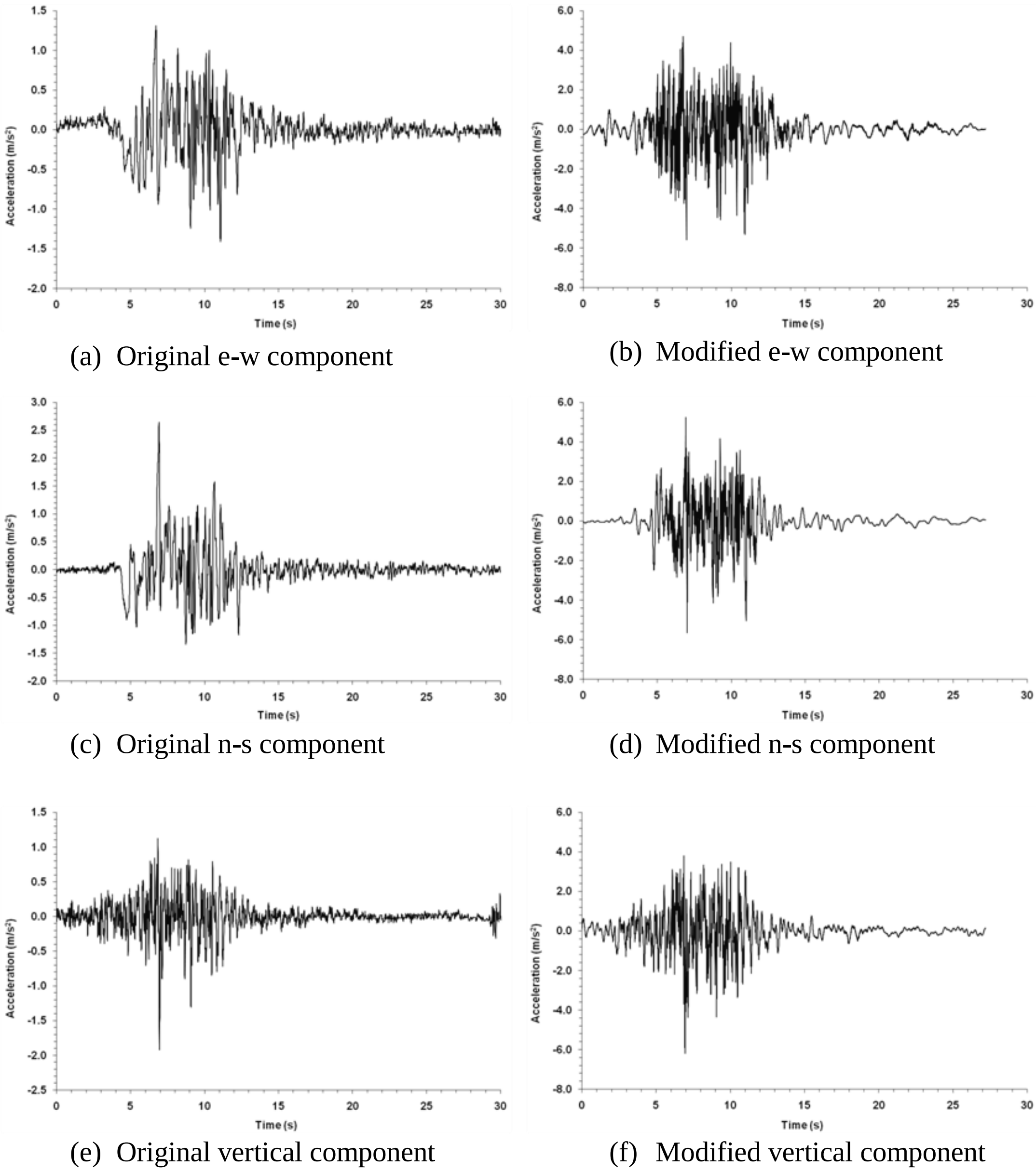

(a) Original e-w component

(b) Modified e-w component

(c) Original n-s component

(d) Modified n-s component

(e) Original vertical component

(f) Modified vertical component

Figure 4.2: Accelerograms of original and modified components of record 1

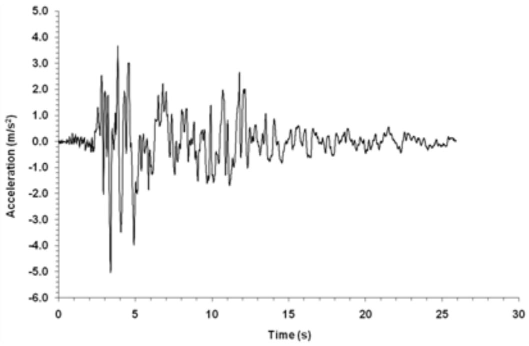

(a) Original e-w component

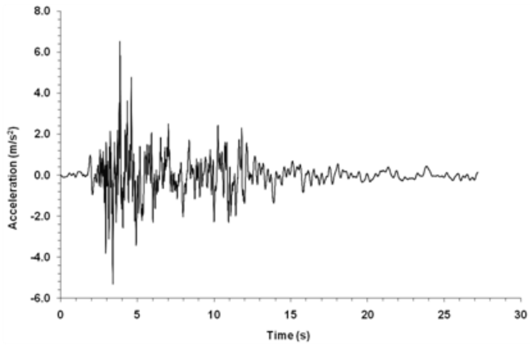

(b) Modified e-w component

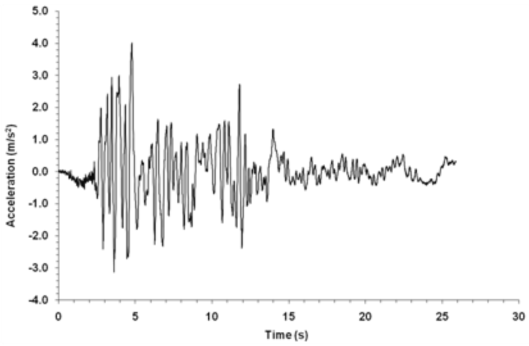

(c) Original n-s component

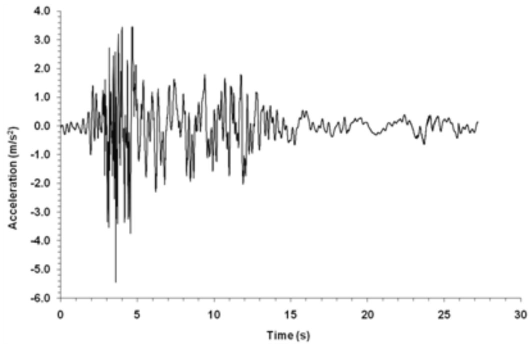

(d) Modified n-s component

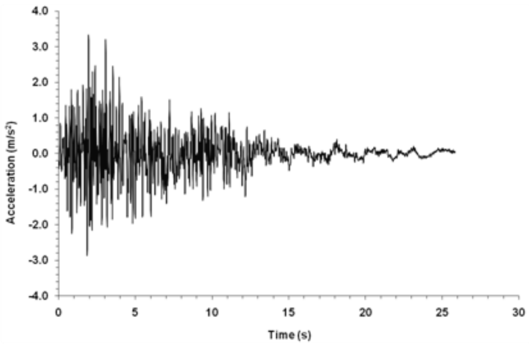

(e) Original vertical component

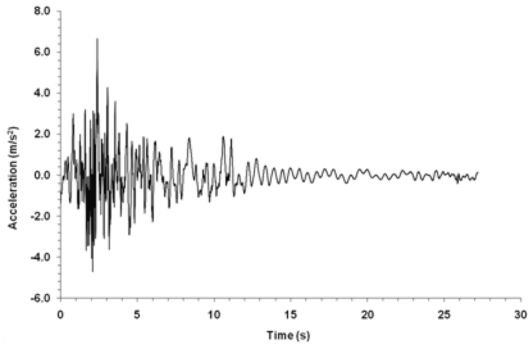

(f) Modified vertical component

Figure 4.3: Accelerograms of original and modified components of record 2

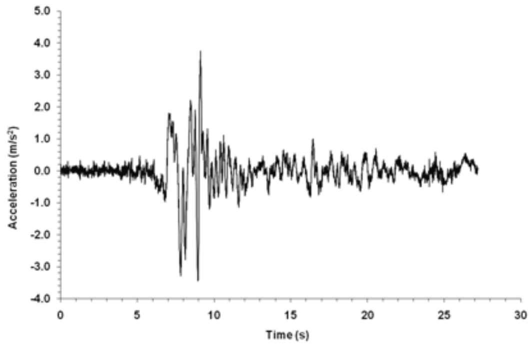

(a) Original e-w component

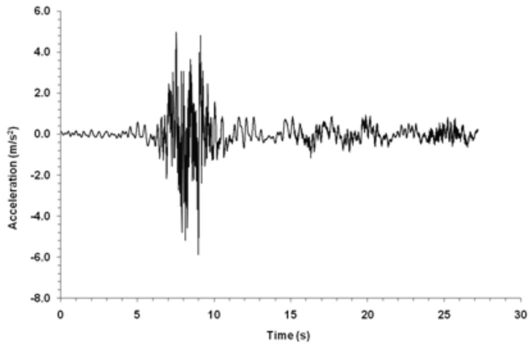

(b) Modified e-w component

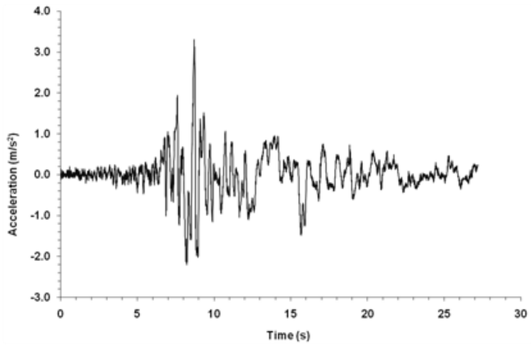

(c) Original n-s component

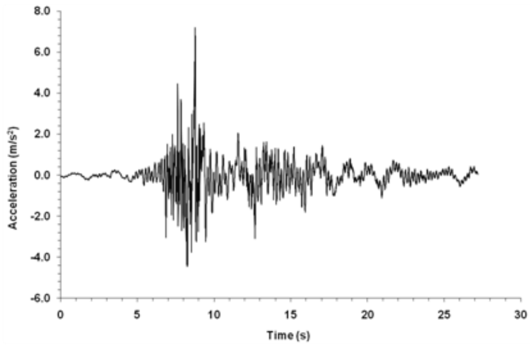

(d) Modified n-s component

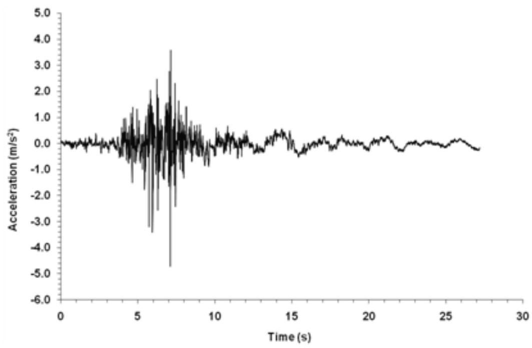

(e) Original vertical component

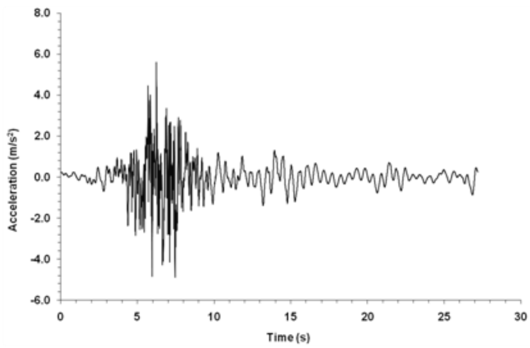

(f) Modified vertical component

Figure 4.4: Accelerograms of original and modified components of record 3

Resultant response spectra before and after modification for the same records are given in APPENDIX E.

Second set was consisted of three synthetic accelerograms, in which all orthogonal directions of a strong ground motion was represented by the same record. Exponential intensity functions were chosen to approximate the characteristics of above mentioned original records, and shown in Figure 4.5.

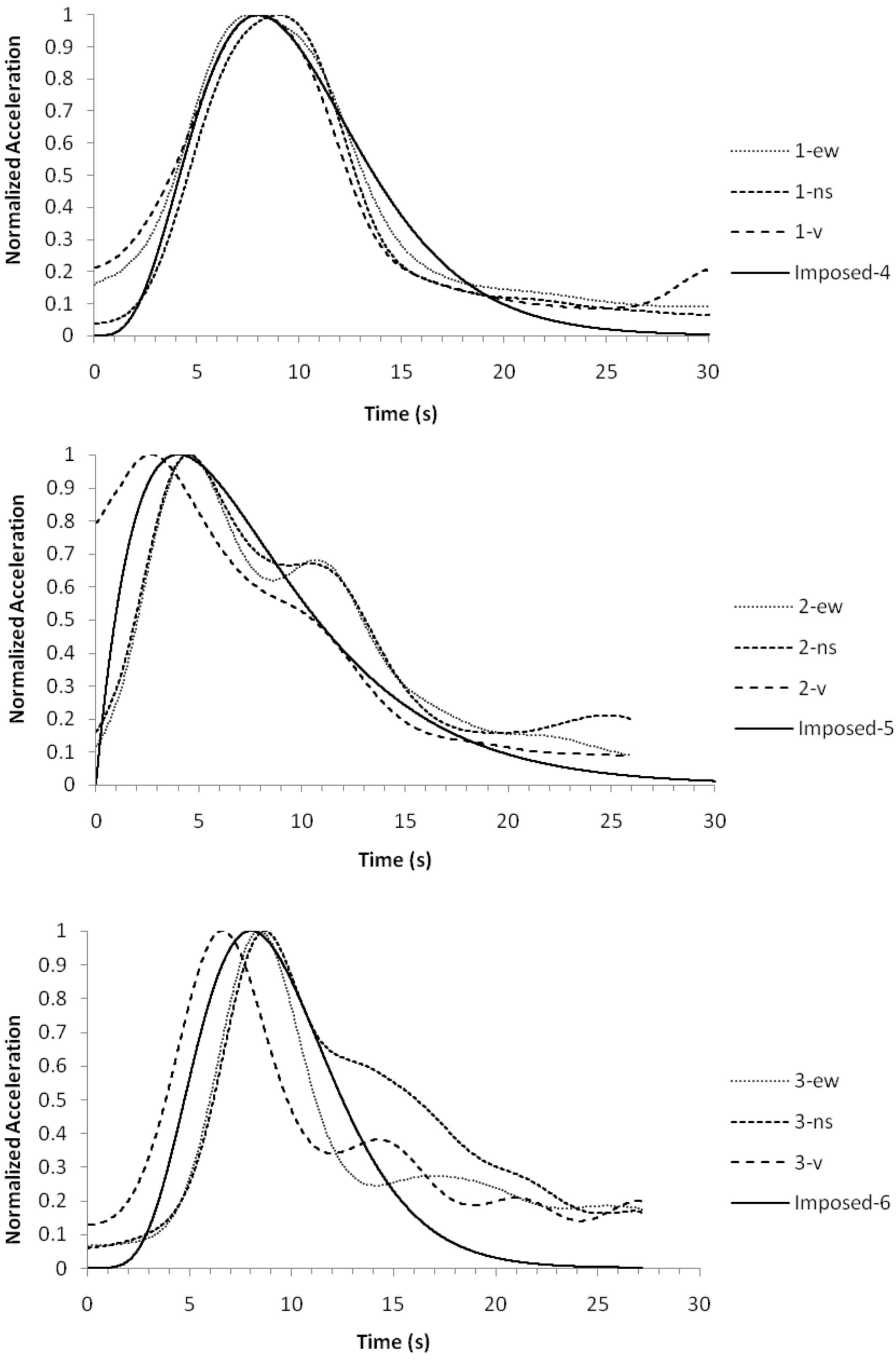

Figure 4.5: Imposed intensity functions for synthetic accelerograms 4, 5 and 6.

Resultant accelerograms that were generated using these intensity functions are presented on the following figure.

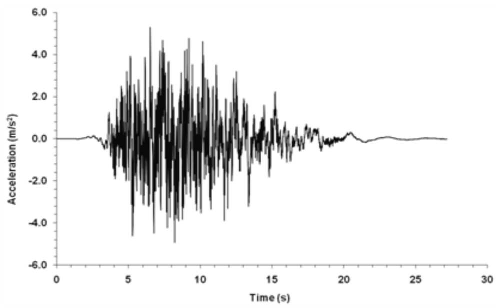

(a) Synthetic record 4

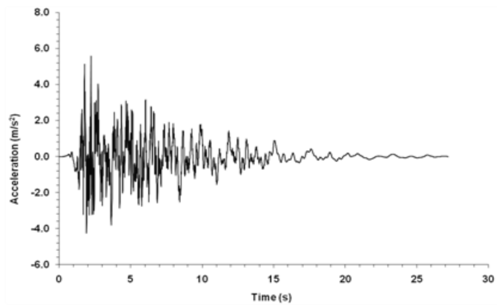

(b) Synthetic record 5

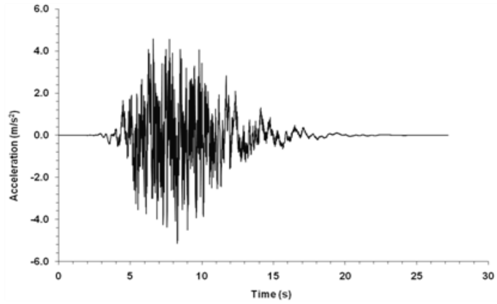

(c) Synthetic record 6

Figure 4.6: Generated synthetic accelerograms 4, 5 and 6.

Resultant response spectra of those records are given in APPENDIX E.

4.1.3 APPLICATION OF GROUND MOTION COMPONENTS

Results of six ground motion records were averaged to obtain seismic demands.

Although spectrum compatible accelerograms were generated for this research; scaling method of [1] explained in Section 3.1.5 was also used to fine tune the horizontal components. Vertical component was included in the analyses simultaneously with those scaled horizontal excitations.

Two sets of ground motions were to be scaled by different factors, as analyses utilizing modified accelerograms were completed already by the time synthetic excitations has been decided to be included in the study.

On the other hand, obtained factors did not differ significantly between those groups, as will be seen in Section 4.3. Thus it is concluded that reliability of average values obtained from individual results were not affected by this separate scaling of two sets.

Recalling the mentioned provisions; ensemble horizontal SRSS spectrum of horizontal components is scaled so that acceleration values does not fall below 1.3 times the design spectrum in the interval between periods T_1 to T_2, which are 0.5 times of fundamental period in the direction under consideration, and 1.5 times of the same.

However, definition of fundamental period is not clearly stated in the reference [1]. In this study, minimum and maximum of fundamental periods in X and Y directions were used to calculate T_1 and T_2 respectively, to acquire a conservative interval which represents vibrations in both directions. That is;

$$T_1 = 0.5 * \min(T_X, T_Y)$$
$$T_2 = 1.5 * \max(T_X, T_Y)$$

4.2 MODELLING TECHNIQUE

Undoubtedly, idealization of a structure has considerably effect on the results. Day by day, advanced modeling techniques are presented to the engineers, making it possible to take into account the actual geometry and construction sequences more realistically.

But it should not be forgotten that, estimations of material behavior and especially strong ground motions are very uncertain and fuzzy subjects. In this respect, the analysis model only provides an approximate representation of the structure.

Certain modeling techniques will be discussed and a choice will be made in this section.

4.2.1 SENSITIVITY ANALYSIS

Four models were prepared to investigate the majorities due to application of staged construction analyses and different modeling techniques. Pre-stressed precast I-girder bridge, which will be explained in Section 4.3.1 was considered in sensitivity analyses.

In the first two types, a detailed superstructure representation was adopted. Each I-girder was represented by beam elements. Concrete slab was modeled using shell elements, and connection with I-girders was established by utilizing rigid beam elements between. Each element passed through the location of its centroid.

Three construction sequences were taken into account in the first model. After erection of columns and placement of cap beams with bearings, I-girders have been added to the system. Finally, slab was formed. Construction stages are visualized on Figure 4.7.

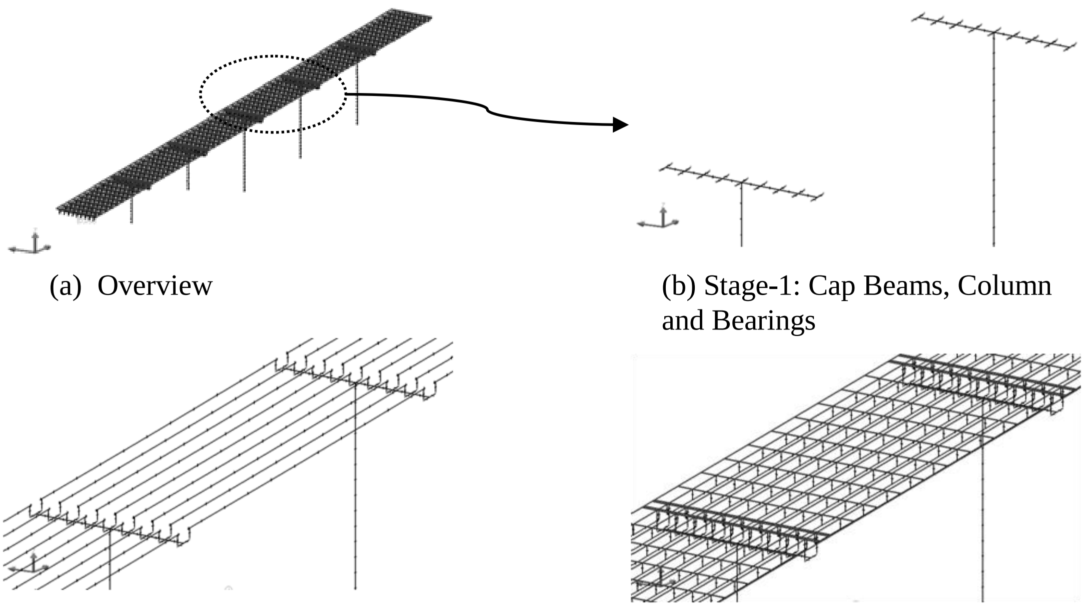

(a) Overview

(b) Stage-1: Cap Beams, Column and Bearings

(c) Stage 2: Precast I-Girders

(d) Stage 3: Slab

Figure 4.7: Overview of detailed models

Second model exhibited same geometry, but a linear static analysis was carried out (i.e. at an instant of time for whole system) omitting construction stages, as typically done for design of standard highway bridges.

In the last two types, superstructure was simulated using a single beam element. Composite material and geometric properties were taken into account by means of an equivalent section. The beam element has been passed through the centroid of composite superstructure. Overview of these models is shown in Figure 4.8.

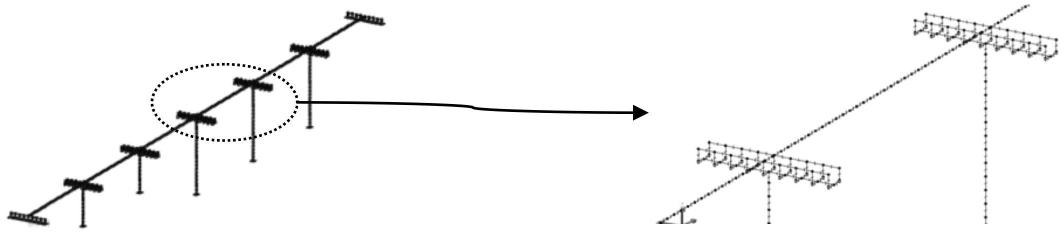

Figure 4.8: Overview of simple models

The difference between these last two lies in the representation of cap beam. Third model included cap beams with actual stiffness. This led to significant errors in bearing forces and cap beam moments under dead loads, as explained in following paragraphs. Thus a fourth model was prepared, using artificially high stiffness values for cap beam, yielding quite accurate results. Summary of these models are tabulated in Table 4.1.

Table 4.1: Models used in sensitivity analyses

ID	Description
S1	Detailed Model, Staged Construction Analyses
S2	Detailed Model
S3	Simple Model, Actual Cap Beam Stiffness
S4	Simple Model, Rigid Cap Beam Stiffness

Comparison of bearing axial forces is presented on Figure 4.9.

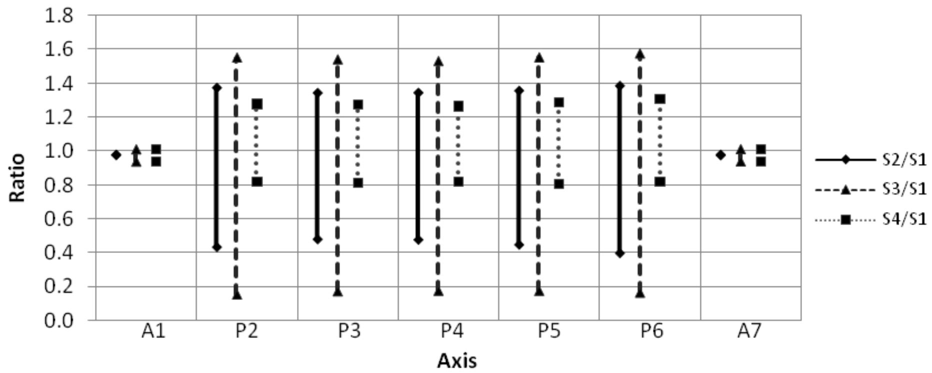

Figure 4.9: Comparison of bearing axial forces under dead loads

Results indicated that, models S2 and S3 yielded inaccurate bearing forces under dead loads, taking those of S1 as reference. Ratios of axial forces obtained from S2 to those of S1 changed from 0.4 to 1.4. Edge bearings experienced significantly lower axial forces (40%), while interior bearings at the middle exhibited high values (140%). Same trend was observed for model S3, with increased error range (20%-160%). Total value at a pier remained constant for all of the models. Here, results of S1 were used as reference because; nearly same values were observed at each bearing in this model. This is a close estimation of actual situation, as all bearings at a pier will exhibit more or less same axial force due to the construction sequence in reality.

Since I-girders are placed separately on bearings in actual situation, each bearing will carry approximately half weight of those at the end of that stage. Slight differences may originate later due to utilization of slab. In this respect, models S2 and S3 did not stand for a good representation of real case. Large error margin included in the results of S2 showed that also; if staged construction analysis is not performed, detailed idealization of superstructure will still not be adequate to obtain accurate bearing forces under dead loads.

Use of rigid cap beams in the last model equalized all bearing forces at a pier, thus yielding more accurate cap beam moments as well. Comparison of those moments is presented on Figure 4.10 with reference to the results of S1.

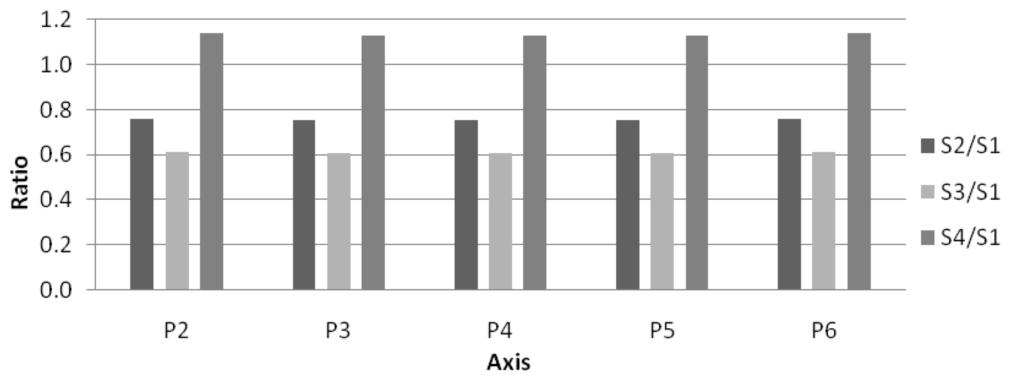

Figure 4.10: Comparison of cap beam moments

Results pointed out that the least error, which was approximately 15% in average, has been observed in the results of model S4.

Periods of fundamental modes are tabulated for each model in Table 4.2. Conformity of results showed that representation of whole superstructure by means of single beam element will not likely introduce a significant error in the overall response under applied seismic loading.

Table 4.2: Fundamental modes of models

ID	**X**	**Y**	**Z**
S1	1.400	0.931	0.325
S2	1.400	0.931	0.325
S3	1.397	0.843	0.319
S4	1.394	0.842	0.316

4.2.2 MODEL TYPE SELECTION

A great number of time-history analyses were carried out through this study. Time and memory requirement of such analyses can be extraordinary when using detailed models. Additionally, this thesis work is indented to contribute to the practical calculations and analyses methods used in design of standard highway bridges. In this sense, use of a simple but effective model that would be usually preferred in design of standard highway bridges meets the case better.

Thus model type of S4 was selected, in which a single beam element is used to represent whole superstructure and rigid members are utilized for cap beams. Bearing layout is to be preserved, in other words not to be simplified. Columns were fixed in rotational degree of freedoms at the bottom, recalling that, soil type was selected as rock and/or stiff soils, to eliminate soil-structure interaction. Finite elements of maximum 1 m lengths were used to increase calculation accuracy.

4.2.3 SIMULATION OF NONLINEAR FEATURES

Three set of analyses were performed to account for nonlinearities in bearings.

1) To observe occurrence of uplift, springs having only compression stiffness were used to simulate bearing elements. Small values were assigned for tensile direction as well to avoid possible convergence problems. Case ID 8 (Table 3.3) is used for these.

2) To verify hold-down device forces, tensile stiffness of these elements were made equal to those of devices and additional set of nonlinear time-history analyses, having ID 9, (Table 3.3) were performed.

3) Last group of analyses, called *lower bound solution* in this study, were performed to investigate the stability condition during occurrence of uplift in the bearings. As the name implies, the most unfavorable condition of bearings, in which they completely lose their shear capacity due to uplift, was considered in these analyses. This is established by eliminating translational stiffness of bearings that were subjected to uplift in nonlinear analyses case 8. NLTH and RSP analyses were included in this group. Cases are donated by NLTH 10, RSP 11, 12 and 13 (Table 3.3).

4.3 INVESTIGATED BRIDGES

One of the key ideas was to investigate the uplift behavior that in bridges of different types and bearing layouts. Four different bridge systems have been analyzed. A brief summary of these are presented in Table 4.3 with labels as well.

Table 4.3: Summary of investigated bridges

ID	**Superstructure Type**	**Span Length (m)**	**Continuity**
Bridge 1	Pre-stressed Precast I-Girders	30	Slab
Bridge 2	Steel I-Girders + Concrete Deck	60	Superstructure
Bridge 3	Post-tensioned Box Section	60	Superstructure
Bridge 4	Steel Box Section + Concrete Deck	60	Superstructure

These bridge types have frequent applications in highway projects. Especially Bridge 1 is the most used type as a standard highway bridge in Turkey. Total span length of bridges was selected to be 180 m for all cases. Superstructures included two lanes, resulting in 12.5 m width. The natural topography they passed through is shown in Figure 4.11.

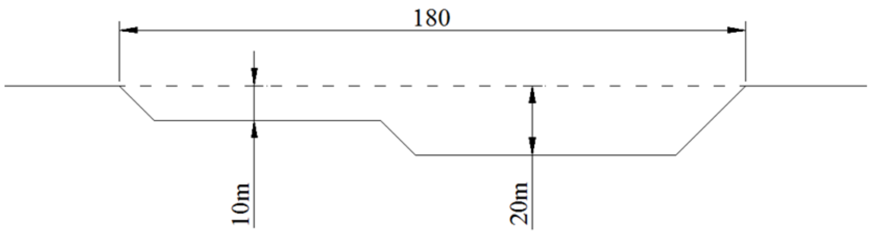

Figure 4.11: Natural topography

The chosen profile made it possible to observe responses at piers of different heights.

Elastomeric bearings that are 80mm in height (4mm external rubber layers at top and bottom, with seven internal plates of 2mm thick steel) were used in all bridges, as typically done in Turkey. Axial and transverse stiffness of those was calculated according to the suggestions of AASHTO [2] as;

$K_A = A.E/t$ (Axial stiffness)

$K_S = A.G/t$ (Transverse stiffness)

where;

$E = 6.G.S^2$ (Elasticity modulus of in axial direction)

$G = 1000\ kPa$ (Shear modulus of rubber)

$S = L.W/(2.h_{ri}.(L+W))$ (Shape factor)

$h_{ri} = 8\ mm$ (Thickness of an internal rubber layer)

$t = 64\ mm$ (Total Thickness of all rubber layers)

and L and W are plan dimensions of the bearings, which are case specific.

In addition to the self weight of superstructure, additional loads were also applied to account for a reasonable portion of vehicle load as suggested in [3], and additional weights due asphalt, curbs, railings, etc. A total load of 61.5 kN/m was assumed for all bridges, considering typical design values used in Turkey.

$F_A = Asphalt + Railings + Curbs + Reduced\ Live\ Load$

$F_A = 25 + 1.5 + 20 + 15 = 61.5$ kN/m

Superstructure properties are tabulated in Table 4.4 for selected case studies. Properties of composite sections were calculated by taking concrete as the reference material.

Table 4.4: Summary of superstructure properties of investigated bridges

ID	**Weight (kN/m)**	**A (m^2)**	**I_Y (m^4)**	**I_Z (m^4)**	**J (m^4)**
Bridge 1	259.7	7.9	1.8	95.1	5.9
Bridge 2	196.5	7.1	3.2	94.2	3.2e-3
Bridge 3	251.0	7.1-16.9	7.1-11.6	70.3-99.6	15.5-27.9
Bridge 4	162.0	5.5	5.3	66.7	1.4e-1

Gross moments of inertias were assigned to superstructures. Those of piers and link slab of were multiplied by some rational factors, 0.4 and 0.3 respectively, to simulate bending stiffness of cracked sections as done in most preliminary and/or final design.

4.3.1 BRIDGE 1: PRE-STRESSED PRECAST I-GIRDER

In Turkey, superstructures composed of pre-stressed precast I-girders undoubtedly constitute the majority of highway bridges. This type is preferred due to ease of construction in most cases.

A section that has frequent use was selected for this case study. Superstructure consists of 9 adjacent I-girders with heights of 120 cm, underlying 25 cm thick concrete slab to span 30 m between pier axes. Dimensions and section properties are shown in Figure 4.12.

1 elastomeric bearing exists under each girder; with plan dimensions of 250x250 mm and height of 80 mm. Shear blocks were placed between precast girders to prevent transverse movement superstructure. Translational stiffness values of bearings were calculated according to [2] as;

Axial stiffness = 357638 kN/m

Longitudinal stiffness = 977 kN/m

Transverse stiffness = very rigid (To account for shear blocks)

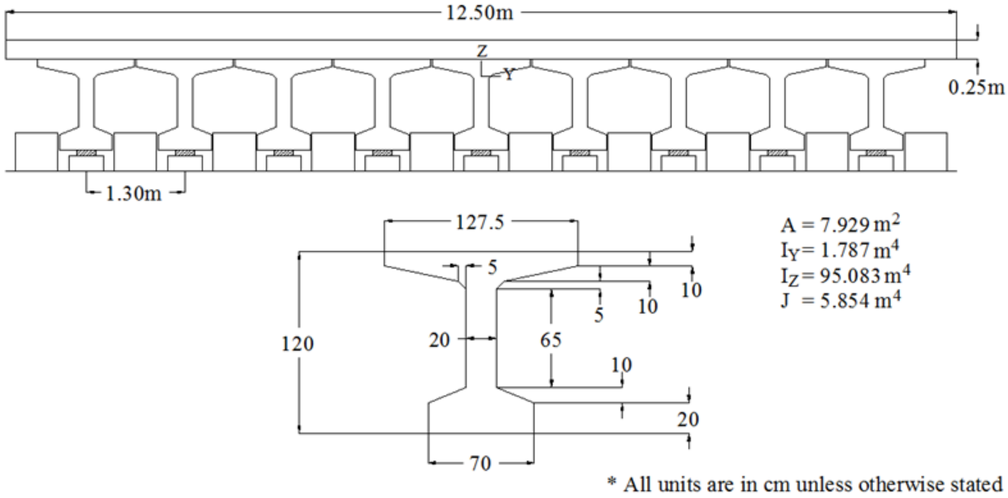

Figure 4.12: Dimensions and section properties of superstructure (Bridge 1)

Inverted-T section and box tube with two cells were used for cap beams and piers respectively. Dimensions and section properties are shown in Figure 4.13.

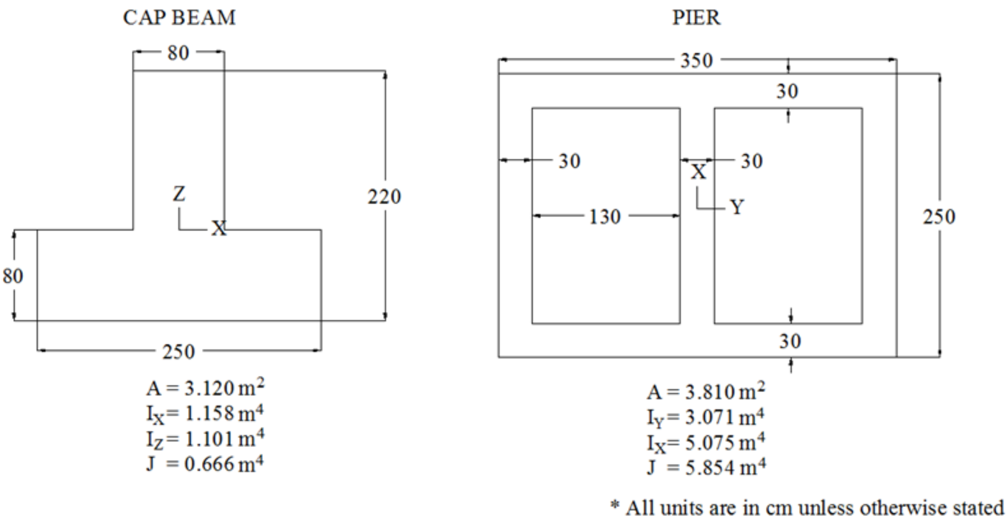

Figure 4.13: Dimensions and section properties of cap beams and piers (Bridge 1)

Idealized analysis model is shown in Figure 4.14.

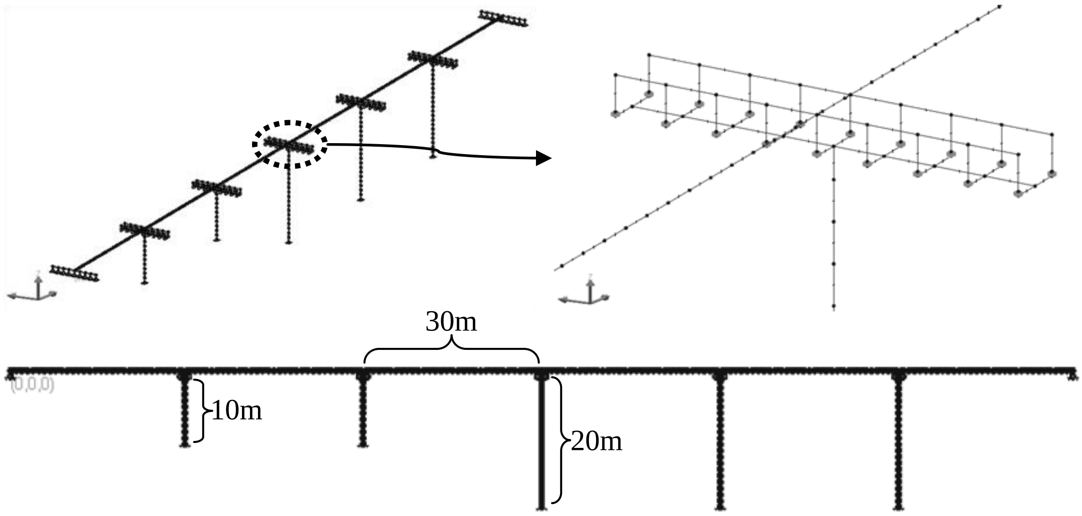

Figure 4.14: Analysis model (Bridge 1)

Modal Analysis

Natural periods of vibration and mass participation factors of first 100 modes are given in APPENDIX A as well as with the shapes of fundamental modes.

Following period intervals accumulated over 90% of modal mass in each orthogonal direction:

X direction : T= 1.635-0.375 s (91.3%)
Y direction : T= 0.956-0.093 s (90.0%)
Z direction : T= 0.389-0.034 s (90.1%)

It was not possible to supply damping ratios close to 5% in the period interval between 0.034 s and 1.635 s, due to nature of Rayleigh damping matrix. Thus as a rational approach, damping coefficients were selected to make average damping ratio equal to 5% between the periods of fundamentals modes governing vibrations in X and Z directions (1.635 s and 0.384 s respectively). Coefficients a = 0.3530 and b = 4.757e-3, which set this ratio to 5% at periods 0.38 s and 1.40 s, were deemed as suitable for this purpose. Plot of damping ratio versus period for these selected values is given on Figure 4.15. Periods of fundamental vibration modes for each orthogonal direction are plotted on the same chart. Verification of these values will be carried out later in this section by means of LTH analyses.

Using related provisions of [1], which are also summarized in Section 3.1, ensemble horizontal SRSS spectrum was scaled so that acceleration values did not fall below 1.3 times the design spectrum in the interval between periods T_1 to T_2 that are 0.5 times of fundamental period of vibration in transverse direction and 1.5 times of the one in longitudinal directions respectively.

T_1 = 0.5*0.956 = 0.478 s

T_2 = 1.5*1.635 = 2.452 s

Minimum ratio of acceleration values of ensemble spectrum to those of design spectrum was found to be 1.368 and 1.350 for modified and synthetic set of records. These led to scale factors of 0.951 and 0.963, which are to be applied to the orthogonal horizontal components of those two sets respectively.

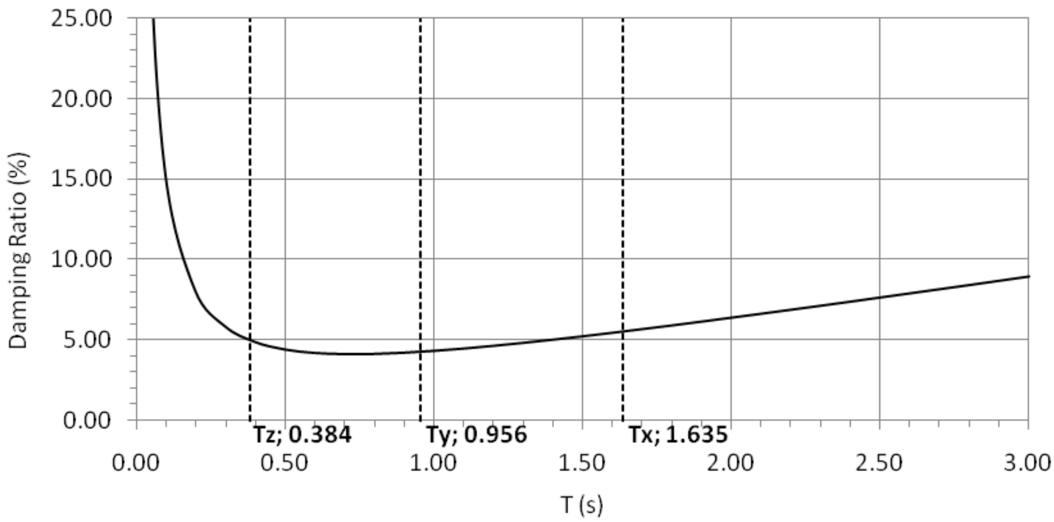

Figure 4.15: Damping ratio vs. period (Bridge 1)

Bearing Axial Forces and Hold-down Device Design

Forces calculated from response spectrum analysis cases in orthogonal directions were summed through the load combinations. Results are tabulated in Table 4.5.

Table 4.5: Bearing axial forces from RSP cases and load combinations (Bridge 1)

Axis	ID	D	1	2	3	C1	C2	C3	C4	C5
A1	1	419	33	130	212	72	140	135	204	261
	2	419	33	98	212	62	108	126	171	251
	3	419	33	65	212	52	75	116	138	241
	4	419	33	33	212	42	42	106	106	231
	5	419	33	0	212	33	10	96	73	221
P2	10	441	520	151	220	565	307	631	373	421
	11	441	520	113	220	554	269	620	335	410
	12	441	520	76	220	543	232	608	297	398
	13	441	520	38	220	531	194	597	260	387
	14	441	520	0	220	520	156	586	222	376
	19	434	531	306	222	623	466	690	532	473
	20	434	531	230	222	600	389	667	456	450
	21	434	531	153	222	577	312	644	379	427
	22	434	531	77	222	554	236	621	303	404
	23	434	531	0	222	531	159	598	226	381
P3	28	434	547	132	221	586	296	653	362	425
	29	434	547	99	221	576	263	643	329	415
	30	434	547	66	221	567	230	633	296	405
	31	434	547	33	221	557	197	623	263	395
	32	434	547	0	221	547	164	613	230	385
	37	437	558	411	220	682	578	748	644	511
	38	437	558	308	220	651	475	717	541	480
	39	437	558	205	220	620	373	686	439	449
	40	437	558	103	220	589	270	655	336	418
	41	437	558	0	220	558	168	624	234	388
P4	46	434	870	64	217	889	325	954	390	497
	47	434	870	48	217	884	309	949	374	492
	48	434	870	32	217	879	293	945	358	488
	49	434	870	16	217	875	277	940	342	483
	50	434	870	0	217	870	261	935	326	478
	55	437	873	126	232	911	388	980	457	531
	56	437	873	95	232	902	356	971	426	522
	57	437	873	63	232	892	325	962	394	512
	58	437	873	32	232	883	294	952	363	503
	59	437	873	0	232	873	262	943	332	494
P5	64	435	880	95	227	909	359	977	427	519
	65	435	880	71	227	901	335	969	403	512
	66	435	880	48	227	894	312	962	380	505
	67	435	880	24	227	887	288	955	356	498
	68	435	880	0	227	880	264	948	332	491
	73	435	880	62	227	898	326	967	394	510
	74	435	880	46	227	894	310	962	379	505
	75	435	880	31	227	889	295	957	363	500
	76	435	880	15	227	885	279	953	348	496
	77	435	880	0	227	880	264	948	332	491
P6	82	436	864	241	224	937	500	1004	567	555
	83	436	864	181	224	918	440	986	507	537

Table 4.5 (continued)

Axis	ID	D	1	2	3	C1	C2	C3	C4	C5
P6	84	436	864	121	224	900	380	968	447	519
	85	436	864	60	224	882	320	949	387	501
	86	436	864	0	224	864	259	931	326	483
	91	440	846	219	224	912	473	979	540	543
	92	440	846	164	224	895	418	962	485	527
	93	440	846	109	224	879	363	946	430	510
	94	440	846	55	224	863	309	930	376	494
	95	440	846	0	224	846	254	913	321	478
A7	100	419	56	281	212	141	298	205	362	314
	101	419	56	211	212	120	228	184	292	293
	102	419	56	141	212	99	158	162	221	272
	103	419	56	70	212	78	87	141	151	250
	104	419	56	0	212	57	17	120	81	229

C1 and C2 load combinations were used to check the requirement of hold-down device design, as well as to calculate the design force at each bearing, in conformity with the suggestions of AASHTO. Design forces are supplied in Table 4.6, where cells containing a hyphen indicate that hold-down device is not needed for that bearing.

Table 4.6: Hold-down device design forces per AASHTO (Bridge 1)

Axis	ID	C1	C2	Max	
A1	1	-	-	-	***Max = 0***
	2	-	-	-	
	3	-	-	-	
	4	-	-	-	
	5	-	-	-	
P2	10	149	44	***149***	***Max = 227***
	11	135	44	***135***	
	12	122	44	***122***	
	13	108	-	***108***	
	14	94	-	***94***	
	19	227	47	***227***	
	20	199	43	***199***	
	21	172	43	***172***	
	22	144	43	***144***	
	23	117	-	***117***	
P3	28	183	43	***183***	***Max = 294***
	29	171	43	***171***	
	30	159	43	***159***	
	31	147	-	***147***	

Table 4.6 (continued)

Axis	Bearing Id	C1	C2	Max	
P3	32	135	-	***135***	***Max = 294***
	37	294	169	***294***	
	38	257	48	***257***	
	39	220	44	***220***	
	40	183	44	***183***	
	41	146	-	***146***	
P4	46	546	43	***546***	***Max = 569***
	47	540	43	***540***	
	48	535	43	***535***	
	49	529	43	***529***	
	50	523	43	***523***	
	55	569	44	***569***	
	56	558	44	***558***	
	57	546	44	***546***	
	58	535	44	***535***	
	59	524	44	***524***	
P5	64	568	44	***568***	***Max = 568***
	65	559	44	***559***	
	66	551	44	***551***	
	67	542	44	***542***	
	68	534	44	***534***	
	73	556	44	***556***	
	74	550	44	***550***	
	75	545	44	***545***	
	76	539	44	***539***	
	77	533	44	***533***	
P6	82	601	78	***601***	***Max = 601***
	83	579	44	***579***	
	84	558	44	***558***	
	85	536	44	***536***	
	86	514	44	***514***	
	91	567	47	***567***	
	92	547	44	***547***	
	93	527	44	***527***	
	94	508	44	***508***	
	95	488	44	***488***	
A7	100	-	42	***42***	***Max = 42***
	101	-	42	***42***	
	102	-	-	-	
	103	-	-	-	
	104	-	-	-	

Results pointed out hold-down device requirements necessitated for almost all bearings except those at A1 axis, using AASHTO combinations.

A simple design of hold-down device will be made by connecting slab to cap beam via steel cables located in front of each bearing. Maximum design force at an abutment or pier axis is to be used for all devices placed along that one.

It may be noted that many applicable device alternatives are possible; but this is out of the scope of this study. The parameter that is to be considered in nonlinear analyses is stiffness of the device. Connection details will not be considered in this sense. A schematic drawing of two types of hold-down devices are shown in Figure 4.16, one for a superstructure composed of adjacent girders, which is the current case and the other for a deck type with spaced girders including transverse beams.

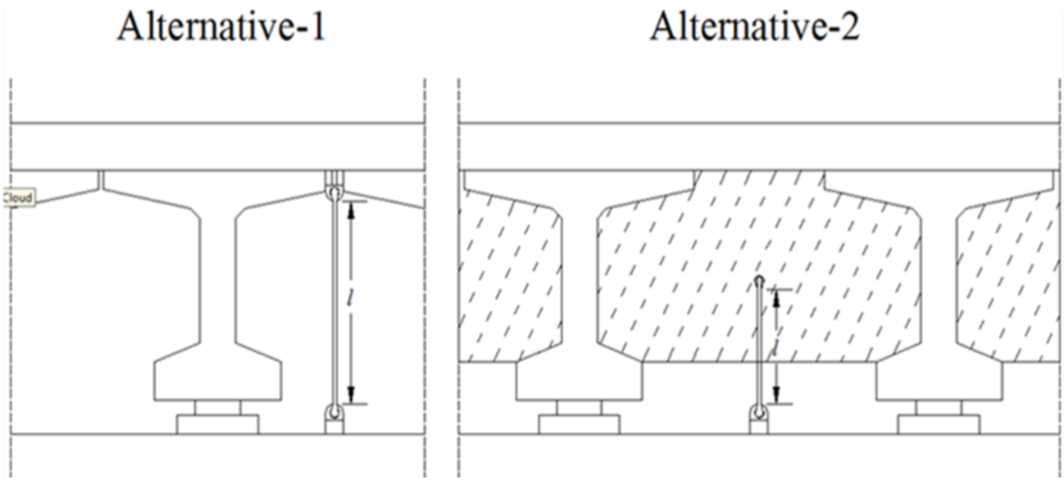

Figure 4.16: Schematic drawing of hold-down device alternatives (Bridge 1)

A rational value for tensile stiffness of a hold down device can be calculated by simplifying the device to a steel rod, ignoring the connecting parts such as clingers, etc…

$$K_{HD} = E.A/l \tag{4.1}$$

The required steel bar area is to be calculated from forces presented on Table 4.6.

$$A = P/\sigma_a \tag{4.2}$$

Combining these two equations gives;

$$K_{HD} = (E.P)/(l.\sigma_a) \tag{4.3}$$

St42 grade steel was preferred, although high strength steel is also used in practice. $E = 200000\ Mpa$ and $\sigma_a = 0.6.\sigma_y = 252$ Mpa were substituted into Equation (4-3) to achieve a conservative design. Clear cable length, l was set equal to 1.2 m, which is the height of I-girder. It should not be forgotten that this value would change according to the detailing, but not result in a significant change of stiffness. Calculated stiffness values are given in Table 4.7. The primary issue is that; in order to represent hold-down devices by means of these tensile stiffness values which are to be assigned to bearings, it is mandatory to place hold-down devices close to bearings, as described above. Otherwise, actual geometry will not be represented with the analysis model, leading to incorrect interpretation of device forces.

Table 4.7: Hold-down device stiffness per bearing at each axis (Bridge 1)

Axis	**Design Force/bearing**	**Calculated Area**	**Stiffness/bearing**
A1	-	-	-
P2	227	900.79	150132
P3	294	1166.67	194444
P4	569	2257.94	376322
P5	568	2253.97	375661
P6	601	2384.92	397486
A7	42	166.67	27778

Bearing axial forces obtained from one-directional linear time-history analysis cases 4, 5 and 6 are shown in Table 4.8. These results were compared with the ones obtained from response spectrum analyses to verify Rayleigh damping coefficients, as well as modified strong ground motion records.

Table 4.8: Bearing axial forces from one-directional LTH analyses (Bridge 1)

Axis	**ID**	**4**	**5**	**6**
	1	31	153	220
	2	31	115	220
A1	3	31	76	220
	4	31	38	220
	5	31	0	220

Table 4.8 (continued)

Axis	ID	4	5	6
P2	10	519	159	228
	11	519	119	228
	12	519	79	228
	13	519	40	228
	14	519	0	228
	19	528	323	227
	20	528	242	227
	21	528	161	227
	22	528	81	227
	23	528	0	227
P3	28	543	146	227
	29	543	109	227
	30	543	73	227
	31	543	36	227
	32	543	0	227
	37	561	434	229
	38	561	326	229
	39	561	217	229
	40	561	109	229
	41	561	0	229
P4	46	841	76	225
	47	841	57	225
	48	841	38	225
	49	841	19	225
	50	841	0	225
	55	851	144	235
	56	851	108	235
	57	851	72	235
	58	851	36	235
	59	851	0	235
P5	64	856	100	230
	65	856	75	230
	66	856	50	230
	67	856	25	230
	68	856	0	230
	73	856	64	232
	74	856	48	232
	75	856	32	232
	76	856	16	232
	77	856	0	232
P6	82	843	255	230
	83	843	191	230
	84	843	128	230
	85	843	64	230
	86	843	0	230
	91	818	235	232
	92	818	177	232

Table 4.8 (continued)

Axis	ID	4	5	6
P6	93	818	118	232
	94	818	59	232
	95	818	0	232
A7	100	53	327	222
	101	53	245	222
	102	53	163	222
	103	53	82	222
	104	53	0	222

To visualize the difference, average ratio of bearing axial forces obtained from LTH analyses over those of RSP cases at each axis are given for orthogonal directions.

The ratios were obtained as;

- 0.98 in average for longitudinal (X) direction.
- 1.10 in average for transverse (Y) direction.
- 1.03 in average for vertical (Z) direction.

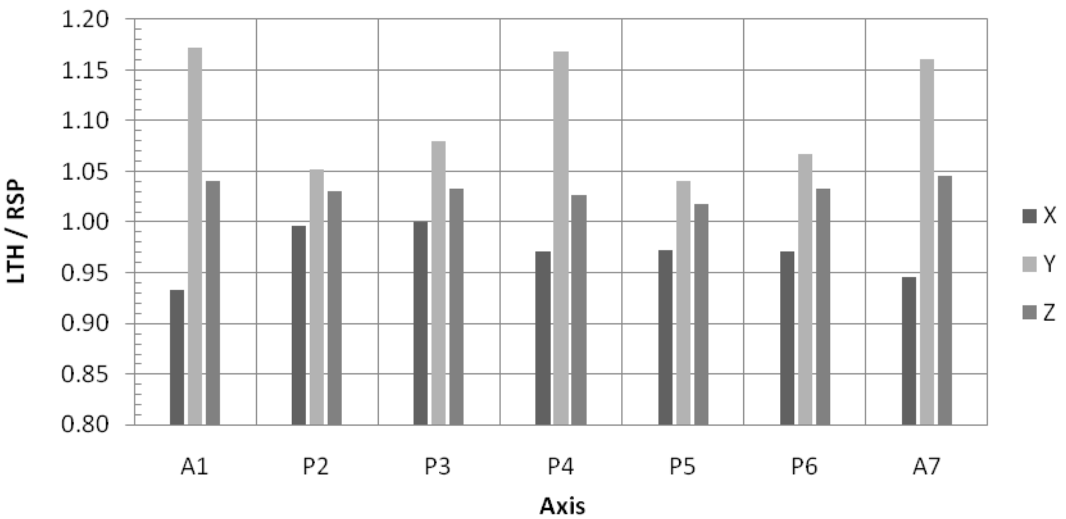

Figure 4.17: Comparison of bearing axial forces (Bridge 1)

Results pointed to the fair compatibility of time-history and response spectrum analyses. Differences were reasonable, being averagely 9.6% in Y direction as maximum, verifying conformity of selected Rayleigh damping coefficients and generated accelerograms.

Moving on with the further analyses, bearing axial forces obtained from multi-directional linear and nonlinear time-history cases 7, 8 and 9 are tabulated in Table 4.9.

Table 4.9: Bearing axial forces from time-history analyses (Bridge 1)

Axis	**ID**	**7**		**8**		**9**	
		T.	**C.**	**T.**	**C.**	**T.**	**C.**
A1	1	-	700	-	698	-	700
	2	-	682	-	681	-	682
	3	-	665	-	663	-	665
	4	-	649	-	648	-	649
	5	-	635	-	634	-	635
P2	10	-162	1081	YES	1163	-125	1094
	11	-150	1066	YES	1143	-113	1081
	12	-138	1052	YES	1127	-102	1069
	13	-125	1038	YES	1113	-91	1056
	14	-113	1024	YES	1098	-80	1043
	19	-301	1091	YES	1172	-235	1113
	20	-256	1057	YES	1134	-207	1076
	21	-224	1024	YES	1101	-179	1044
	22	-193	993	YES	1076	-151	1015
	23	-162	964	YES	1057	-124	989
P3	28	-166	1089	YES	1194	-136	1100
	29	-158	1073	YES	1163	-130	1085
	30	-152	1058	YES	1141	-124	1071
	31	-146	1044	YES	1123	-118	1058
	32	-139	1031	YES	1107	-113	1045
	37	-420	1179	YES	1278	-349	1202
	38	-348	1128	YES	1210	-294	1146
	39	-289	1078	YES	1155	-248	1098
	40	-240	1030	YES	1104	-203	1051
	41	-191	993	YES	1072	-159	1015
P4	46	-381	1264	YES	1407	-387	1261
	47	-377	1259	YES	1396	-383	1256
	48	-372	1254	YES	1385	-378	1251
	49	-368	1249	YES	1373	-374	1247

Table 4.9 (continued)

Axis	ID	7		8		9	
		T.	C.	T.	C.	T.	C.
P4	50	-364	1245	YES	1363	-370	1243
	55	-542	1312	YES	1424	-548	1311
	56	-525	1299	YES	1405	-531	1298
	57	-507	1287	YES	1388	-513	1286
	58	-490	1275	YES	1372	-496	1274
	59	-473	1263	YES	1358	-478	1262
P5	64	-405	1299	YES	1404	-410	1298
	65	-396	1289	YES	1389	-401	1288
	66	-388	1280	YES	1377	-393	1280
	67	-381	1273	YES	1366	-386	1272
	68	-374	1266	YES	1355	-380	1265
	73	-498	1284	YES	1390	-504	1284
	74	-493	1280	YES	1379	-499	1279
	75	-489	1275	YES	1368	-495	1275
	76	-484	1271	YES	1358	-490	1270
	77	-480	1267	YES	1348	-486	1266
P6	82	-458	1363	YES	1496	-469	1360
	83	-432	1330	YES	1458	-443	1327
	84	-409	1299	YES	1419	-419	1297
	85	-388	1275	YES	1385	-398	1274
	86	-367	1256	YES	1359	-378	1254
	91	-551	1326	YES	1452	-564	1324
	92	-523	1304	YES	1426	-535	1302
	93	-494	1282	YES	1400	-506	1280
	94	-466	1261	YES	1375	-478	1259
	95	-438	1241	YES	1355	-450	1239
A7	100	-	782	-	779	-	783
	101	-	731	-	728	-	732
	102	-	692	-	688	-	693
	103	-	664	-	656	-	664
	104	-	644	-	638	-	644

Design forces obtained from load combinations C3, C4 and C5 were included in Table 4.10 for comparisons.

Table 4.10: Hold-down device forces from C3, C4 and C5 (Bridge 1)

Axis	Bearing Id	C3	C4	C5	Max	
A1	1	-	-	-	-	***Max = 0***
	2	-	-	-	-	
	3	-	-	-	-	
	4	-	-	-	-	
	5	-	-	-	-	
P2	10	190	-	-	***190***	***Max = 256***
	11	179	-	-	***179***	
	12	167	-	-	***167***	
	13	156	-	-	***156***	
	14	145	-	-	***145***	
	19	256	98	39	***256***	
	20	233	22	16	***233***	
	21	210	-	-	***210***	
	22	187	-	-	***187***	
	23	164	-	-	***164***	
P3	28	219	-	-	***219***	***Max = 311***
	29	209	-	-	***209***	
	30	199	-	-	***199***	
	31	189	-	-	***189***	
	32	179	-	-	***179***	
	37	311	207	74	***311***	
	38	280	104	43	***280***	
	39	249	2	12	***249***	
	40	218	-	-	***218***	
	41	188	-	-	***188***	
P4	46	520	-	63	***520***	***Max = 544***
	47	515	-	58	***515***	
	48	511	-	54	***511***	
	49	506	-	49	***506***	
	50	501	-	44	***501***	
	55	544	21	95	***544***	
	56	534	-	85	***534***	
	57	525	-	76	***525***	
	58	515	-	66	***515***	
	59	506	-	57	***506***	
P5	64	541	-	84	***541***	***Max = 541***
	65	534	-	77	***534***	
	66	527	-	70	***527***	
	67	520	-	62	***520***	
	68	513	-	55	***513***	
	73	531	-	74	***531***	
	74	527	-	70	***527***	
	75	522	-	65	***522***	
	76	517	-	60	***517***	
	77	513	-	56	***513***	
P6	82	568	132	120	***568***	***Max = 568***
	83	550	72	102	***550***	

Table 4.10 (continued)

Axis	Bearing Id	C3	C4	C5		Max
P6	84	532	11	84	***532***	***Max = 568***
	85	514	-	65	***514***	
	86	496	-	47	***496***	
	91	539	100	104	***539***	
	92	523	45	87	***523***	
	93	506	-	71	***506***	
	94	490	-	54	***490***	
	95	474	-	38	***474***	
A7	100	-	-	-	-	***Max = 0***
	101	-	-	-	-	
	102	-	-	-	-	
	103	-	-	-	-	
	104	-	-	-	-	

Tensile axial forces in bearings (i.e. hold-down device forces), which were obtained from NLTH case 9, were compared with those used in the design of hold-down devices. Results of LTH case 8 and C3, C4, C5 load combinations are included as well on Figure 4.18.

Bearing ID's that required application of a hold-down device matched for all time-history analyses cases and AASHTO load combinations (C1, C2), except those with ID's 100 and 101 at A7 axis. This outcome can be easily verified just by scanning Table 4.6 for bearing ID's having hold-down design forces greater than zero and, Table 4.9 for the ones exposed to tensile axial forces.

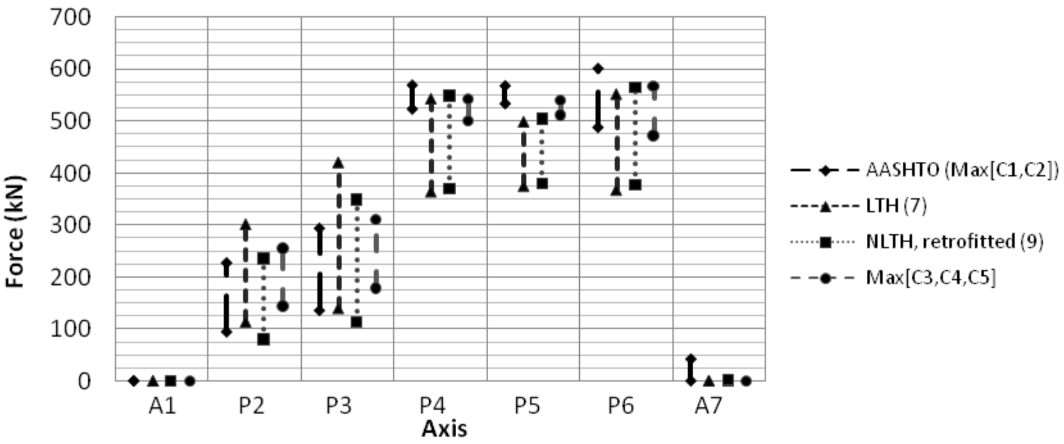

Figure 4.18: Hold-down device forces (Bridge 1)

On the other hand, individual results of NTLH case 9 of modified record 1 indicated these ones also exhibited uplift. But this outcome could not be observed by the remaining, thus was not taken into account in average values shown in Table 4.9.

However, AASHTO hold-down device design forces could not be exactly verified by time-history analyses at all, especially for those on short piers (P2, P3). Figure 4.18 indicates that, AASHTO load combinations (C1 and C2) tended to give smaller design forces up to 15.8% at P3 axis. On the other hand, for hold-down devices at relatively long piers P4, P5 and P6 (20 m), AASHTO approach seemed to produce close results, which were maximum 12.6% greater at pier P5. In average for all bearings, AASHTO predictions were 0.7% greater than the actual NLTH case 9. Load combinations C3, C4 and C5 supplied slightly more accurate values as shown in Figure 4.18, reducing deviations to 10.9% and 7.4% at P3 and P6 axes respectively, but increasing average exceedance to 1%. Linear analyses results supplied 24.3% greater forces at P2 and P3 axes, due to higher tensile stiffness of bearings then those of hold-down devices shown in Table 4.7.

Another interesting phenomenon was that, bearings on long piers experienced much greater uplift forces than the others, especially under longitudinal excitation (X direction). At first glance, this fact may seem absence of sense, as one usually expects that short piers will exhibit greater moments at bottom, which will possibly result in greater top moments and thus bearing forces for such a continuous bridge. But the actual case was completely the opposite, short piers exhibited smaller top moments, thus lesser bearing axial forces under longitudinal excitation. An analytical verification is developed and presented in APPENDIX F, including the effects of transverse excitation as well.

Compressive axial forces in bearings under applied earthquake excitations are plotted for the same analyses cases on Figure 4.19. Comparison of results of NLTH case 8 and 9 indicated that uplift of bearings on one side of the cap beam created minor increase in compression forces of those on the opposing side. The alteration is 5.4 % in average, being maximum 10% at pier P6.

It is hard to develop a quantitative explanation of this outcome, because the nonlinearity of bearings concerned in the problem removes the possibility of superposing individual responses due to each excitation. That is, resultant bearing axial forces cannot be separated into such components that arise due to an individual orthogonal excitation.

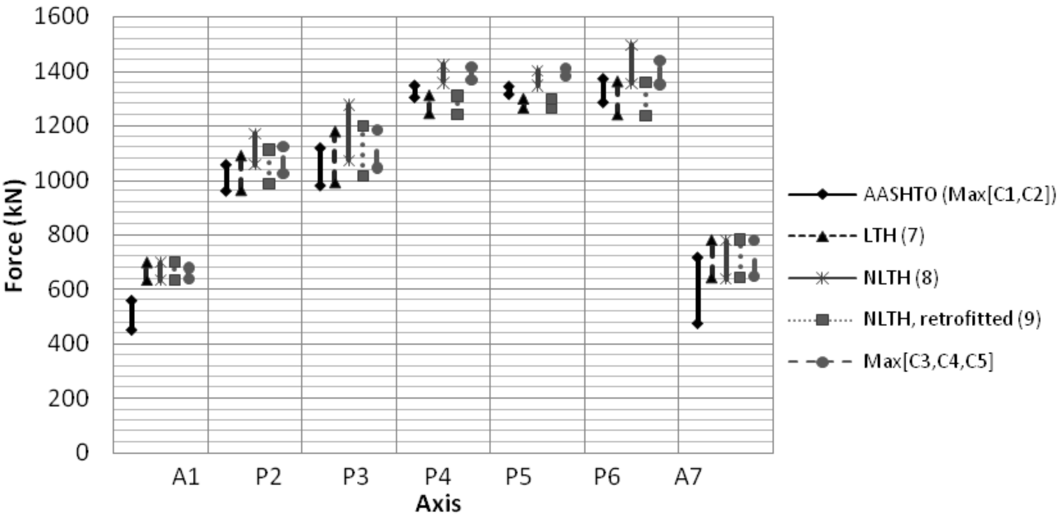

Figure 4.19: Comparison of compressive bearing axial forces (Bridge 1)

Furthermore, it cannot be investigated when contribution from one individual ground motion component is maximum or minimum in terms of bearing axial forces. Only a sensitive judgment shall be made instead; as high number of bearings supplied adequate redundancy on a pier, significant increase of axial force in any bearing due to uplift of others was not observed. Forces obtained from AASHTO load combinations tended to be smaller up to 20.0% at A1 axis, underestimating all values 5.8% in average, taking results of NLTH case 9 as reference. Load combinations C3, C4 and C5 supplied more accurate values, which are 2.8% and 8.8% smaller in average and at P3 axis respectively.

Cap Beam Moments

Maximum moments in cap beams are presented in the following tables.

Table 4.11: Maximum cap beam moments from Dead and RSP analysis (Bridge 1)

Axis	**D**	**1**	**2**	**3**
P2	7421	183	1166	3471
P3	7386	395	2087	3466
P4	7385	431	759	3568
P5	7385	21	608	3638
P6	7420	446	464	3549

Table 4.12: Maximum cap beam moments from RSP load combinations (Bridge 1)

Axis	D+C1	D+C2	D+C3	D+C4	D+C5
P2	7953	8642	8994	9683	11296
P3	8408	9592	9448	10631	11597
P4	8043	8273	9114	9343	11310
P5	7588	7999	8680	9091	11212
P6	7588	7999	8680	9091	11212

Table 4.13: Maximum cap beam moments from time-history analyses (Bridge 1)

Axis	7	8	9
P2	11262	11268	11262
P3	11737	11808	11725
P4	11108	11110	11108
P5	11098	10964	11099
P6	11163	10998	11166

Results are plotted for these analyses cases on Figure 4.20. Outcomes indicated that cap beam moments do not differ significantly between actual and retrofitted cases (NLTH cases 8 and 9 respectively). Unlike the case of compressive axial forces in bearings, here it will be helpful to examine the responses of individual orthogonal ground motions on cap beams.

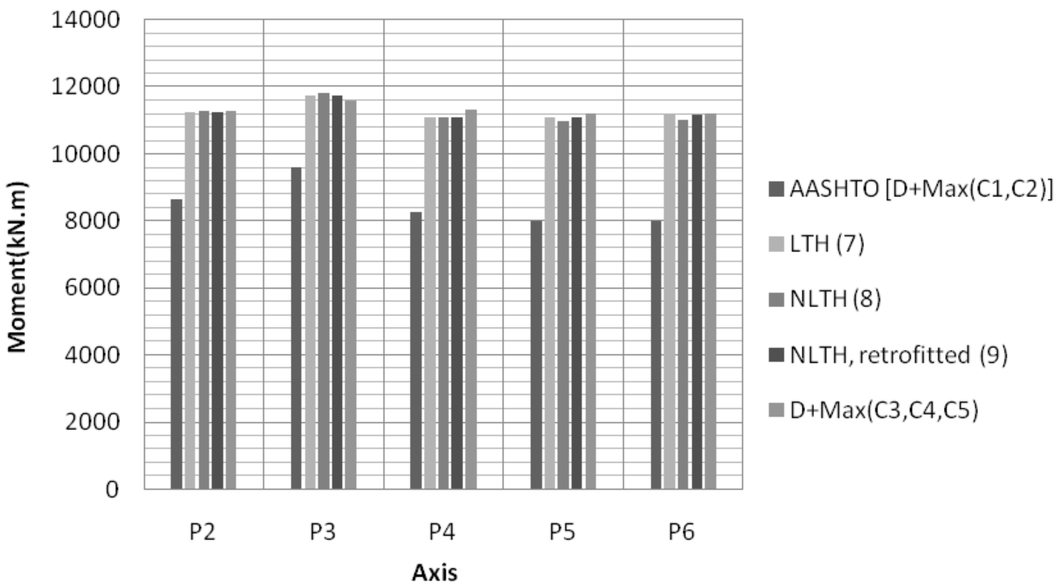

Figure 4.20: Comparison of cap beam moments (Bridge 1)

Uplift movement of bearings during longitudinal excitation does not alter cap beam moments significantly in both cases. When bearings on one side of the beam loose compression, the others on the opposing side gain approximately that much equal. In other words, all bearings that are in compression have to carry same span loads, which do not change at any time instant under longitudinal excitation. Thus total vertical load along cap beam and moments do not change remarkably, which leads to nearly same values at any time instant under longitudinal excitation. Figure 4.21 illustrates this concept.

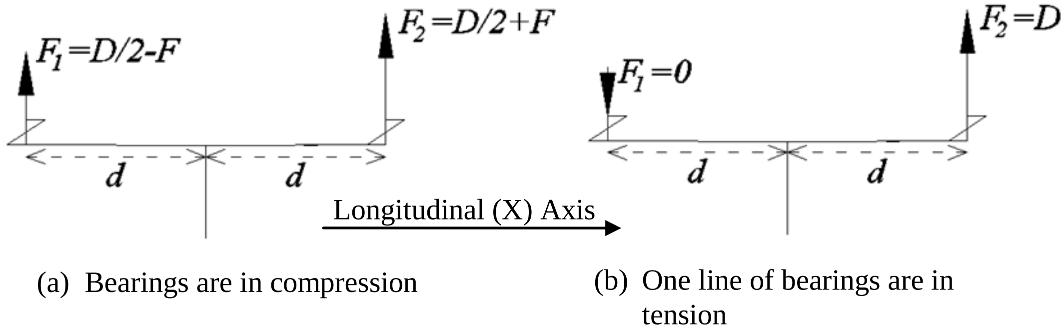

Figure 4.21: Cap beam moments under longitudinal excitation (D denotes dead load carried by a cap beam).

There occurred some major moment increase of 13% in average, being maximum 28.2% at P3 axis due to transverse excitation. Recalling earlier explanations in this section about alteration of bearing forces due to transverse excitation, and also considering the bearing layout back in Figure , one can clearly understand this increase of moments originate due to the increase in bearing axial forces, even uplift does not occur. The most significant alteration originated from vertical excitation. Recalling Table 4.5, it can be seen that the increase in bearing compressive forces was 51.1% of those under dead load, in average. This is the action that caused increase of cap beam moments, which was approximately equal to the same value (48.2%) as can be investigated from Table 4.11, with reference to moments under dead load.

Due to these explanations, AASHTO load combinations (C1 and C2) underestimated cap beam moments 24.7% in average, as they do not take account the effects of vertical excitation. On the other hand, load combinations that consider these effects as well (C3, C4 and C5) provided quite accurate results, which are only 0.5% higher in average.

Pier Forces

Maximum pier moments about longitudinal (X) and transverse (Y) directions of bridge are presented on the following tables for all analysis cases.

Table 4.14: Maximum pier moments about transverse direction (Bridge 1)

Axis	D+[Max(C1,C2)]	7	8	9	D+[Max(C3,C4,C5)]
P2	32218	30749	32468	31027	32326
P3	32011	30503	32488	30656	32107
P4	32996	30887	32027	30891	33143
P5	33098	31019	32162	31015	33154
P6	33012	30898	31903	30894	33133

Table 4.15: Maximum pier moments about longitudinal direction (Bridge 1)

Axis	D+[Max(C1,C2)]	7	8	9	D+[Max(C3,C4,C5)]
P2	41988	43521	43441	42961	41988
P3	92318	93245	93210	92026	92318
P4	43765	43950	43943	43614	43765
P5	46271	47162	47181	46782	46271
P6	29704	31103	31142	30841	29704

Comparison of those results is provided on Figure 4.22 and Figure 4.23.

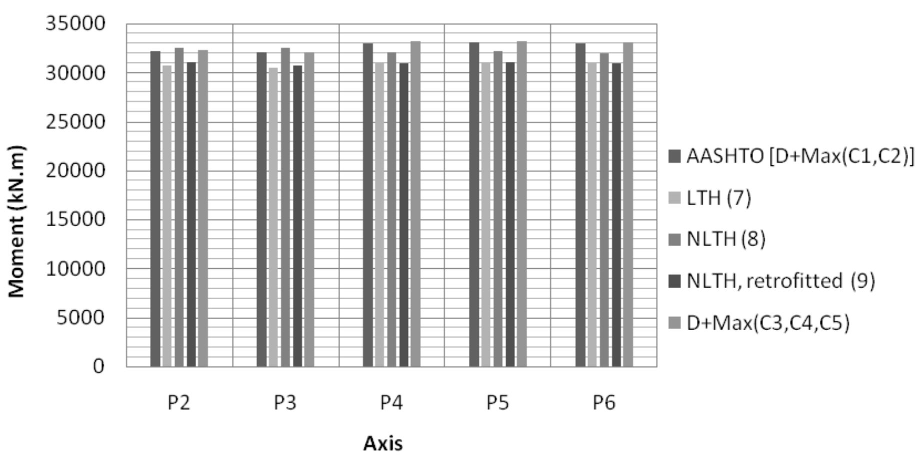

Figure 4.22: Pier moments about transverse (Y) direction (Bridge 1)

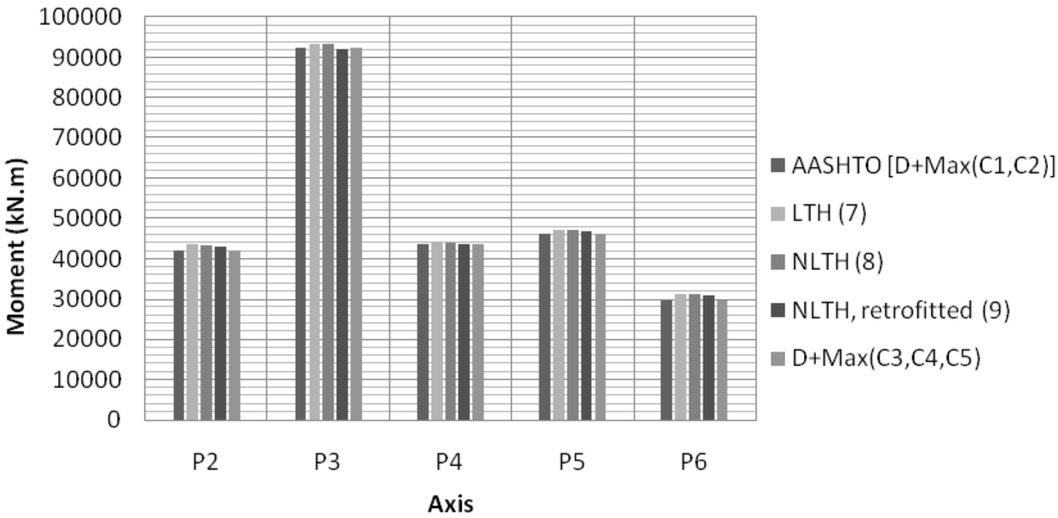

Figure 4.23: Pier moments about longitudinal (X) direction (Bridge 1)

Results pointed out that differences between RSP load combinations and NLTH case 9 are 5.8% in average, for moments under longitudinal excitation (about transverse direction), and 1.3% under transverse excitation (about longitudinal direction) in average. Those values did not change for retrofitted case also. As seen, differences were negligible for all analysis cases. Discussion of this outcome is included in the paragraphs below.

Under horizontal ground motion, no moment coupling occurred in piers. In other words; noticing straight alignment of Bridge 1, directional pier responses resulted due to related excitations only, that is; moments about transverse axis originate from longitudinal excitation only and vice versa. In view of this fact, it is concluded that these variations have originated due to the nature of Rayleigh damping matrix and minor unconformities between pseudo acceleration spectra of scaled accelerograms and design response spectrum.

Larger pier moments of P3 axis is directly related to the fundamental mode shape of the structure in transverse direction, shown in Figure 4.24. One shall remember from Table A.1 that, mass participation factor of this mode was 88.4%, indicating vibration due to transverse excitation will induce approximately same deformation shape on structure. Thus it can be judged that pier P3 will exhibit greatest shear force and thus moment among the others due to this vibration mode, as it is the shortest one. Although pier P2 has the same length, it will not yield that much moment, as movement of superstructure in transverse direction is constrained at the abutment.

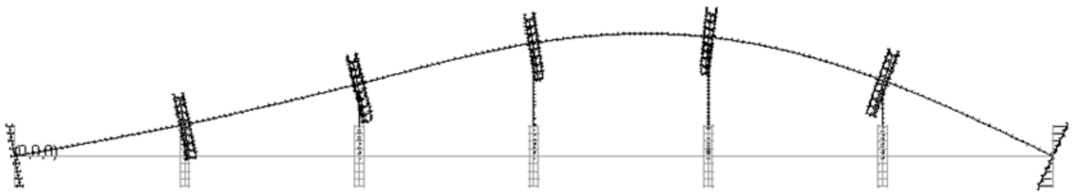

Figure 4.24: Mode shape governing transverse (Y) direction (Bridge 1)

Vertical excitation creates no considerable moments on piers as expected. Thus all load combinations, including those suggested by AASHTO, were deemed to be accurate.

Pier axial forces are tabulated in Table 4.16 and Table 4.17.

Table 4.16: Absolute maximum pier axial forces from Dead and RSP analysis (Bridge 1)

Axis	D	1	2	3
P2	9642	228	0	4056
P3	9602	470	0	4051
P4	10553	518	1	4315
P5	10553	47	0	4441
P6	10594	523	1	4267

Table 4.17: Maximum and minimum pier axial forces from load combinations (Bridge 1)

Direction	Axis	D+C1	D+C2	D+C3	D+C4	D+C5
Minimum	P2	9414	9573	8197	8356	5517
	P3	9132	9461	7916	8246	5410
	P4	10035	10397	8740	9102	6082
	P5	10506	10539	9174	9207	6098
	P6	10070	10436	8790	9155	6169
Maximum	P2	9870	9710	11086	10927	13766
	P3	10073	9743	11288	10959	13794
	P4	11071	10709	12366	12004	15024
	P5	10600	10568	11933	11900	15008
	P6	11117	10752	12397	12032	15018

As explained in Section 3.3, AASHTO Standard Specifications [2] suggest the use a load factor of 0.75, to reduce dead loads when checking maximum pier moments, for bridges of SPC A. Although this case study is of SPC D, reduced tensile forces are still included in comparisons and tabulated in Table 4.18 and Table 4.19.

Table 4.18: Reduced minimum pier axial forces per AASHTO (Bridge 1)

Direction	**Axis**	**0.75D+C1**	**0.75D +C2**
Minimum	P2	7003	7163
	P3	6731	7060
	P4	7396	7758
	P5	7868	7901
	P6	7422	7787

Table 4.19: Maximum and minimum pier axial forces, LTH and NLTH cases (Bridge 1)

Direction	**Axis**	**7**	**8**	**9**
Minimum	P2	5441	5804	5782
	P3	5433	5864	5787
	P4	6193	6656	6568
	P5	6156	6603	6494
	P6	6153	6511	6431
Maximum	P2	13500	13823	13841
	P3	13416	13775	13770
	P4	14541	14937	14912
	P5	14612	14844	14951
	P6	14756	14930	15034

Results are plotted on Figure 4.25 and Figure 4.26.

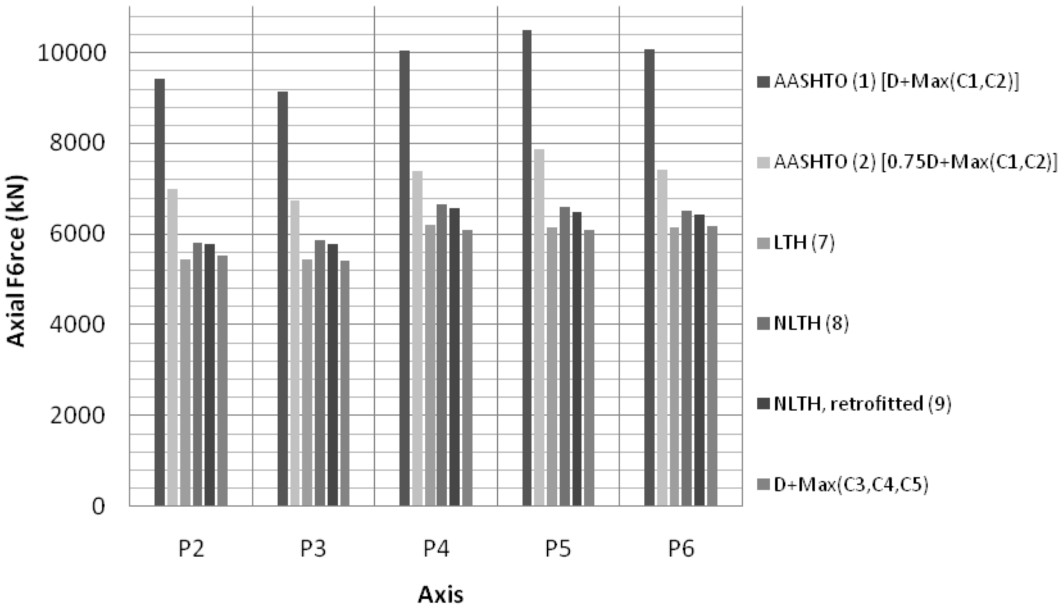

Figure 4.25: Minimum pier axial forces (Bridge 1)

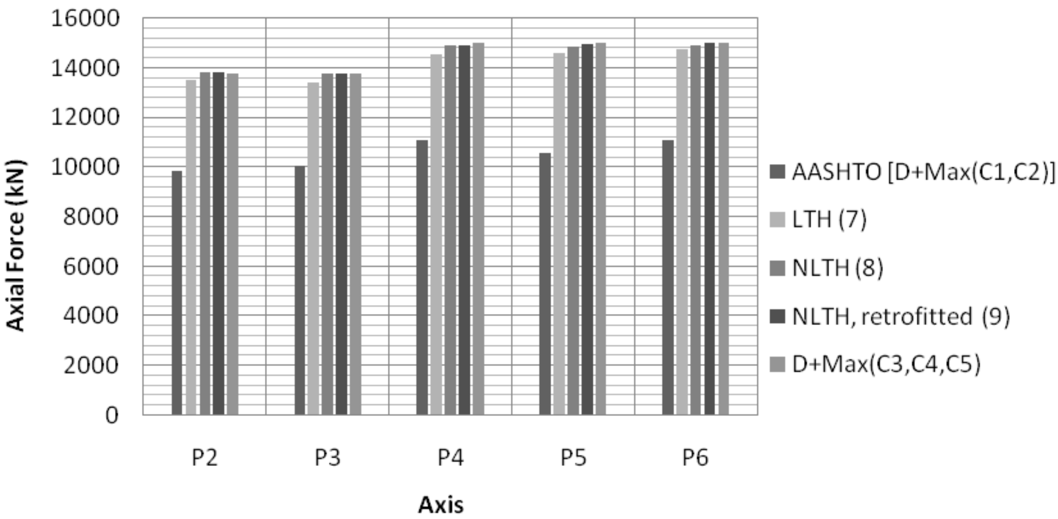

Figure 4.26: Maximum pier axial forces (Bridge 1)

Results pointed out that vertical excitation had a considerable effect on pier axial forces, altering them by 41.5% in average. This value is close to those observed in bearing axial forces and cap beam moments. AASHTO load combinations significantly overestimated (58.3%) and underestimated (27.3%) minimum and maximum axial forces in piers.

Combinations C3, C4 and C5 produced accurate results for both responses (5.7% smaller for maximum axial forces and 0.1% greater for minimums). Reduced AASHTO approach provided minimum axial forces that are greater up to 21.1%, being 17.3% in average.

Lower Bound Analyses

Due to all of these discussions included from the beginning of this section, one important question comes into mind, what are the consequences of sacrificing hold-down devices for this bridge? Lower bound nonlinear time-history and response spectrum analyses, of which assumptions had been described in Section 4.2.3 were performed to seek the answer.

Recalling Equation (3.2), the minimum required support length of this bridge according to AASHTO is;

$$N = (305 + 2.5L + 10H)(1 + 0.000125S^2)$$

Where;

$L = 180\ m$ length of whole superstructure
$H = 16\ m, 10\ m\ and\ 20\ m$ for abutments, short and long piers respectively
$S = 0$ since bright alignment is straight

This leads to three values of 915 mm, 855 mm and 955 mm for abutments, short and long piers respectively. From now on, assuming these requirements are satisfied, relative displacement of superstructure to the bottom face of bearings will be investigated. Only longitudinal displacements are to be examined, as shear blocks prevent transverse displacement of bearings.

Bearings with ID's 1, 10, 28, 46, 64, 82 and 100, which are the side bearings on A1, P2,P3,P4, P5,P6 and A7 axes, were inspected for this purpose. Results are tabulated in Table 4.20 and Table 4.21. Relevant directions for abutments were considered only, that is; positive X direction for A1 and negative for A7 axis where superstructure tends to displace apart from the abutments. For piers, maximum responses in both directions are tabulated, since a symmetric bearing exists on the opposing side of the cap beam (i.e. results will be of same magnitude but in different direction for 10 and 19, etc.).

Table 4.20: Relative superstructure displacements with respect to the bottom of bearings, LTH case 10 (Bridge 1)

ID	10-1	10-2	10-3	10-4	10-5	10-6	Avg.	Max
1	240	262	212	223	192	179	218	262
10	242	256	208	219	187	177	215	256
28	241	257	209	219	187	177	215	257
46	292	254	246	238	214	195	240	292
64	297	248	247	238	218	200	241	297
82	293	256	246	239	218	196	241	293
100	214	207	199	202	169	199	198	214

Table 4.21: Relative superstructure displacements with respect to the bottom of bearings, RSP analyses cases (Bridge 1)

ID	11	12	13
1	610	7	3
10	613	2	3
28	612	2	3
46	615	1	3
64	615	0	3
82	616	1	3
100	610	18	3

Differences between results of LTH and RSP analyses were again due to nature of Rayleigh damping matrix. Selected coefficients provided significantly high damping values, reaching up to approximately 10% at increased fundamental period in longitudinal direction (3.269 sec) in this lower bound case. Thus displacements of LTH cases were much lower (33.8% in average) than those of RSP analyses. As seen from Table 4.21, longitudinal displacements of bearings were governed only by excitation in the same direction, which is sensible. Due to these discussions, results of RSP case 11 were used in evaluation.

Outcomes indicated that average of the values obtained from different excitations was in the limits of provided seat width. Also the maximum ones were observed to be so, thus it may be concluded that stability loss of structure will not occur bearings due to loss of support under I-girders, if minimum support length requirement per AASHTO is provided. However, longitudinal displacements of superstructure relative to the bottom end of the bearings increased up to 2.6 times at abutments and 5.7 times at piers, due to the extended fundamental period of the structure in the same direction. Those for the earlier RSP cases 1, 2 and 3 are tabulated in Table 4.22.

Table 4.22: Relative superstructure displacements with respect to the bottom of bearings, RSP analyses cases (Bridge 1)

ID	1	2	3
1	238	7	3
10	198	2	3
28	199	2	3
46	108	1	4
64	109	0	3
82	108	1	3
100	239	18	3

4.3.2 BRIDGE 2: STEEL I-GIRDERS AND CONCRETE DECK

This type of superstructure is widely used in Europe, however rarely utilized in Turkey.

Superstructure consists of 5 steel I-girders spaced 2.6 m apart from center-to-center. Height of I-girders is 155 cm and thickness of overlying concrete slab is 25 cm. Span length is 60 m between pier axes. Dimensions and section properties are shown in Figure 4.27.

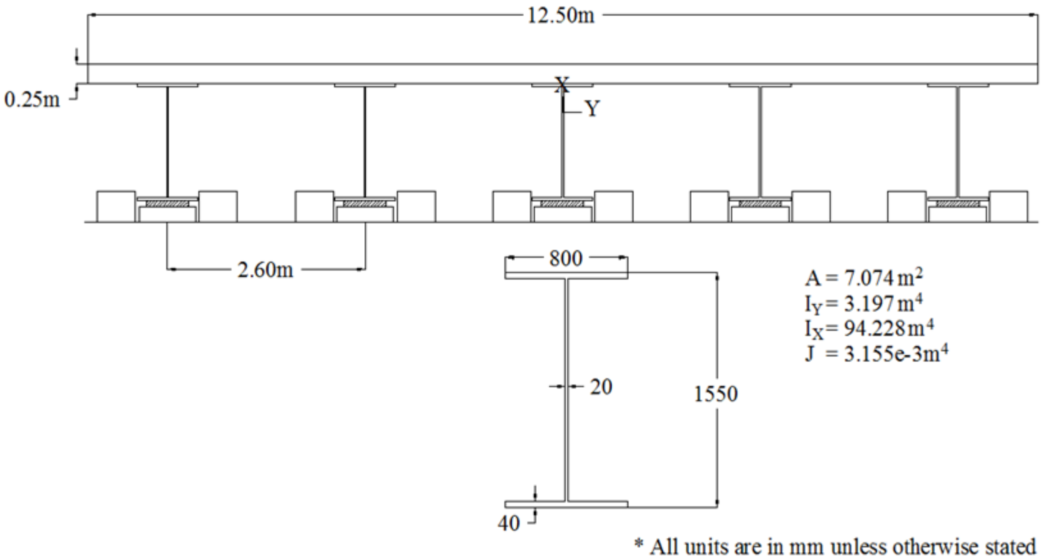

Figure 4.27: Dimensions and section properties of superstructure (Bridge 2)

One elastomeric bearing exists under each girder; with plan dimensions of 550x550 mm at piers and 400x400 mm at abutments, both with height of 80 mm. Shear blocks were placed between precast girders to prevent transverse movement of superstructure. Translational stiffness's of bearings are as follows (for piers and abutments respectively);

Axial stiffness = 8377647, 2343757 kN/m
Longitudinal stiffness = 4727, 2500 kN/m
Transverse stiffness = very rigid (To account for shear blocks)

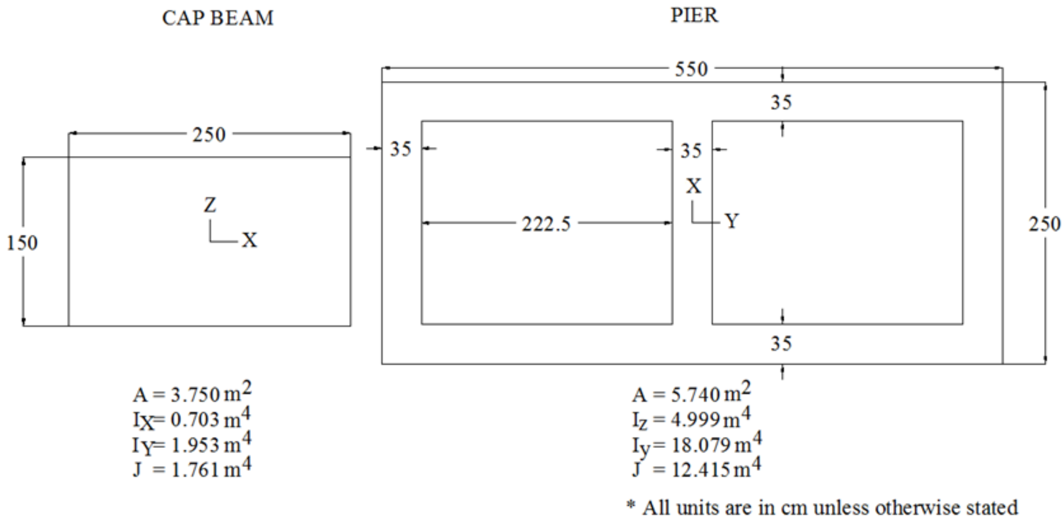

Figure 4.28: Dimensions and section properties of cap beams and piers (Bridge 2)

Rectangular section and box tube with two cells was used for cap beams and piers respectively. Dimensions and section properties are shown in Figure 4.28.

Idealized analysis model is shown in Figure 4.29.

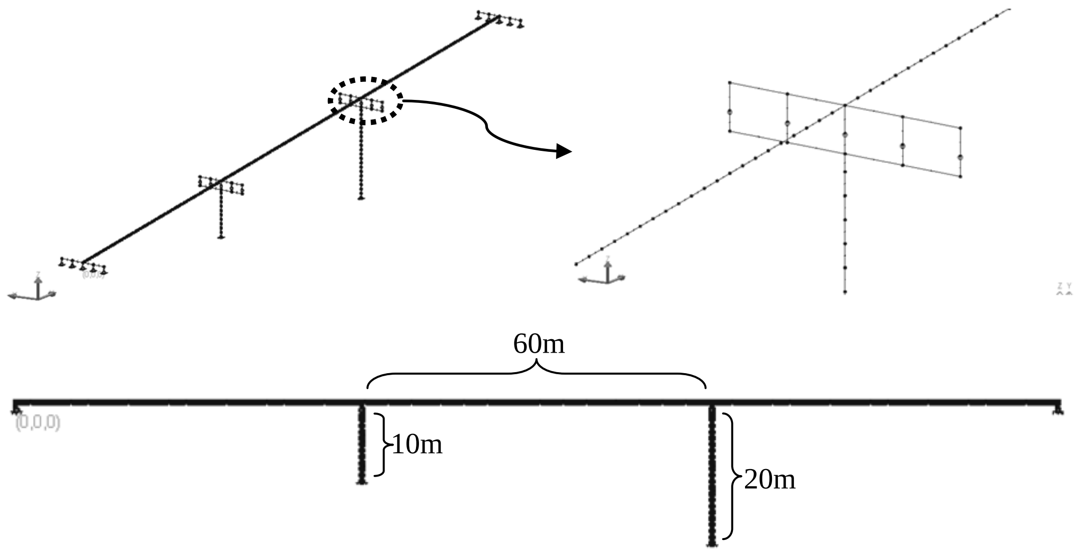

Figure 4.29: Analysis model (Bridge 2)

Modal Analysis

Natural periods of vibration and mass participation factors of first 100 modes are given in APPENDIX B as well as with the shapes of fundamental modes.

Following period intervals accumulated over 90% of modal mass in each orthogonal direction:

X direction : T= 1.653 (90.9%)
Y direction : T= 0.704-0.071 (90.7%)
Z direction : T= 1.120-0.035 (90.1%)

Rayleigh damping coefficients were selected to make average damping ratio equal to 5% between the periods of fundamentals modes governing vibrations in X and Z directions (1.653 s and 0.637 s respectively). Coefficients a = 0.3142 and b = 6.983e-3, which set damping ratio to 5% at periods 0.65 s and 1.35 s, were deemed as suitable for this purpose. Plot of damping ratio versus period is given on Figure 4.30. Periods of fundamental vibration modes for each orthogonal direction are plotted on the same chart.

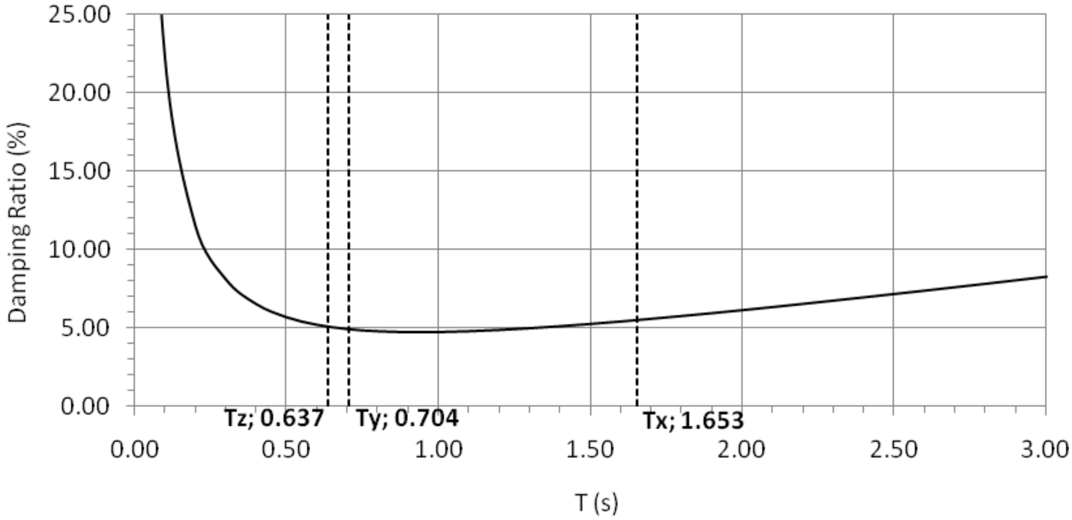

Figure 4.30: Damping ratio vs. period (Bridge 2)

Using related provisions of [1] that are mentioned in Section 3.1, ensemble horizontal SRSS spectrum was scaled so that acceleration values does not fall below 1.3 times the design spectrum in the interval between periods T_1 to T_2, which are 0.5 times of fundamental period of vibration in transverse direction and 1.5 times of the one in longitudinal directions respectively.

T_1 = 0.5*0.704 = 0.352 s

T_2 = 1.5*1.653 = 2.480 s

Minimum ratio of acceleration values of ensemble spectrum to those of design spectrum was found to be 1.368 and 1.350 for modified and synthetic set records. These led to scale factors of 0.951 and 0.963 to be applied to horizontal components of these sets respectively.

Bearing Axial Forces and Hold-down Device Design

Results are tabulated in Table 4.23.

Table 4.23: Bearing axial forces from RSP cases and load combinations (Bridge 2)

Axis	**ID**	**D**	**1**	**2**	**3**	**C1**	**C2**	**C3**	**C4**	**C5**
A1	1	965	30	264	257	109	273	186	350	345
	2	965	30	132	257	70	141	147	218	305
	3	965	30	0	257	30	9	107	86	266
P2	6	2671	26	882	860	291	890	549	1148	1132
	7	2672	26	441	860	159	449	417	707	1000
	8	2673	26	0	860	26	8	284	266	868
P3	11	2670	25	303	867	116	311	376	571	966
	12	2671	25	152	868	71	159	331	419	921
	13	2671	25	0	868	25	8	286	268	875
A4	16	965	35	429	256	164	440	241	517	396
	17	965	35	215	256	100	225	177	302	331
	18	965	35	0	256	35	11	112	88	267

C1 and C2 load combinations were used as to check the requirement of hold-down device according to AASHTO. Design forces are supplied in Table 4.24 for each bearing. Cells containing a slash, “-”, indicates that hold-down device is not needed for that bearing. Forces obtained from load combinations C3, C4 and C5 are included as well.

Table 4.24: AASHTO Hold-down device design forces (Bridge 2)

Axis	**ID**	**C1**	**C2**	**C3**	**C4**	**C5**
A1	1	-	-	-	-	-
	2	-	-	-	-	-
	3	-	-	-	-	-
P2	6	-	-	-	-	-
	7	-	-	-	-	-
	8	-	-	-	-	-
P3	11	-	-	-	-	-
	12	-	-	-	-	-
	13	-	-	-	-	-
A4	16	-	-	-	-	-
	17	-	-	-	-	-
	18	-	-	-	-	-

Results indicated that hold-down requirement did not materialize for any of the bearings. At this point, it will be helpful to make a comparison with the results of Bridge 1. The dissimilarity of the results of Bridge 1 and Bridge 2 primarily originated from the difference in bearing layouts.

As shown in Figure 4.31 and also explained in APPENDIX F, bearings in Bridge 1 were placed in two opposing sides of cap-beam, due to discontinuity of pre-stressed I-girders. On the other hand, for Bridge 2, continuous girder structure enables placement of a single line of bearings on a pier. Thus top piers moments due to longitudinal excitation did not create an axial force couple in bearings, preventing occurrence of uplift forces.

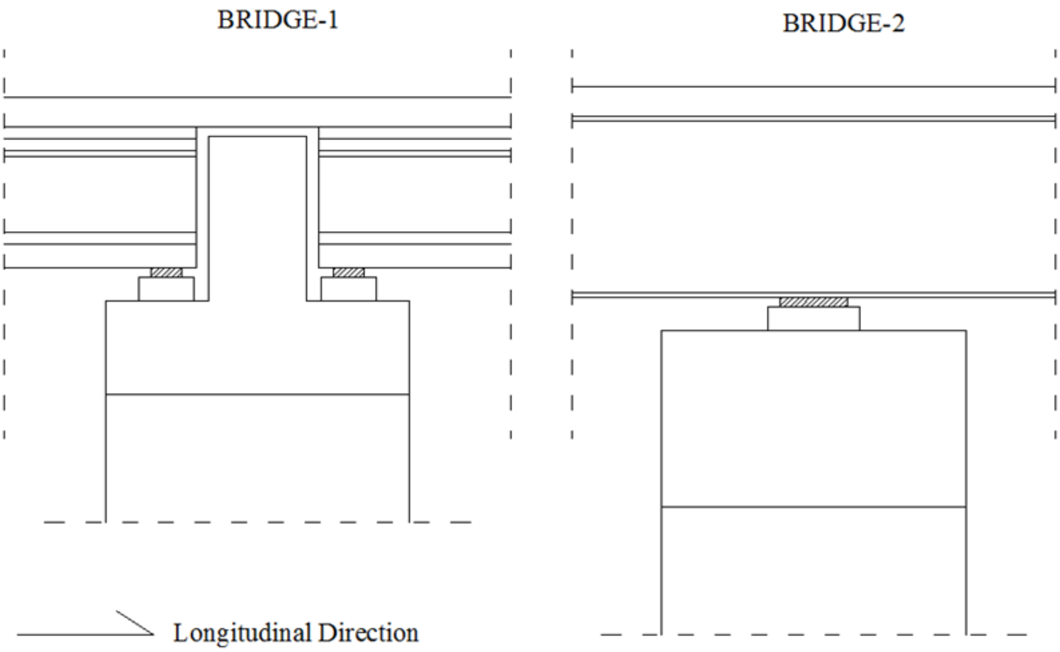

Figure 4.31: Bearing Layouts of Bridge 1 and Bridge 2

Reader will normally question that why transverse excitation does not trigger hold-down device requirements in bearings as it does for Bridge 1, which can be examined from Table 4.6. A solution using Equation (F.16) developed in APPENDIX F will be helpful to reveal the answer of this question. Recalling the axial force in bearing numbered n due to transverse excitation from Equation (F.16);

$$F_n = n.F_1 = n.M_{top} / (2.d.\sum_{i=1}^{i=n} i^2)$$

Assuming identical top pier moments two bridges, axial force ratio becomes a function of total number and spacing of bearings on a pier;

$$\frac{F_{n_1}}{F_{n_2}} = \frac{n_1.d_2.\sum_{i=1}^{i=n_2} i^2}{n_2.d_1.\sum_{i=1}^{i=n_1} i^2}$$

Substituting $n_1 = 4$, $d_1 = 1.3$ and $n_2 = 2$, $d_2 = 2.6$ for Bridge 1 and Bridge 2 respectively, this ratio will be equal to 2/3, meaning that Bridge 2 will experience 1.5 times larger uplift forces in bearings under transverse motion. But the assumption of identical pier moments is not unrealistic, and hold-down device requirement of AASHTO not only depends on axial forces due to excitation, but also those under dead loads. Dead loads responses were different for both bridges recalling Table 4.5 and Table 4.23. Those parameters will be taken into account to make a sound verification of axial forces given in Table 4.23.

Equation (F.16) needs a modification for Bridge 2 because transverse shear forces in bearings also contributes to the moment M_{top} as shown in Figure 4.32, since line of action of these shear forces are at a distance h from top of pier. This difference originated from dissimilarity of cap beam sections used in both bridges, which resulted in different centroid locations with respect to bearings that cap beam elements pass through. Due to transverse movement, all bearings of a pier will be displaced by the same amount due to the high rigidity of superstructure, thus will exhibit same shear forces. Under these circumstances Equation (F.16) becomes;

$$F_n = n.F_1 = n.(M_{top} - F_{shear}.(2n+1).h)/(2.d.\sum_{i=1}^{i=n} i^2) \tag{4.4}$$

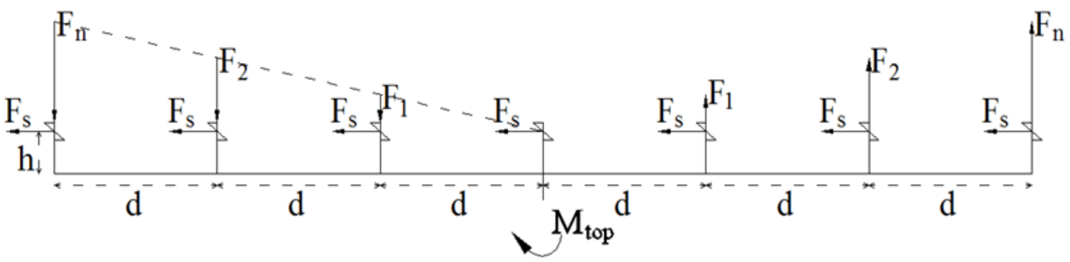

Figure 4.32: Modification to Equation (F.16) for Bridge 2

Top pier moments and bearing shear forces for P2 axis of Bridge 2 under transverse excitation were obtained from RSP analysis case 2. Undoubtedly, at the same time instant axial forces in the side bearings, which are to be calculated, will be at their maximum. Substituting obtained values into Equation (4.4);

$$F_2 = 2.(19412 - 1959 * 5 * 0.750)/(2 * 2.6 * 5) \cong 928\ kN$$

Result obtained from RSP analysis case 2 is equal to 882 kN for the same bearing. This 5% difference primarily originates due to the fact that Equation (4.4) ignores the mass of the cap beam, as explained earlier in APPENDIX F for the case of Bridge 1. But, it is seen that this approach is very useful to verify the magnitude of axial forces of bearings resulting under transverse excitation.

Pier top moments depends on transverse bending stiffness of piers for both bridges as well as other properties, which are, tributary masses carried by piers and torsional stiffness contributions of superstructure to the top of piers. All of these variables affect the magnitude of fundamental period of vibration in transverse direction as well as rotational rigidity of pier top. These variations shall be investigated by a parametric study, which is out of scope of this thesis work.

Recalling hold-down device requirement of AASHTO; if uplift force in a bearing exceeds 50% of axial force under dead loads, it is necessary to utilize a hold-down device [2, 3]. For bearings at P2 axis;

$$\frac{F_2}{F_{2-dead}} = \frac{882}{2671} \cong 0.330$$

Thus hold-down device requirement did not arise for this bridge.

To move on with time-history analyses, bearing axial forces calculated from one-directional LTH cases 4, 5 and 6 were shown in Table 4.25.

Table 4.25: Bearing axial forces from one-directional LTH analyses (Bridge 2)

Axis	ID	4	5	6
A1	1	36	252	277
	2	36	126	277
	3	36	0	277
P2	6	29	944	865
	7	29	472	865
	8	29	0	865
P3	11	28	307	859

Table 4.25 (continued)

Axis	ID	4	5	6
P3	12	28	154	859
	13	28	0	859
A4	16	40	466	278
	17	40	233	278
	18	40	0	278

Average ratio of bearing axial forces obtained from LTH analyses to those of RSP cases at each axis are given on Figure 4.33 for orthogonal directions.

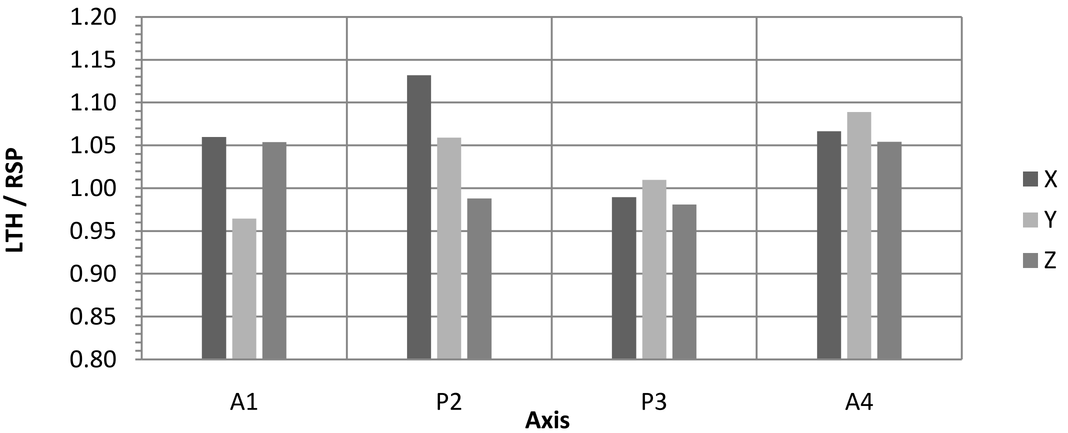

Figure 4.33: Ratio of bearing axial forces for LTH/RSP (Bridge 2)

The ratios are;

- 1.06% in average in X direction.
- 1.03% in average in Y direction.
- 1.02% in average in Z direction.

Results pointed out compatibility of time-history and response spectrum analyses. Small deviations have confirmed the appropriateness of both used Rayleigh damping coefficients and accelerograms for this case also.

Bearing axial forces obtained from multi-directional linear time-history case 7 are shown in following tables. Since tensile bearing forces were not observed from the results of multi-directional LTH analysis cases, no necessity aroused to perform any NLTH analyses further.

Table 4.26: Bearing axial forces from multi-directional LTH analyses (Bridge 2)

Axis	**ID**	**7**	
		T.	**C.**
A1	1	-	1320
	2	-	1257
	3	-	1222
P2	6	-	3912
	7	-	3665
	8	-	3482
P3	11	-	3618
	12	-	3546
	13	-	3482
A4	16	-	1552
	17	-	1377
	18	-	1230

Results were found to be in complete agreement with those of AASHTO load combinations (C1 and C2). As need of hold-down device design was not necessitated, provisions of AASHTO were deemed as accurate. Load combinations C3, C4 and C5 also produced the same outcome.

Compressive axial forces which bearings were exposed to under applied earthquake excitations are plotted for the same analyses cases on Figure 4.34.

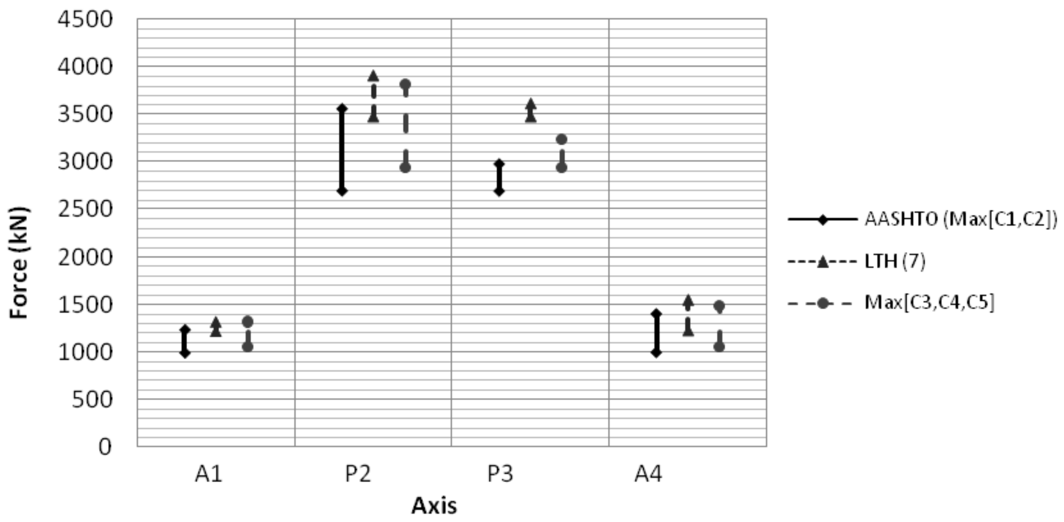

Figure 4.34: Comparison of Compressive Bearing Axial Forces (Bridge 2)

Results showed that AASHTO load combinations (C1 and C2) underestimated axial forces in bearings up to 17.6% at P3 axis, and 10.6% in average. Since bearings did not exhibit uplift in this case, responses due to excitations can be examined separately.

Significant contribution occurred due to motions in both transverse and vertical direction as seen from Table 4.23, yielding almost equal increase in axial forces (27.3% and 29.5%) in the edge bearings of the superstructure. Peak responses resulting from these two motions did not occur exactly at the same time instant in time-history analyses, but the magnitude of resultant axial force obtained from LTH case 7 was close to the sum of individual components computed from RSP cases 2 and 3.

In view of these facts, load combinations C3, C4 and C5 produced more accurate estimate of bearing axial forces. Recalling these combinations;

- C3: 1.0X+0.3Y+0.3Z
- C4: 0.3X+1.0Y+0.3Z
- C5: 0.3X+0.3Y+1.0Z

Although the factor of 0.3 underestimated the combinations of those earthquake responses for this case, error decreased to 10.5% for P3 axis and to 4.5% in average.

Cap Beam Moments

Maximum moments in cap beams are presented in the following tables and figure.

Table 4.27: Maximum cap beam moments from Dead and RSP analysis (Bridge 2)

Axis	**D**	**1**	**2**	**3**
P2	7262	68	3861	2257
P3	7258	66	1449	2291

Table 4.28: Maximum cap beam moments from load combinations (Bridge 2)

Axis	**D+C1**	**D+C2**	**D+C3**	**D+C4**	**D+C5**
P2	8489	11144	9166	11821	10698
P3	7759	8727	8446	9414	10004

Table 4.29: Maximum cap beam moments from LTH case 7 (Bridge 2)

Axis	**7**
P2	12425
P3	10025

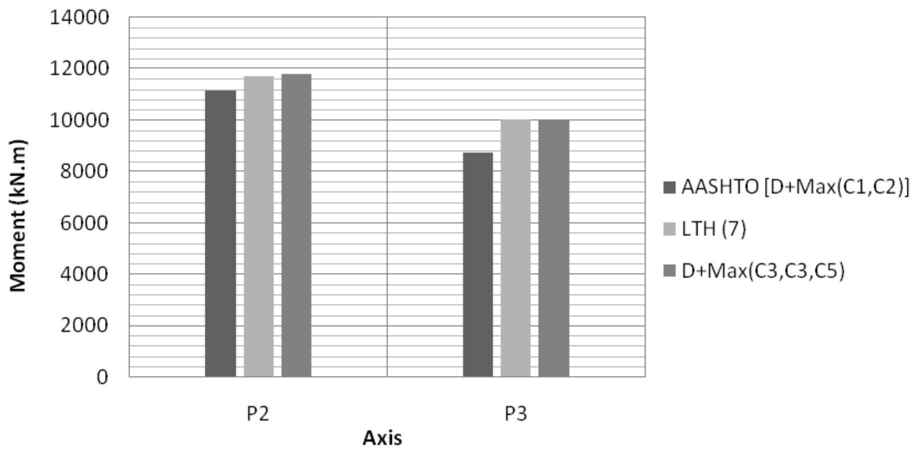

Figure 4.35: Comparison of cap beam moments (Bridge 2)

As explained earlier in this section, axial forces in bearings did not change during longitudinal excitation. Thus it is not expected to observe an alteration in cap beam moments, which was verified by Figure 4.35. Transverse excitation had a major influence on cap beam moments for this bridge. From earlier discussions, it can be recalled that top pier moments were much greater than those of Bridge 1. This also led to the larger increase in bearing axial forces and thus cap beams moments for this case. This alteration was 53.2% at P2 axis (short pier) and 20% at (P3) axis, of the values under dead loads.

As in the case of Bridge 1, a significant increase in cap beam moments also originated from vertical excitation, which was approximately 31% for all cap beams, with respect to values under dead loads. The increase in bearing axial forces due to vertical motion was approximately the same (29.5%), as seen from Table 4.23. AASHTO load combinations (C1 and C2) underestimated cap beam moments 4.8% and 13.2% for P2 and P3 axes respectively, since they do not account for the effects of vertical excitation. Load combinations C3, C4 and C5, which includes vertical direction as well, produced results that are 1.0% greater and 0.4% smaller for the same axis as seen from Figure 4.35, thus deemed to provide accurate estimates.

Pier Forces

Forces are tabulated in Table 4.30 and Table 4.31.

Table 4.30: Maximum pier moments about transverse axis (Bridge 2)

Axis	**D+[Max(C1,C2)]**	**7**	**D+[Max(C3,C4,C5)]**
P2	51119	47872	51456
P3	50188	44926	50293

Table 4.31: Maximum pier moments about longitudinal axis (Bridge 2)

Axis	**D+[Max(C1,C2)]**	**7**	**D+[Max(C3,C4,C5)]**
P2	130023	132859	130024
P3	101287	99115	101287

Pier moments are plotted for these analyses cases on Figure 4.36 and Figure 4.37.

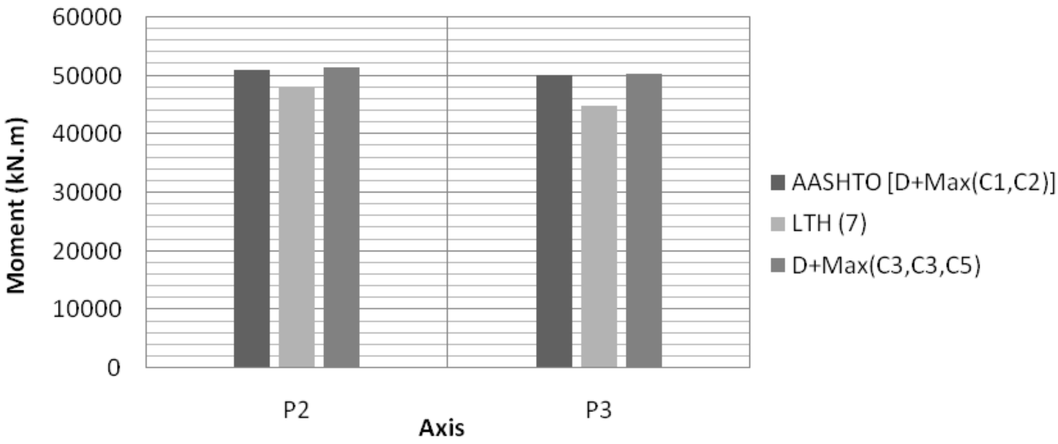

Figure 4.36: Pier moments about transverse (X) axis (Bridge 2)

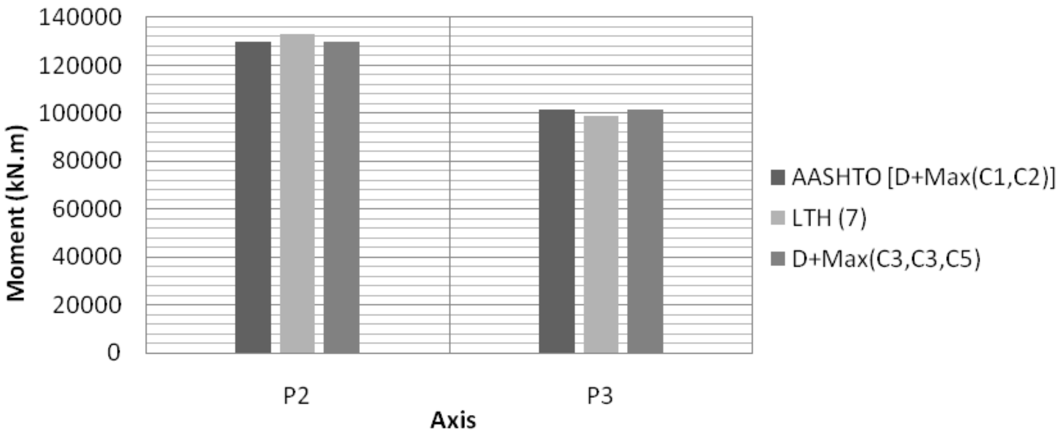

Figure 4.37: Pier moments about longitudinal (Y) axis (Bridge 2)

Deviations between results of AASHTO load combinations and LTH case 7 were 9.2% in average for moments under longitudinal excitation (about Y axis), and ± 2.2% under transverse excitation (about Y axis), being equal in average. Load combinations C3, C4 and C5 produced nearly the same results with those of C1 and C2, just slightly increasing the difference to 9.7% in average under longitudinal excitation. In accordance with the remarks made in earlier in this section for Bridge 1, these negligible differences originated from nature of Rayleigh damping matrix and small unconformity of pseudo acceleration spectra of scaled accelerograms with design response spectrum.

Vertical excitation created no considerable moments on piers as expected.

Load combinations suggested by AASHTO gave accurate results, noticing again the straight alignment of the bridge.

Pier axial forces are tabulated in Table 4.32, Table 4.33 and Table 4.34.

Table 4.32: Absolute maximum pier axial forces from Dead and RSP analysis (Bridge 2)

Axis	**D**	**1**	**2**	**3**
P2	15770	132	1	4435
P3	17197	128	1	4705

Table 4.33: Maximum and minimum pier axial forces, RSP load combinations (Bridge 2)

Direction	**Axis**	**D+C1**	**D+C2**	**D+C3**	**D+C4**	**D+C5**
Minimum	P2	15638	15730	14307	14399	11295
	P3	17069	17158	15657	15747	12454
Maximum	P2	15902	15810	17233	17141	20244
	P3	17325	17236	18737	18648	21941

Table 4.34: Maximum and minimum pier axial forces from LTH case 7 (Bridge 2)

Direction	**Axis**	**7**
Minimum	P2	11435
	P3	12593
Maximum	P2	20215
	P3	21910

Reduced axial forces per AASHTO load combinations are also tabulated in Table 4.35.

Table 4.35: Reduced minimum pier axial forces, RSP load combinations (Bridge 2)

Direction	**Axis**	**D+C1**	**D+C2**
Minimum	P2	11695	11787
	P3	12770	12859

Results are plotted on Figure 4.38.

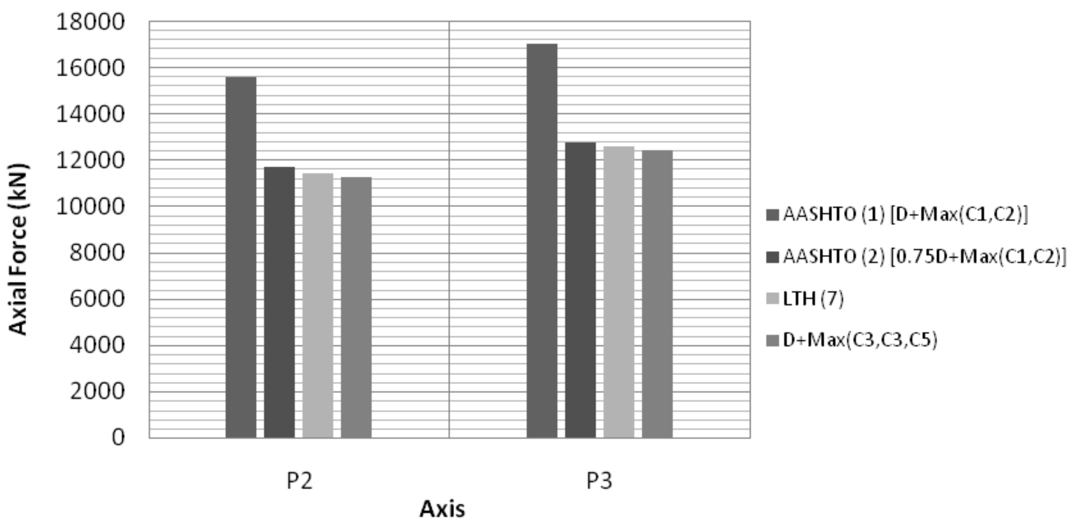

Figure 4.38: Minimum pier axial forces (Bridge 2)

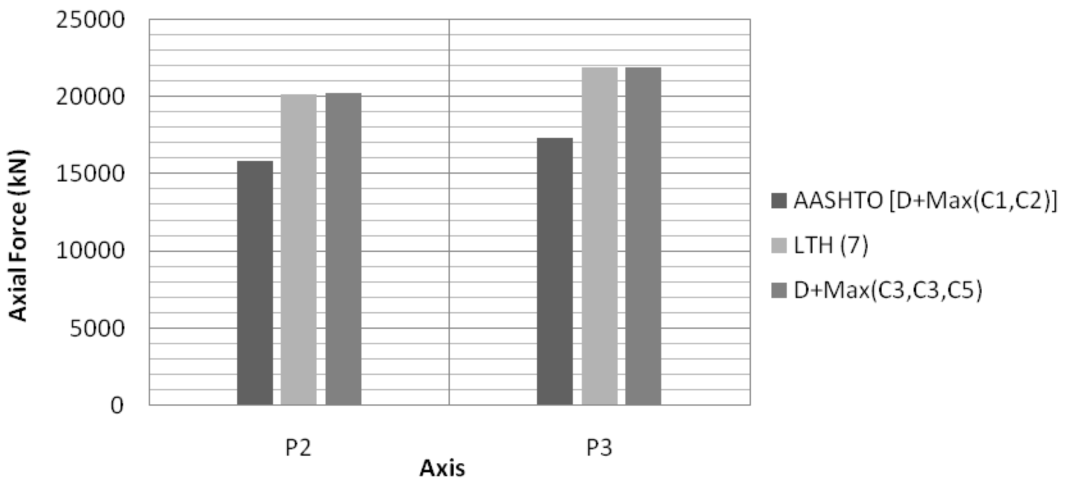

Figure 4.39: Maximum pier axial forces (Bridge 2)

Results pointed out vertical excitation altered pier axial forces by 27.7% in average, which is of nearly the same value of change in compressive bearing forces and cap beam moments. AASHTO load combinations overestimated (36.1%) and underestimated (21.1%) minimum and maximum axial forces in piers. Combinations C3, C4 and C5 produced accurate results for both responses (1.1% smaller for maximum axial forces and 0.1% greater for minimums). Reduced AASHTO load combinations also provided accurate results, which are 1.8% greater in average.

4.3.3 BRIDGE 3: POST_TENSIONED BOX SECTION

Another superstructure type, which is widely used in especially United States and Europe, is post-tensioned concrete box section. Although this type has some applications in Turkey, but these are very few in number.

For this study, AASHTO-PCI-ASBI 2700-2 type post-tensioned box section was selected to span a length of 60 m between axes. Three different variations were used through the span, of which dimensions and properties are shown in Figure 4.40 and Figure 4.41. This configuration is a slightly modified version of the design example described in [31].

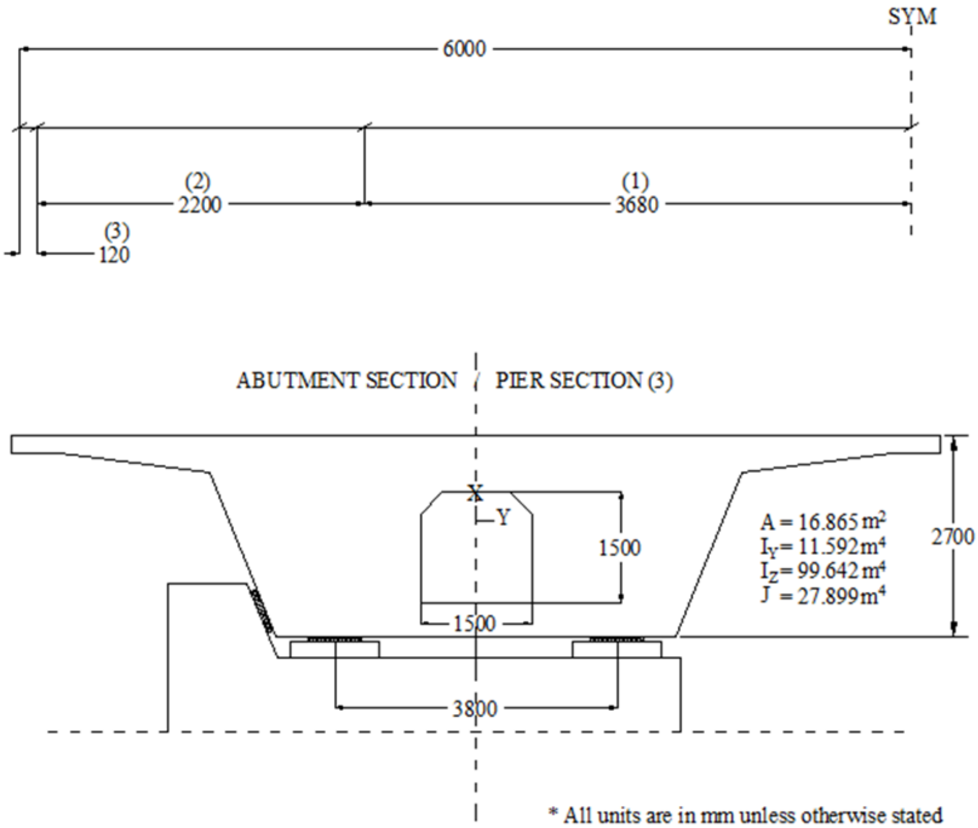

Figure 4.40: Superstructure dimensions - 1 (Bridge 3)

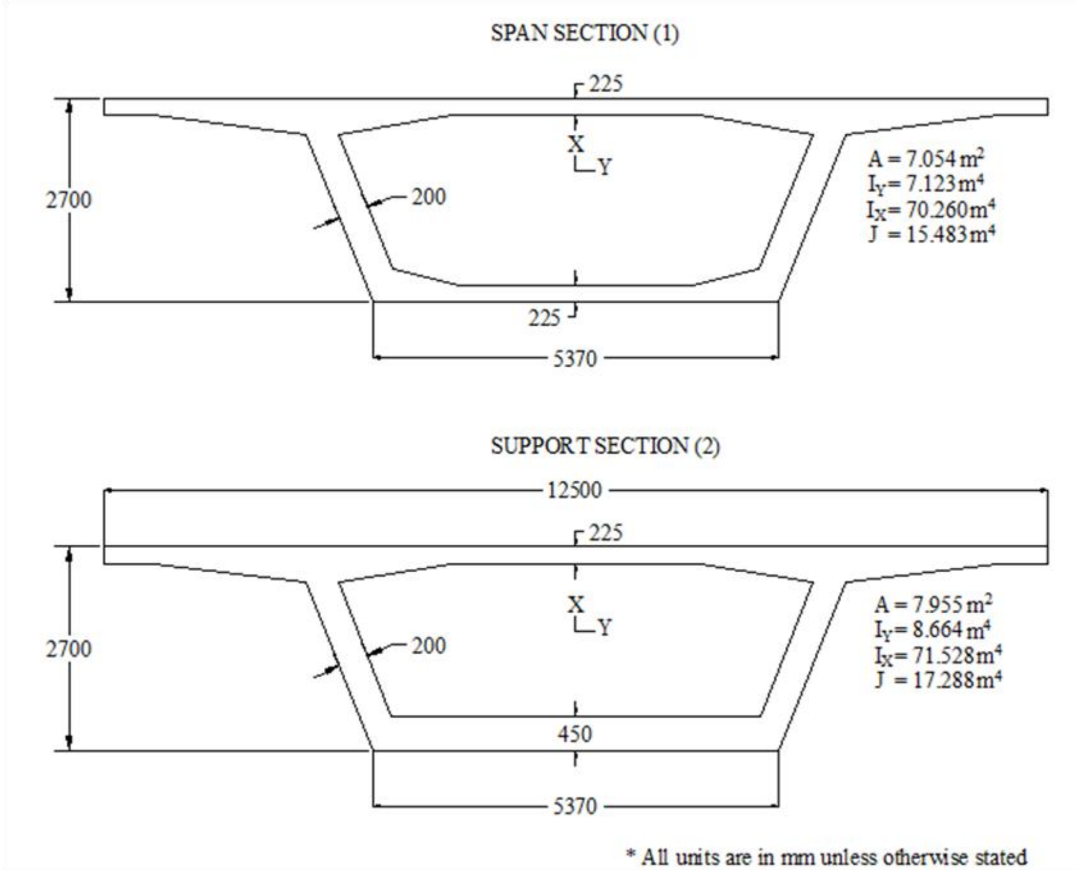

Figure 4.41: Superstructure dimensions - 2 (Bridge 3)

2 elastomeric bearing were placed under the box section; with plan dimensions of 700x700 mm for piers and 1000x1000 mm for abutments, both with height of 80 mm. Shear keys were utilized at abutments, to prevent transverse movement of superstructure. Translational stiffness values of bearings are as follows (for piers and abutments respectively);

Axial stiffness = 91552734, 21981812 kN/m
Longitudinal stiffness = 15625, 7656 kN/m
Transverse stiffness = 15625, very rigid (To account for shear keys at abutments)

Dimensions and section properties of piers are shown in Figure 4.42.

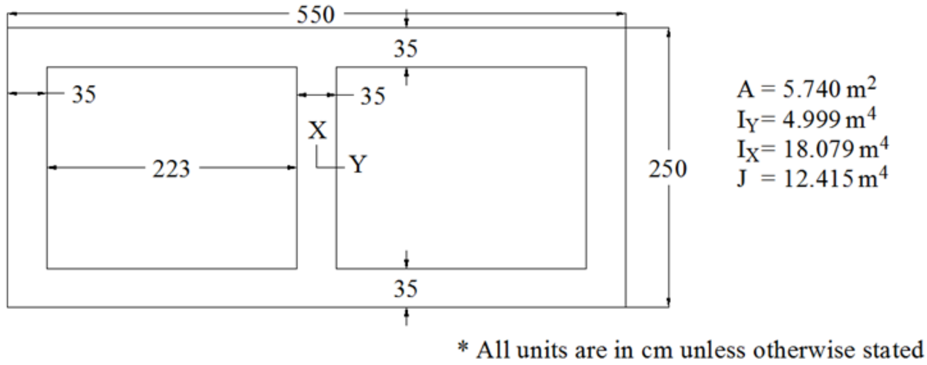

Figure 4.42: Dimensions and section properties of piers (Bridge 3)

Idealized analysis model is shown in Figure 4.43.

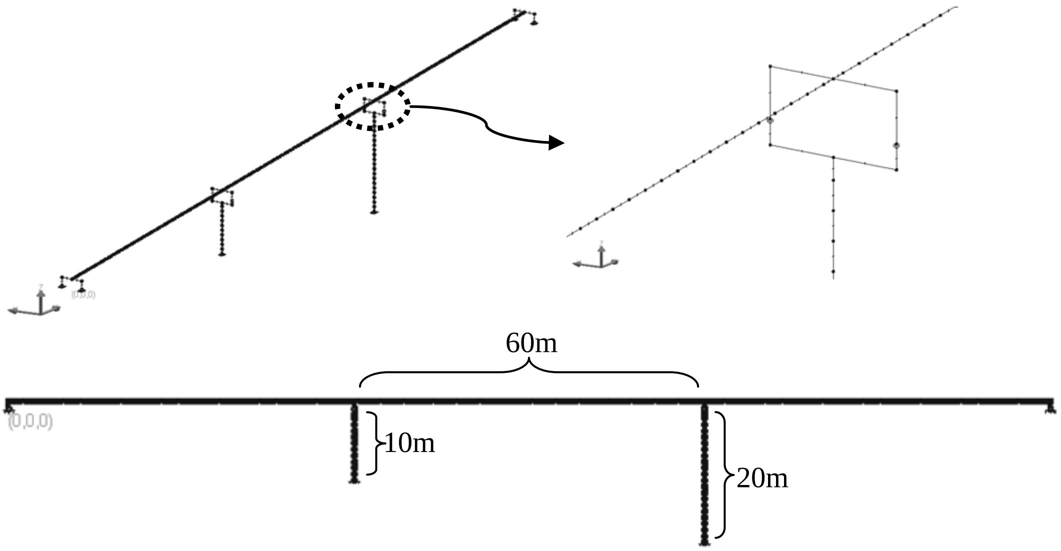

Figure 4.43: Analysis model (Bridge 3)

Modal Analysis

Natural periods of vibration and mass participation factors of first 100 modes are given in APPENDIX C as well as with the shapes of fundamental modes.

Following period intervals are found to accumulate over 90% of modal mass in each orthogonal direction:

X direction : T= 1.583 (93.1%)
Y direction : T= 1.323-0.073 (90.3%)
Z direction : T= 0.699-0.039 (91.7%)

Rayleigh damping coefficients were selected to make average damping ratio equal to 5% between the periods of fundamentals modes governing vibrations in X and Z directions (1.583 s and 0.399 s respectively). Coefficients a = 0.3396 and b = 5.807e-3, which set damping ratio to 5% at periods 0.50 s and 1.35 s, were deemed to be suitable for this purpose. Plot of damping ratio versus period is given on Figure 4.44. Periods of fundamental vibration modes for each orthogonal direction are plotted on the same chart.

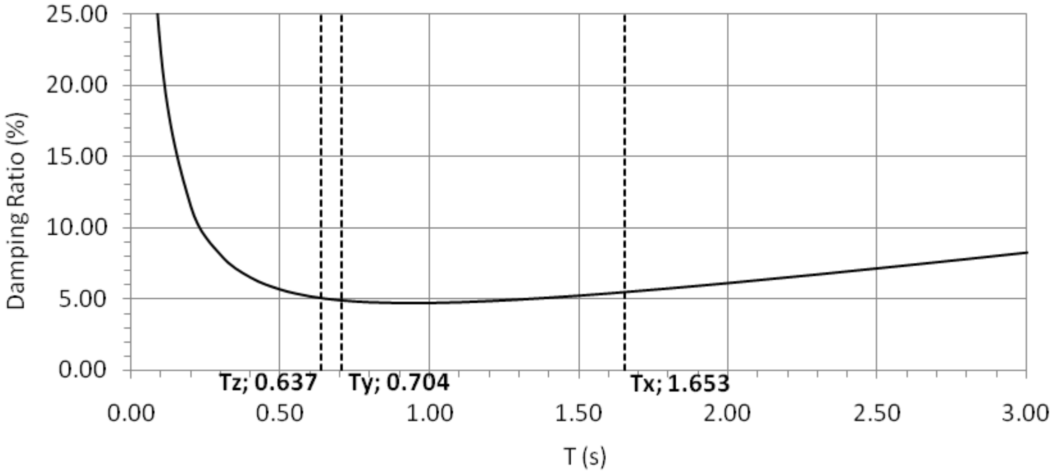

Figure 4.44: Damping ratio vs. period (Bridge 3)

Ensemble horizontal SRSS spectrum was scaled so that acceleration values did not fall below 1.3 times design spectrum between periods T_1 to T_2, where;

T_1 = 0.5*1.323 = 0.662 s

T_2 = 1.5*1.583 = 2.375 s

Minimum ratio of acceleration values of ensemble spectrum to those of design spectrum was found to be 1.368 and 1.350 for modified and synthetic set of records respectively. These led to scale factors of 0.951 and 0.963, which are to be applied to the orthogonal horizontal components of those.

Bearing Axial Forces and Hold-down Device Design Forces

Results of RSP load combinations are presented Table 4.36 and Table 4.37.

Table 4.36: Bearing axial forces from RSP cases and load combinations (Bridge 3)

Axis	**ID**	**D**	**1**	**2**	**3**	**C1**	**C2**	**C3**	**C4**	**C5**
A1	1	3108	205	3416	1083	1230	3478	1554	3803	2169
P2	3	8458	332	1742	3583	854	1841	1929	2916	4205
P3	5	8445	306	3204	3611	1267	3296	2350	4379	4664
A4	7	3116	250	5043	1071	1763	5118	2084	5439	2658

Design forces are supplied for AASHTO load combinations in Table 4.37, where cells containing a slash, “-”, indicates that hold-down device was not needed for that bearing.

Table 4.37: Hold-down device design forces (Bridge 3)

Axis	**ID**	**C1**	**C2**	**Max**
A1	1	-	443	***443***
P2	3	-	-	-
P3	5	-	-	-
A4	7	312	2403	***2403***

Conceptual design was performed by connecting superstructure to the top of piers via steel bars in front of each bearing as done for Bridge 1. Maximum design force of bearing couple at an abutment or pier axis was for hold-down devices to be placed for all at that axis. As discussed in Section 4.3.1, this study is only concerned with the tensile stiffness of the device. Thus connection details were not considered. A schematic drawing of hold-down device for Bridge 2 is shown in Figure 4.45.

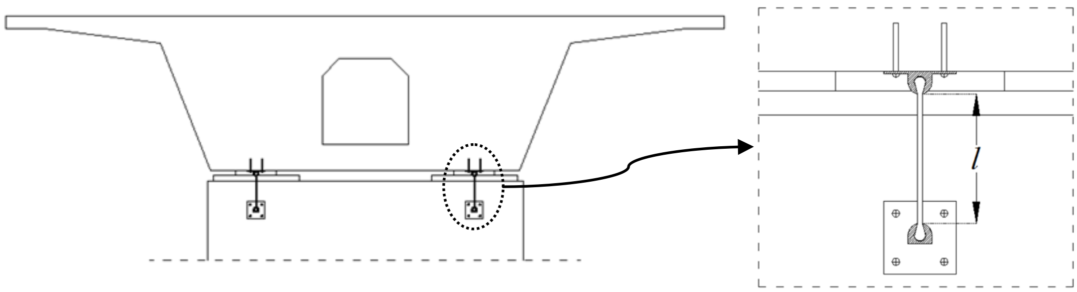

Figure 4.45: Schematic drawing of hold-down device (Bridge 3)

Recalling Equation (4-3), tensile stiffness of hold-down device is;

$$K_{HD} = (E.P)/(l.\sigma_a) \tag{4-3}$$

Calculations were done by substituting E = 200000 Mpa and σ_a = 252 Mpa into Equation (4-3), as in the case of Bridge 1. l was set equal to 0.5 m, which is a rational value suiting this geometry. Calculated stiffness values are given in Table 4.38.

Table 4.38: Hold-down device stiffness per bearing at each axis (Bridge 3)

Axis	**Design Force/bearing**	**Calculated Area (mm^2)**	**Stiffness/bearing (kN/m)**
A1	443	1757.94	703174
P2	-	-	-
P3	-	-	-
A4	2403	9535.71	3814282

Bearing axial forces calculated from one-directional linear time-history analysis cases 4, 5 and 6 are shown in Table 4.39.

Table 4.39: Bearing axial forces from one-directional LTH analyses (Bridge 3)

Axis	**ID**	**4**	**5**	**6**
A1	1	207	3993	1063
P2	2	347	1840	3554
P3	3	300	3448	3578
A4	4	273	5652	1056

These results are compared with the ones obtained from response spectrum analyses to verify Rayleigh damping coefficients, as well as modified strong ground motion records. Average ratio of bearing axial forces obtained from LTH to those of RSP cases at each axis are given on Figure 4.46 for orthogonal directions.

Obtained ratios are;

- 0.99 in average in X direction.
- 1.01 in average in Y direction.
- 1.01 in average in Z direction.

Negligible differences indicated that selected Rayleigh damping coefficients and modified accelerograms were appropriate.

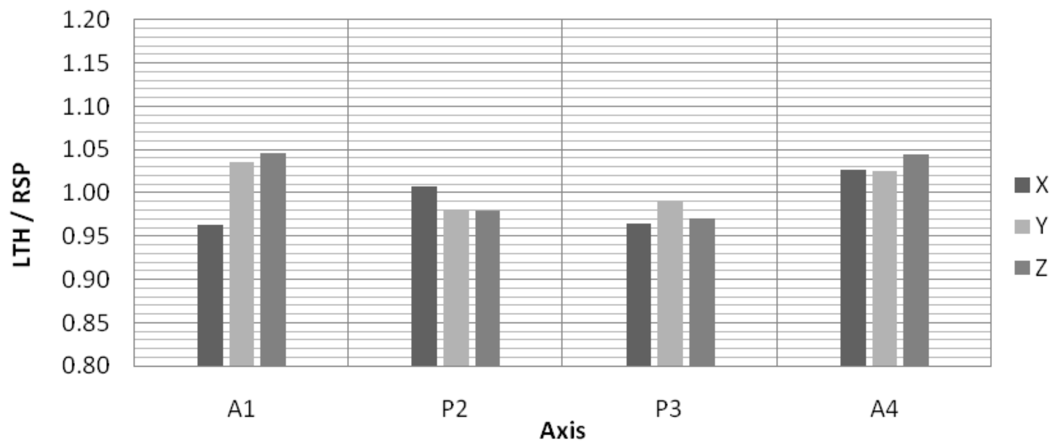

Figure 4.46: Ratio of bearing axial forces for LTH/RSP (Bridge 3)

Bearing axial forces obtained from LTH and NLTH cases 7, 8 and 9 as well as with hold-down device forces of load combinations C3, C4 and C5 are shown in Table 4.40 and Table 4.41.

Table 4.40: Bearing axial forces from multi-directional LTH analyses (Bridge 3)

Axis	**ID**	**7**		**8**		**9**	
		T.	**C.**	**T.**	**C.**	**T.**	**C.**
A1	1	-307	6559	YES	10726	-286	8350
P2	3	-	12307	-	12810	0	12803
P3	5	-	13115	-	13642	0	13663
A4	7	-1637	8148	YES	16545	-1430	9302

Table 4.41: Hold-down device forces from load combinations C3, C4 and C5 (Bridge 3)

Axis	**ID**	**C3**	**C4**	**C5**	**Max**
A1	1	-	694	-	*694*
P2	3	-	-	-	
P3	5	-	-	-	
A4	7	-	2323	-	*2323*

These results are plotted on Figure 4.18.

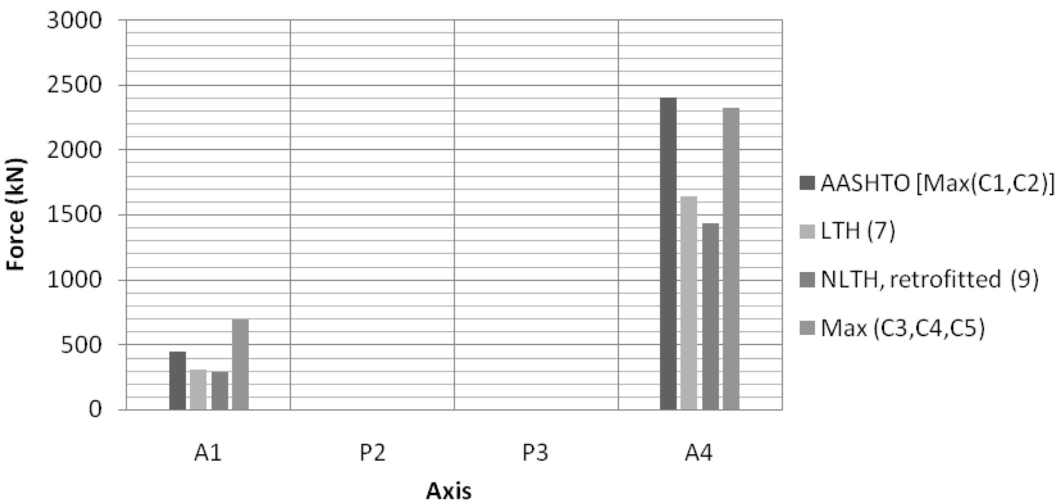

Figure 4.47: Comparison of Hold-Down Device Forces (Bridge 3)

The number and location of bearings that required application of a hold-down device exactly matched for all time-history analyses cases and AASHTO load combinations (C1, C2), as in the case of Bridge 1.

A verification of this observation can be done by scanning Table 4.37 for bearing ID's having hold-down design forces greater than zero and, Table 4.40 for the ones exposed to tensile axial forces.

AASHTO load combinations (C1 and C2) produced conservative results which are 55.3% and 68% greater for A1 and A4 axis respectively, than those of NLTH case 9. Load combinations C3, C4 and C5 gave even higher deviation for A1 axis, which is 143.2% and slightly lower for A2 axis as 62.5%. LTH case 7 produced slightly higher device forces, which are 11.1% greater in average.

For this bridge, uplift forces occurred due to the transverse and vertical excitations as seen from Table 4.36. Results of LTH case 7 indicated that total uplift force was approximately equal to the value coming from transverse direction only. This observation pointed out to the fact; peak responses due to excitation in both these directions did not occur at the same time instant. To be able to examine individual response histories, forces in bearings 1 and 7 were plotted vs. time for transverse and orthogonal directions separately for ground motion record 3, excluding dead loads. Tension forces are shown as positive.

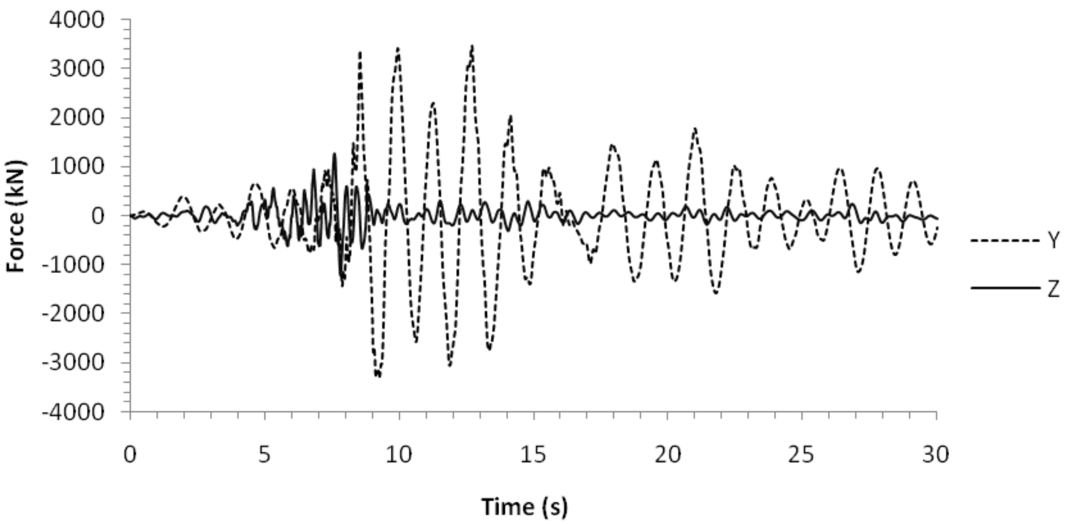

Figure 4.48: Axial forces for bearing 1 under excitation 3 in Y and Z directions

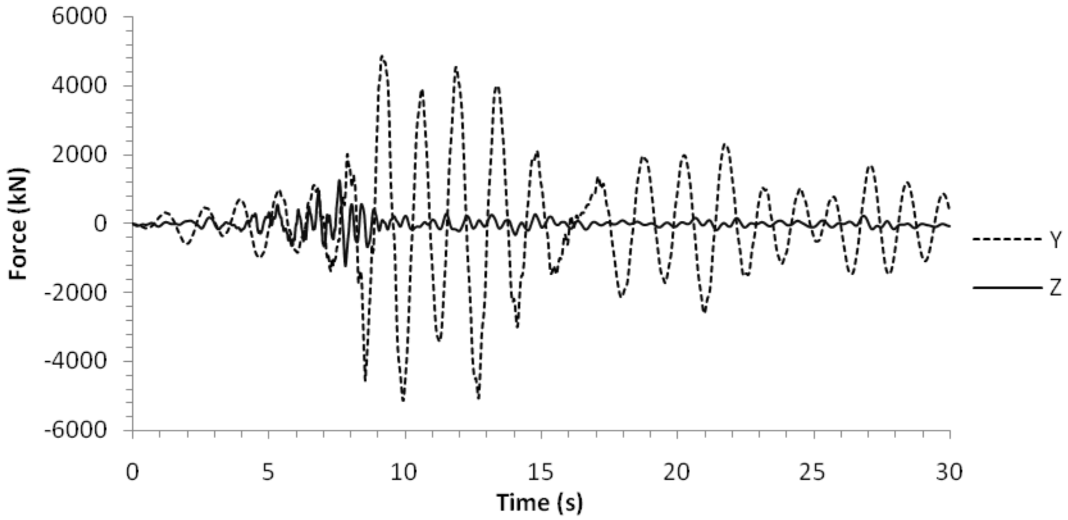

Figure 4.49: Axial forces for bearing 7 under excitation 3 Y and Z directions

Figure 4.48 and Figure 4.49 clearly shows that contribution of vertical excitation was negligible at time instant where resultant bearing forces were at maximum. Here, one may wonder if the situation is the same under all generated records. To investigate further cases, similar plots of record 6 are provided Figure 4.50 and Figure 4.51. Author believes that providing such plots for the remaining records will create useless mass on these pages, rather than providing further clarification of the subject.

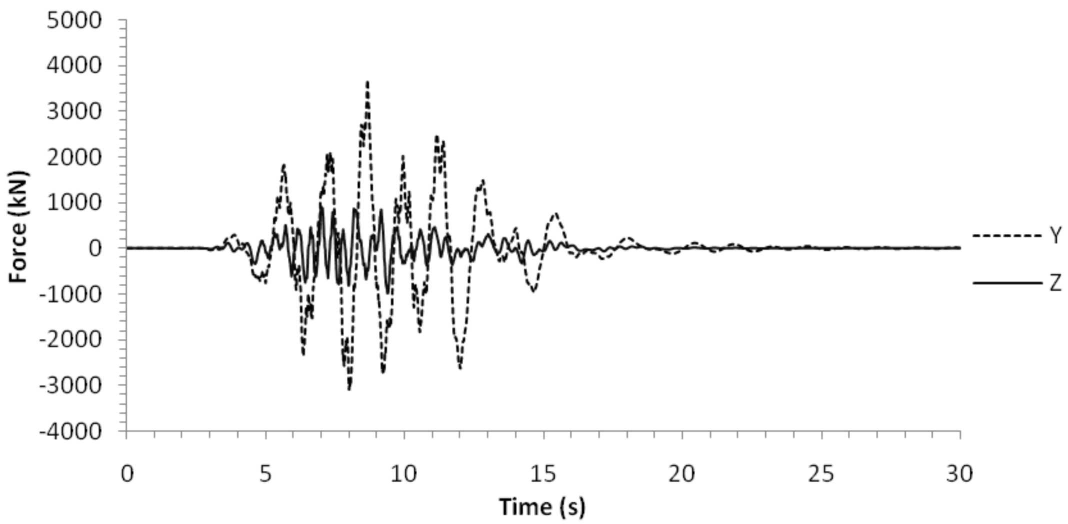

Figure 4.50: Axial forces vs. time for bearing 1 under excitation 6

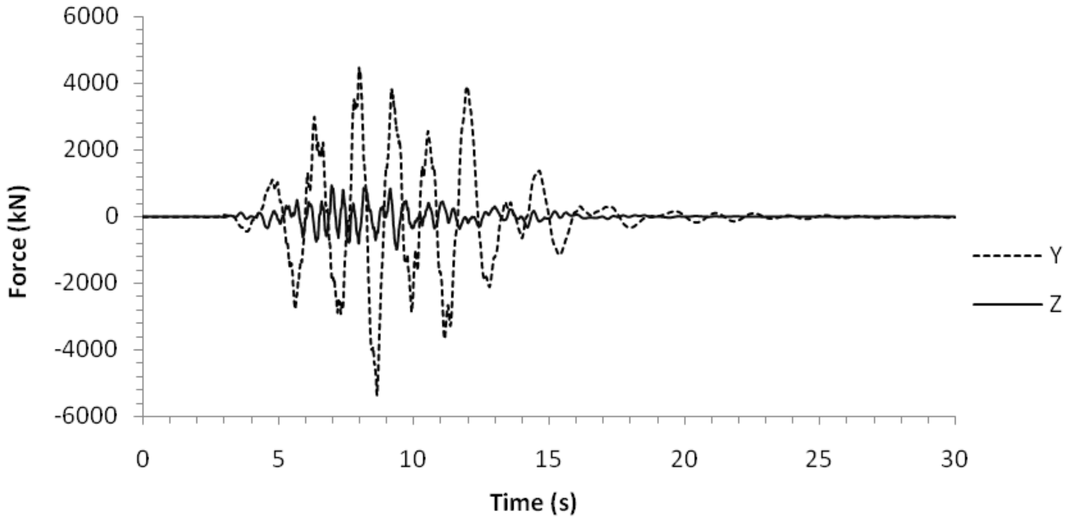

Figure 4.51: Axial forces vs. time for bearing 7 under excitation 6

Again these plots indicate occurrence times of peak responses due transverse and vertical excitations did not match, and even vertical response could have a negative contribution to the peak values of horizontal one. As this is a probabilistic issue, the mentioned action may not be observed in different further excitation records. But for current case, 0.3 coefficients introduced in all load combinations overestimated resultant uplift forces.

Although differences were small in terms of bearing axial forces, they further increased the deviations of hold-down device forces. Suppose axial forces in bearings under dead loads and strong ground motion were denoted by D and E respectively. Hence uplift force a bearing will be $U = E - D$. Here, deviations of the results will be greater for uplift force U. To demonstrate, actual values of bearing ID:1, $D = 3108$ for dead loads, and $E_1 = 3478$ and $E_2 = 3415$ for load combination C2 and LTH case 7 respectively are substituted.

Hence E_1/E_2 becomes 1.02 and U_1/U_2 will be 1.21 respectively. One shall recall that AASHTO also includes the multiplication factor of 1.2 for hold-down device design forces, increase ratio of U_1/U_2 to 1.45. As tensile stiffness hold-down devices are smaller than those of bearings, NLTH case 9 produced even slightly smaller uplift forces, which increased this ratio to 1.55 in percentage as explained in early paragraphs.

Compressive bearing axial forces are plotted on Figure 4.52.

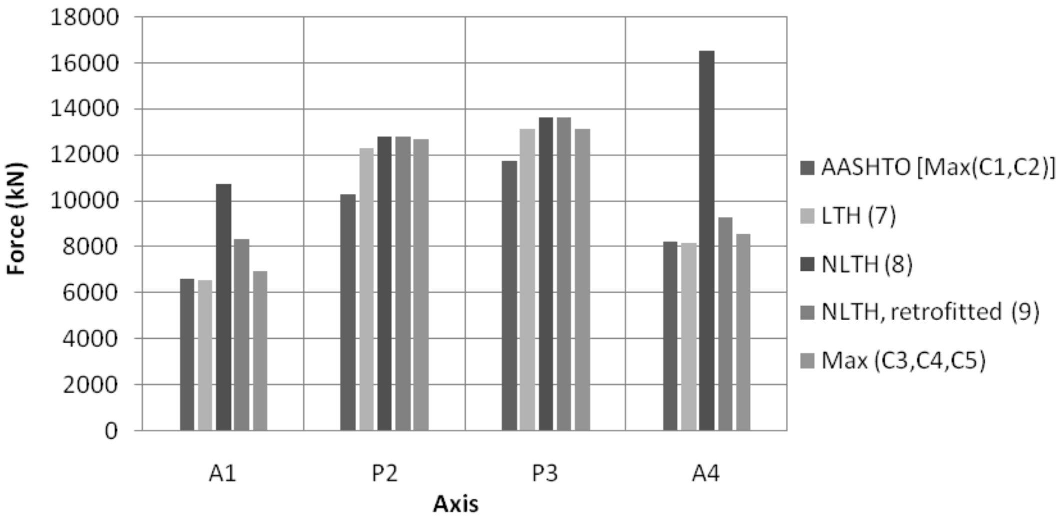

Figure 4.52: Comparison of Compressive Bearing Axial Forces (Bridge 3)

Results of NLTH case 8 indicated that uplift of bearings increases compression forces at bearings on the opposite side significantly. This alteration was 28.4% and 77.9% at abutments A1 and A4 respectively, when compared to the results obtained from retrofitted NLTH case 9. To be able to interpret these results, one shall consider that superstructure sits on two bearings, being very different from Bridge 1. Thus uplift of a bearing under transverse excitation is expected to increase the compression forces on its neighbor in greater means, as no redundancy of supports exists as it did in the case of Bridge 1. However, it could not be possible again to develop a quantitative explanation of such a non-linear problem under three orthogonal excitations.

Forces obtained from AASHTO combinations tend to be 21.1% and 11.5 smaller at A1 and A4 axes, and 19.6% and 14.1% smaller at P2 and P3 axes respectively. Load combinations C3, C4 and C5 produced more accurate results, reducing underestimation ratios to 17.2%, 1.1%, 4.1% and 8.1% for the same axes, A1, A4, P2 and P3.

Pier Moments

Maximum pier moments for all analysis cases are presented in the tables.

Table 4.42: Maximum pier moments about transverse direction (Bridge 3)

Axis	D+[Max(C1,C2)]	7	8	9	D+[Max(C3,C4,C5)]
P2	46144	45002	42404	42386	47115
P3	52759	50011	51064	51064	53045

Table 4.43: Maximum pier moments about longitudinal direction (Bridge 3)

Axis	D+[Max(C1,C2)]	7	8	9	D+[Max(C3,C4,C5)]
P2	66146	66250	68987	69264	66146
P3	76492	77609	80049	80338	76493

Pier moments are plotted for these analyses cases on Figure 4.53 and Figure 4.54. Results indicated that differences between RSP load combinations and time-history analyses are 2.3% for moments under longitudinal excitation (moments about transverse direction), and 2.6% under transverse excitation (moments about longitudinal direction) in average. Same ratios were 3.6% and 2.6% for load combinations C3, C4 and C5. As explained in earlier cases, these quite small deviations were deemed to be originated from analyses parameters such as damping matrix and spectrum-compatible excitations.

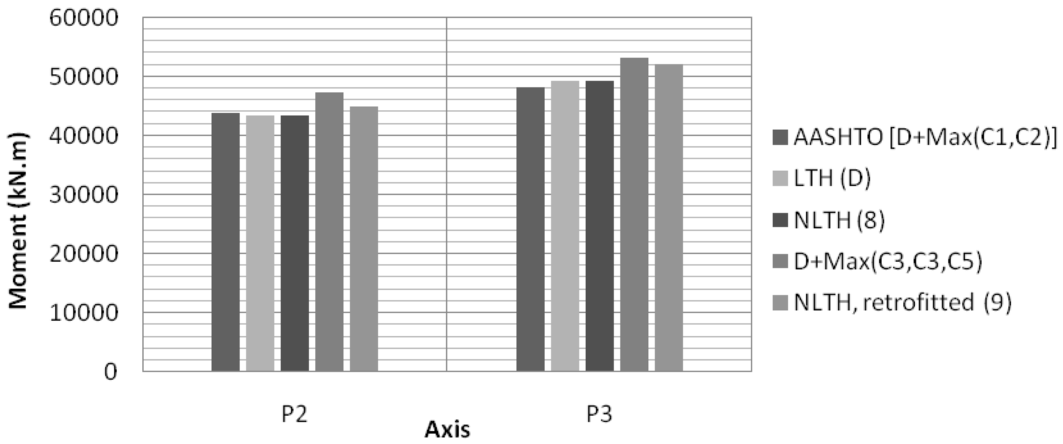

Figure 4.53: Pier moments about transverse (Y) axis (Bridge 3)

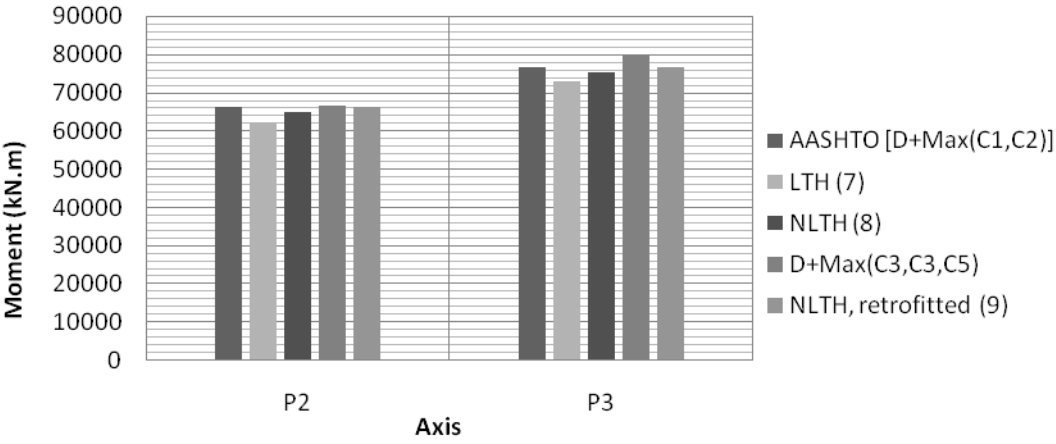

Figure 4.54: Pier moments about longitudinal (X) axis (Bridge 3)

Pier axial forces are tabulated in Table 4.44, Table 4.45 and Table 4.46. Results are shown in Figure 4.55 and Figure 4.56 as well.

Table 4.44: Absolute maximum pier axial forces, Dead and RSP cases (Bridge 3)

Axis	D	1	2	3
P2	18707	666	1	7265
P3	20117	624	0	7499

Table 4.45: Maximum and minimum pier axial forces, Load combinations (Bridge 3)

Direction	Axis	D+C1	D+C2	D+C3	D+C4	D+C5
Minimum	P2	18040	18506	15860	16327	11242
	P3	19492	19929	17242	17679	12430
Maximum	P2	19373	18907	21553	21087	26172
	P3	20741	20304	22991	22554	27803

Table 4.46: Reduced minimum pier axial forces, AASHTO Load combinations (Bridge 3)

Direction	Axis	0.75D+C1	0.75D+C2
Minimum	P2	13363	13829
	P3	14463	14900

Table 4.47: Maximum and minimum pier axial forces, LTH and NLTH cases (Bridge 3)

Direction	Axis	7	8	9
Minimum	P2	11558	11789	11792
	P3	12577	12955	12921
Maximum	P2	25216	26017	26020
	P3	26939	27825	27827

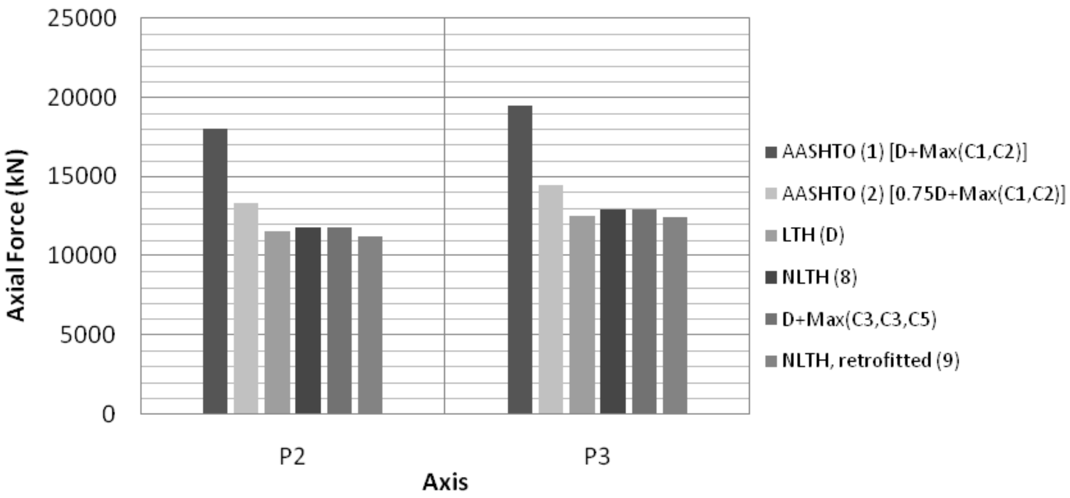

Figure 4.55: Minimum pier axial forces (Bridge 3)

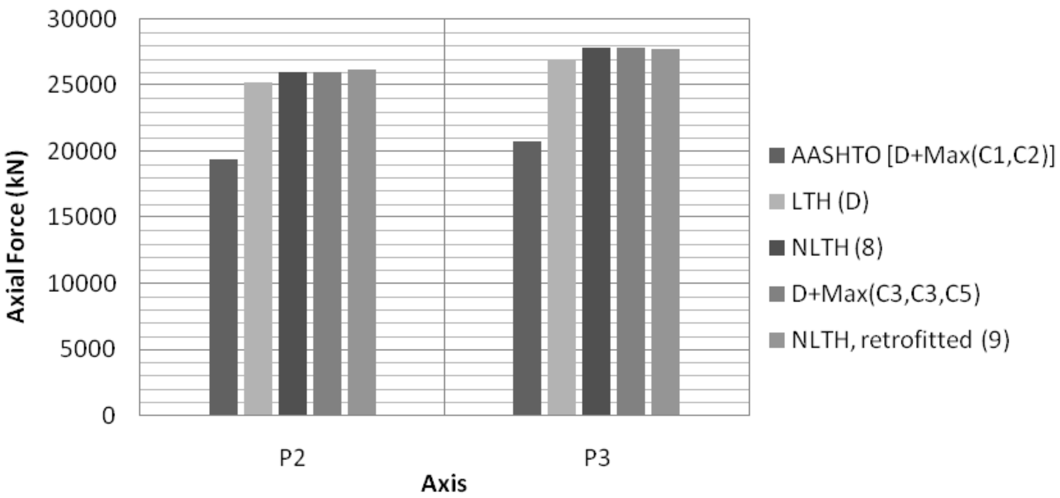

Figure 4.56: Maximum pier axial forces (Bridge 3)

Results pointed out vertical excitation altered pier axial forces by 38.1% in average, which is of nearly the same value of change in compressive bearing forces. AASHTO load combinations overestimated (51.9%) and underestimated (25.5%) minimum and maximum axial forces in piers. Combinations C3, C4 and C5 produced accurate results for both responses (4.2% smaller for maximum axial forces and 0.2% greater for minimums). Reduced AASHTO combinations supplied axial forces that were greater by 12.6% in average.

Lower Bound Analyses

Recalling Equation (3.2), the minimum required support lengths AASHTO are;

$$N = (305 + 2.5L + 10H)(1 + 0.000125S^2)$$

Where;

$L = 180\ m$ length of whole superstructure
$H = 15\ m, 10\ m\ and\ 20\ m$ for abutments, short and long piers respectively
$S = 0$ since bright alignment is straight

This leads to three values of 905 mm, 855 mm and 955 mm for abutments, short and long piers respectively. Assuming these requirements are satisfied, relative displacement of superstructure to the bottom face of bearings was investigated. Longitudinal displacements were examined only, as shear blocks prevents transverse displacement of bearings at abutments and those at the piers were not subjected to uplift during NLTH case 8.

Bearings with ID's 1, 3, 5 and 7, which are the side bearings on A1, P2,P3 and A4 axes respectively, were inspected for this purpose. Only relevant directions for abutments were considered, that is; positive X direction for A1 and negative for A4 axis where superstructure tends to displace apart from the abutments. For piers, maximum of reponses in both directions were tabulated, as a symmetric bearing exists on the opposing side of the pier (i.e. results will be of same magnitude but in different direction for 3 and 4, etc.). Indeed, for this bridge it is not possible for bearings on the piers to experience unseating due to longitudinal excitation, as superstructure is fully continuous. But results of those were also provided in Table 4.48 and Table 4.49.

Table 4.48: Bearing displacements NLTH case 10 (Bridge 3)

ID	10-1	10-2	10-3	10-4	10-5	10-6	Avg.	Max
1	273	228	292	306	305	304	285	306
3	262	258	248	245	259	251	254	262
5	159	129	173	177	167	165	162	177
7	308	302	281	284	303	296	296	308

Table 4.49: Relative superstructure displacements with respect to the bottom of bearings, RSP analyses cases (Bridge 3)

ID	11	12	13
1	318	7	3
3	271	4	7
5	173	3	9
7	319	8	3

Differences between results of LTH and RSP analyses were smaller than those in the case of Bridge 1. Selected damping coefficients still provided high damping values reaching up to approximately 6.5% at lower bound fundamental period (2.064 sec), but not as much as they did in Bridge 1, in which damping ratio was approximately 10%. Thus displacements of LTH cases are closer (9.9% smaller in average) to those of RSP analyses. As seen from Table 4.21, longitudinal displacements of bearings were governed only by excitation in the same direction. Thus, outcomes of RSP case 11 were used in evaluation.

Results indicated that average of the values obtained from all excitations did not exceed provided seat width. Also the maximum ones were observed to be so, thus it is concluded that stability loss of structure may not occur due to loss of support under I-girders, if minimum support length requirement per AASHTO is provided. Bearing displacements increased 42.7% in average for all. This smaller increase compared to Bridge 1 is again due to the lesser change of longitudinal fundamental period, since only half of bearings were modified to lose their shear capacity where same amount was 83.3% for Bridge 1. Bearing displacements for earlier RSP cases 1, 2 and 3 are tabulated on Table 4.50.

Table 4.50: Bearing displacements from RSP analyses cases (Bridge 3)

ID	1	2	3
1	222	7	3
3	191	4	7
5	121	3	9
7	223	8	3

4.3.4 BRIDGE 4: STEEL BOX SECTION AND CONCRETE DECK

This type of superstructure is widely used in United States and partly in Europe.

Superstructure consists of double steel box girders with 6.15 m center-to-center spacing. Height of box girders is 230 cm and thickness of overlying concrete slab is 25 cm. Section dimensions and properties are shown in Figure 4.27.

Two elastomeric bearing exists under each girder; with plan dimensions of 600x600 mm for piers and 400x450 mm for abutments, both with height of 80 cm. Shear blocks were placed at the abutments. Translational stiffness values of bearings are as follows [2] (for piers and abutments respectively);

Axial stiffness = 11865234, 2956045 kN/m
Longitudinal stiffness = 5625, 2813 kN/m
Transverse stiffness = 5625, very rigid (To account for shear blocks)

Dimensions of pier section and idealized analysis model are shown in Figure 4.58 and Figure 4.59.

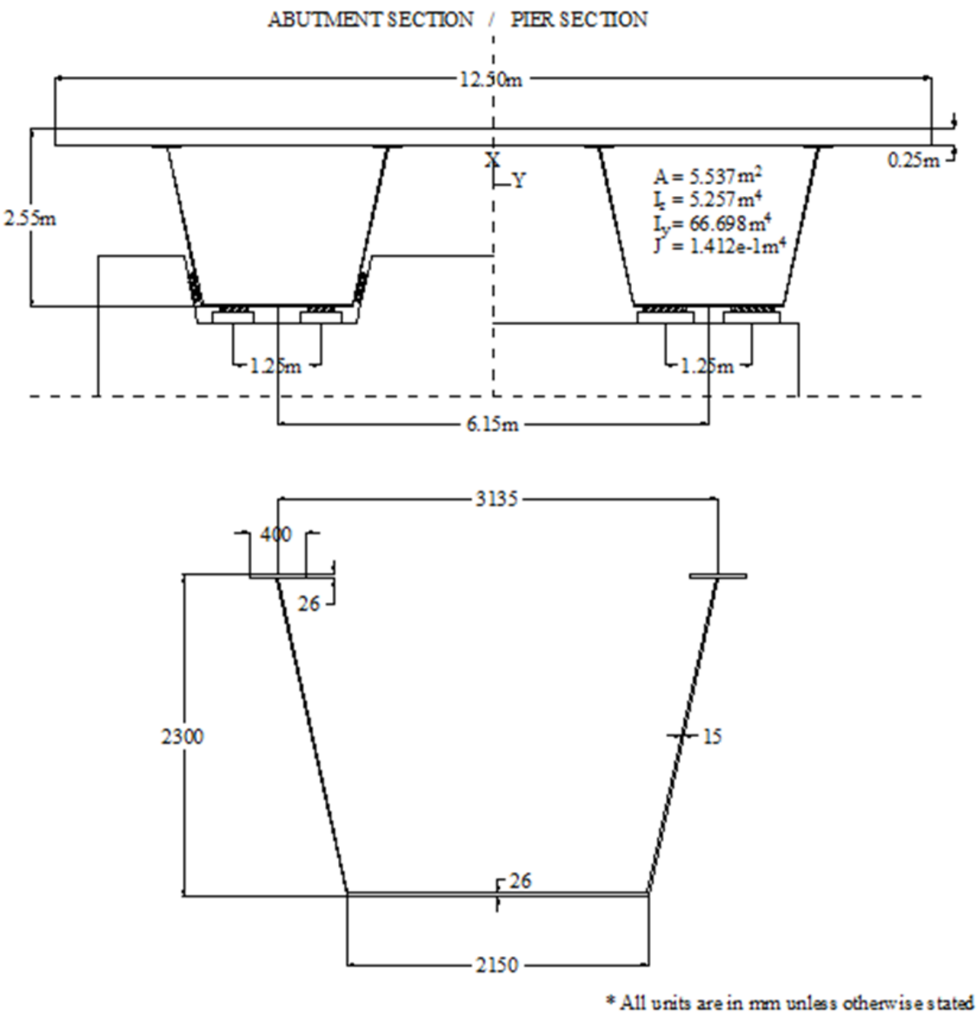

Figure 4.57: Superstructure dimensions (Bridge 4)

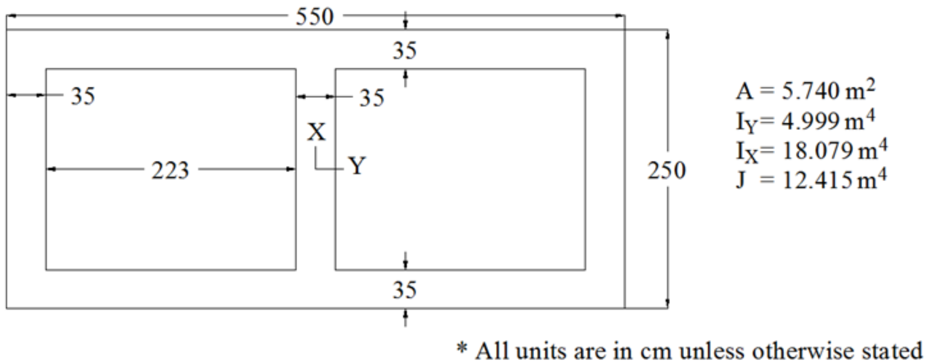

Figure 4.58: Dimensions and section properties of piers (Bridge 4)

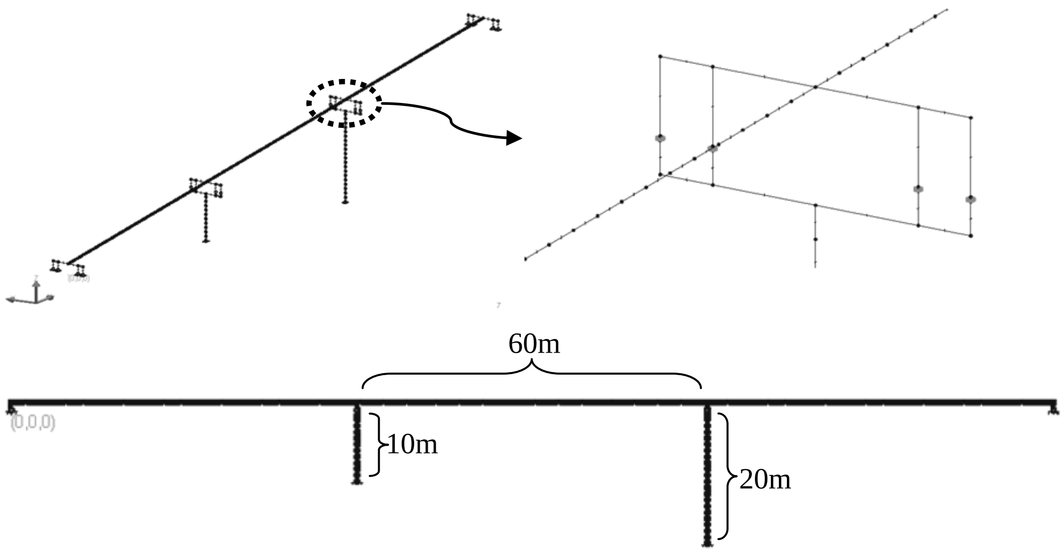

Figure 4.59: Analysis model (Bridge 4)

Modal Analysis

Natural periods of vibration and mass participation factors of first 100 modes are given in APPENDIX D as well as with the shapes of fundamental modes.

Following period intervals were found to accumulate over 90% of modal mass in each orthogonal direction:

X direction : T= 1.552-0.345 (92.1%)
Y direction : T= 1.253-0.052 (92.6%)
Z direction : T= 0.807-0.036 (90.9%)

Rayleigh damping coefficients were chosen to set average damping ratio equal to 5% between periods 0.459 s and 1.552 s. Coefficients a = 0.3491 and b = 6.079e-3e-3, which equals damping ratio to 5% at periods 0.55 s and 1.25 s, were suitable to achieve this. A plot of damping ratio versus period is presented on Figure 4.60. Periods of fundamental vibration modes for each orthogonal direction are plotted on the same figure.

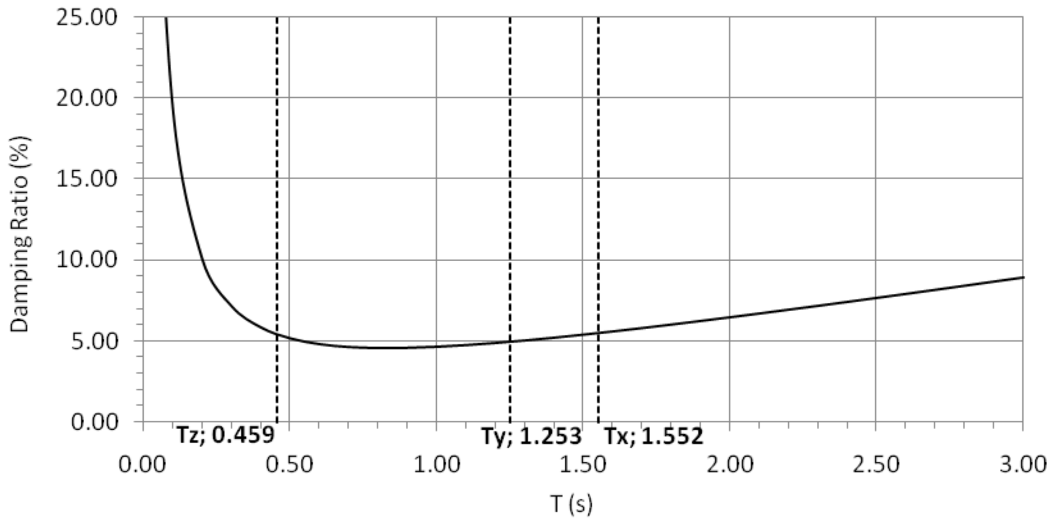

Figure 4.60: Damping Ratio vs. Period (Bridge 4)

Using the related provisions given in Section 3.1.5, ensemble horizontal SRSS spectrum was scaled between T_1 to T_2 where;

T_1 = 0.5*1.253 = 0.627 s
T_2 = 1.5*1.552 = 2.328 s

These led to scale factors of 0.951 and 0.963, which are to be applied to the orthogonal horizontal components of modified and synthetic excitation sets respectively.

Bearing Axial Forces and Hold-down Device Design Forces

Table 4.51: Bearing axial forces (Bridge 4)

Axis	ID	D	1	2	3	C1	C2	C3	C4	C5
A1	1	1006	44	410	327	210	595	541	927	1292
	2	1006	44	271	327	167	423	265	521	463
P2	5	2788	34	585	1106	126	285	224	383	422
	6	2788	34	387	1106	150	398	482	729	1232
P3	9	2785	34	416	1111	158	426	492	760	1246
	10	2786	34	276	1111	210	595	541	927	1292
A4	13	1007	48	458	326	139	318	450	619	1204
	14	1007	48	303	326	158	426	492	760	1246

Results indicated that hold-down requirement arises for none of the bearings. AASHTO requirements were not triggered, and also load combinations C3, C4 and C5 affirmed so. Recalling earlier explanations made in this chapter for Bridges 1 and 2, it is expected that longitudinal earthquake motion would not create uplift forces in bearings, as it was the case indeed. Also it was explained for the same bridges that, since bearing numbers on a pier increase, loss of compression forces decrease as a consequence of greater redundancy. Thus outcomes of this case can be justified by sense, considering the similarity with the bearing layout with that of Bridge 2.

Bearing axial forces calculated from one-directional LTH cases are shown in Table 4.52.

Table 4.52: Bearing axial forces from one-directional LTH analyses (Bridge 4)

Axis	**ID**	**4**	**5**	**6**
A1	1	44	424	345
	2	44	281	345
P2	5	32	605	1078
	6	32	400	1078
P3	9	30	436	1082
	10	30	288	1082
A4	13	49	478	342
	14	49	317	342

Table 4.52 (continued)

Ratios of maximum bearing axial forces calculated from LTH analyses to the ones obtained from RSP analyses were compared to verify modified accelerograms and chosen Rayleigh damping coefficients in Figure 4.61.

The ratios are;

- 1.04 in average in X direction.
- 1.04 in average in Y direction.
- 1.01 in average in Z direction.

Results verified the conformity of selected Rayleigh damping coefficient and generated accelerograms.

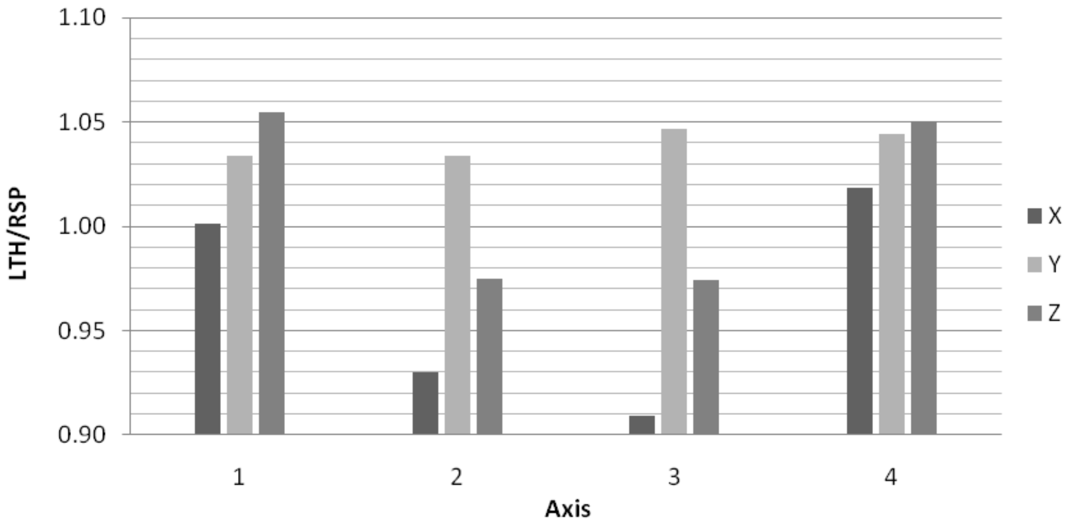

Figure 4.61: Comparison of bearing forces of LTH and RSP analyses (Bridge 4)

Bearing axial forces obtained from LTH case 7 are shown in Table 4.53. Since no tensile bearing forces were observed from the results multi-directional LTH analysis cases, there is no need to perform any NLTH analyses further.

Table 4.53: Bearing axial forces from multi-directional LTH analyses (Bridge 4)

Axis	**ID**	**7**	
		T.	**C.**
A1	1	-	1577
	2	-	1472
P2	5	-	4111
	6	-	4012
P3	9	-	4019
	10	-	3958
A4	13	-	1639
	14	-	1521

Compressive axial forces which bearings are exposed to under applied earthquake excitations are plotted for the same analyses cases on Figure 4.62.

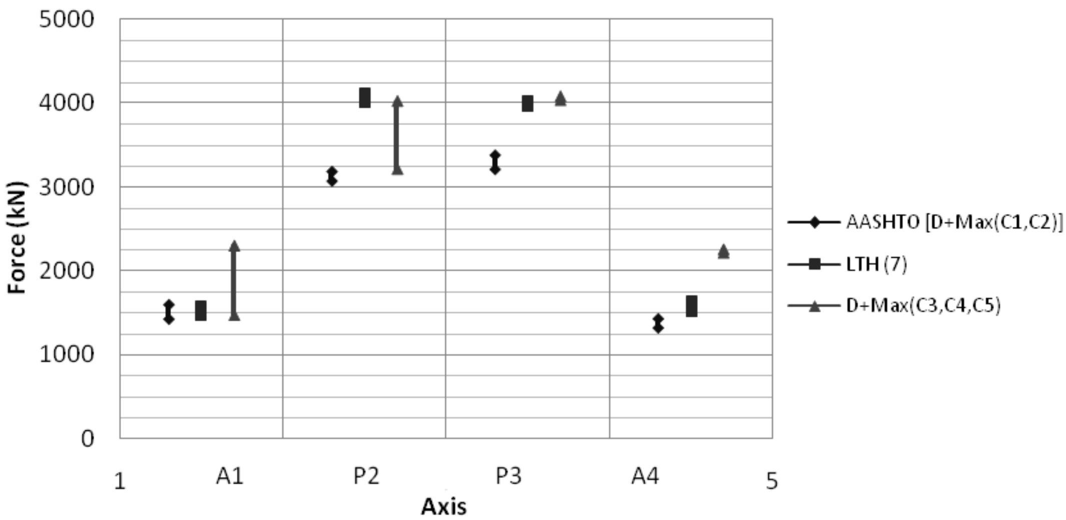

Figure 4.62: Comparison of Compressive Bearing Axial Forces (Bridge 4)

Results showed that AASHTO load combinations (C1 and C2) tended to underestimate bearing forces up to 22.5% at P2 axis, being 12.4% in average. This outcome matched those of earlier cases, as mentioned load combinations do not take into account the responses due to vertical excitation.

Load combinations C3, C4 and C5 produced overestimated results, being 45.7% and 37.4% greater at abutments A1 and A4, and 20.6% larger in average.

Pier Forces

Results are tabulated in Table 4.54 and Table 4.55

Table 4.54: Maximum pier moments about transverse direction (Bridge 4)

Axis	**D+[Max(C1,C2)]**	**7, 8**	**D+[Max(C3,C4,C5)]**
P2	43717	43494	43997
P3	44839	44131	44971

Table 4.55: Maximum pier moments about longitudinal direction (Bridge 4)

Axis	**D+[Max(C1,C2)]**	**7, 8**	**D+[Max(C3,C4,C5)]**
P2	48869	48510	48869
P3	67730	66947	67731

Pier moments are plotted for these analyses cases on Figure 4.36 and Figure 4.37.

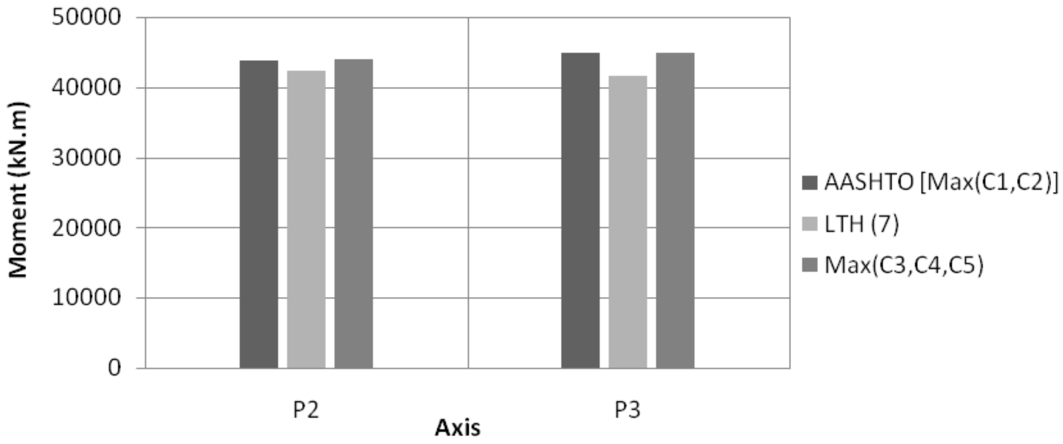

Figure 4.63: Pier moments about transverse (Y) axis (Bridge 4)

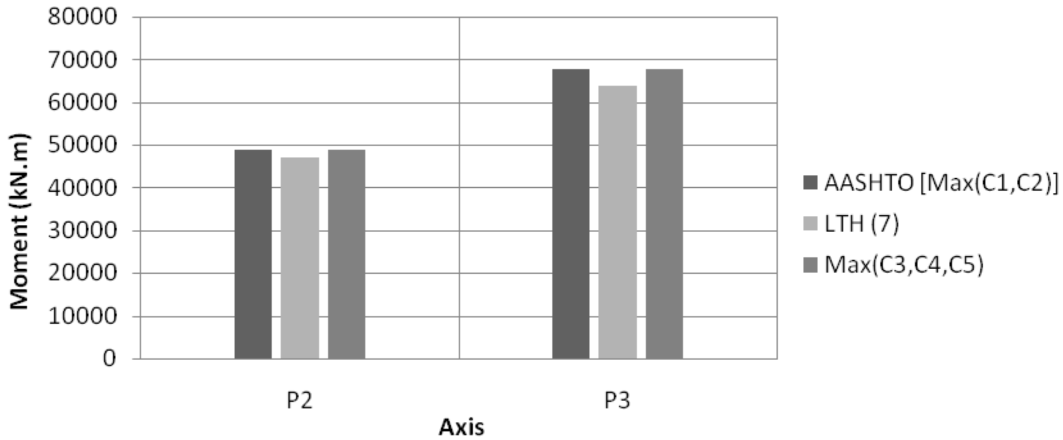

Figure 4.64: Pier moments about longitudinal (X) axis (Bridge 4)

Results pointed out that differences between RSP load combinations and time-history analyses are 5.7% for moments under longitudinal excitation (moments about transverse direction), and 5% under transverse excitation (moments about longitudinal direction) in average. Same deviations were obtained as 6.2% and 5% for combinations C3, C4 and C5. In conformity with the results obtained earlier, it is concluded that this difference originated from the nature of Rayleigh damping matrix and small unconformity of pseudo acceleration spectrum of scaled accelerograms with design response spectrum.

Vertical excitation had no considerable effect on pier moments as in other cases.

All load combinations were deemed to be accurate for this case.

Pier axial forces are tabulated Table 4.56, Table 4.57, Table 4.58 and Table 4.59.

Table 4.56: Absolute maximum pier axial forces from Dead and RSP analysis (Bridge 4)

Axis	**D**	**1**	**2**	**3**
P2	13281	138	0	4528
P3	14705	139	0	4755

Table 4.57: Maximum and minimum pier axial forces, RSP load combinations (Bridge 4)

Direction	**Axis**	**D+C1**	**D+C2**	**D+C3**	**D+C4**	**D+C5**
Minimum	P2	13143	13240	11785	11881	8712
	P3	14567	14664	13140	13237	9909
Maximum	P2	13420	13323	14778	14681	17851
	P3	14844	14747	16271	16174	19502

Table 4.58: Maximum and minimum pier axial forces from LTH case 7 (Bridge 4)

Direction	**Axis**	**7**
Minimum	P2	8764
	P3	9860
Maximum	P2	17609
	P3	19261

Table 4.59: AASHTO Reduced minimum pier axial forces (Bridge 4)

Direction	Axis	0.75D+C1	0.75D+C2
Minimum	P2	9823	9919
	P3	10890	10987

Results are plotted on Figure 4.65 and Figure 4.66.

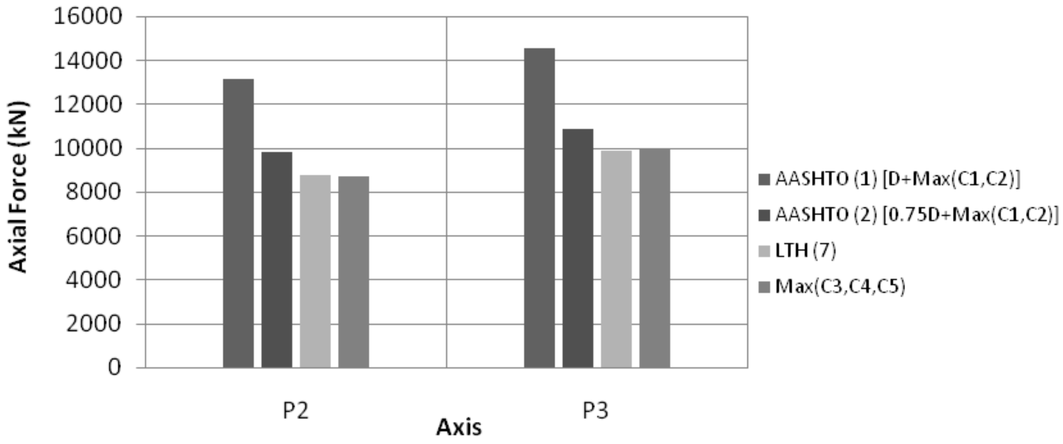

Figure 4.65: Minimum pier axial forces (Bridge 4)

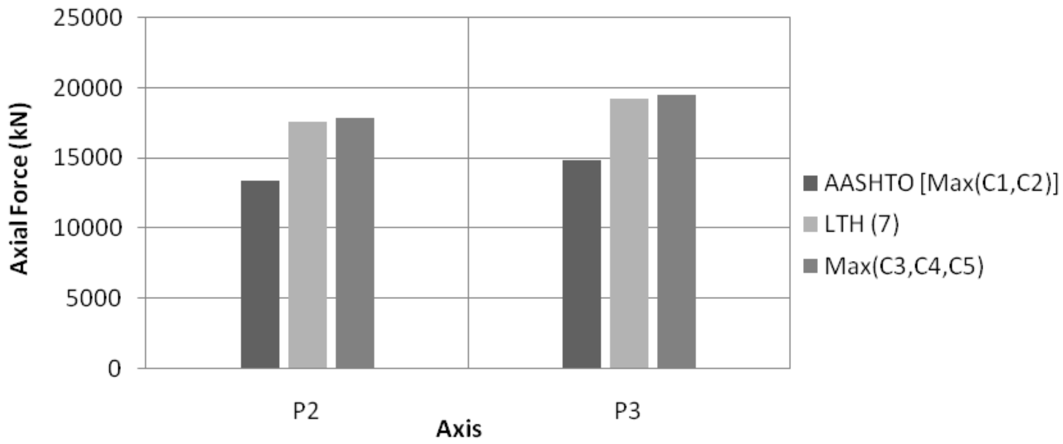

Figure 4.66: Maximum pier axial forces (Bridge 4)

Results pointed out vertical excitation altered pier axial forces by 33.2% in average, which is of nearly the same value of change in compressive bearing forces and cap beam moments. AASHTO load combinations overestimated (48.9%) and underestimated (23.4%) minimum and maximum axial forces in piers. Combinations C3, C4 and C5 produced accurate results for both responses (0.1% smaller for maximum axial forces and 1.3% greater for minimums). Reduced AASHTO load combinations provided axial forces that were greater by 11.3% in average.

CHAPTER 5

SUMMARY AND DISCUSSIONS

Investigated case studies are summarized in Table 5.1.

Table 5.1: Summary of analysis models

Id	Superstructure Type	Span Length (m)	Continuity
Bridge 1	Pre-stressed Precast I-Girders	30	Slab
Bridge 2	Steel I-Girders + Concrete Deck	60	Superstructure
Bridge 3	Post-tensioned Box Section	60	Superstructure
Bridge 4	Steel Box Section + Concrete Deck	60	Superstructure

Following responses were examined for each model through this study:

1) Hold-down device requirement and design forces
2) Compressive forces in bearings
3) Moments in cap beams
4) Moments and axial forces in piers

Deviations of results obtained from AASHTO load combinations, and C3, C4 and C5 are presented in Table 5.2 and Table 5.3 respectively, in terms of *percentage*. Results of NLTH case 9 are taken as reference for bridges 1 and 2, where hold-down devices were utilized. In the remaining ones, results of LTH case 7 are used for same purpose. Responses that are not available for a specific case are left blank on these tables. Comparison of pier moments is not included in this summary, since only minor deviations of those resulted from inevitable side effects as explained earlier in Section 4.3.

Table 5.2: Summary of results of load combinations C1 and C2

ID	HD Forces			Bearing Compressive Forces			Cap Beam Moments			Pier Axial Forces	
	+	-	*Avg.*	+	-	*Avg.*	+	-	*Avg.*	*Min.*	*Max.*
1	15.8	-12.6	0.7	2.8	-20.0	-5.8		-28.4	-24.7	58.3	-27.3
2					-17.6	-10.6		-13.2	-9.0	36.1	-21.1
3	68.0		61.7		-21.1	-16.6				51.9	-25.5
4					-22.5	-12.4				48.9	-23.4

Table 5.3: Summary of results of load combinations C3, C4 and C5

ID	HD Forces			Bearing Compressive Forces			Cap Beam Moments			Pier Axial Forces	
	+	-	*Avg.*	+	-	*Avg.*	+	-	*Avg.*	*Min.*	*Max.*
1	7.2	-10.9	1.0	8.8	-2.8	2.8	1.8	-1.1	0.5	-5.7	0.1
2					-10.5	-4.5	1.0	-0.4	0.3	-1.1	0.1
3	143.2		102.9		-17.2	-7.6				-4.2	0.2
4				45.7		20.6				-0.1	1.3

Average deviations are visualized on Figure 5.1, Figure 5.2, Figure 5.3 and Figure 5.4.

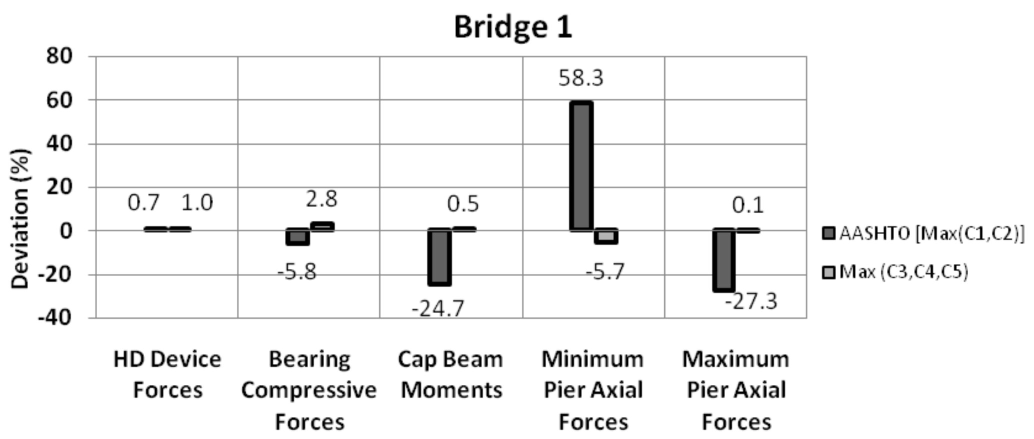

Figure 5.1: Average deviations for case study 1

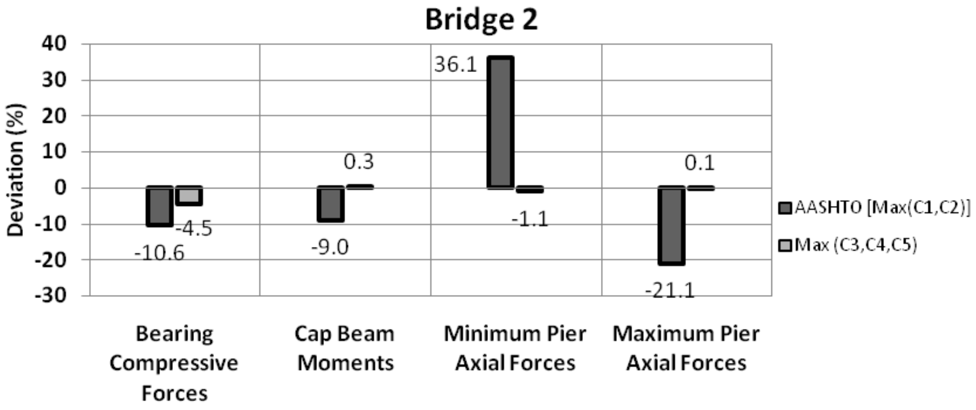

Figure 5.2: Average deviations for case study 2

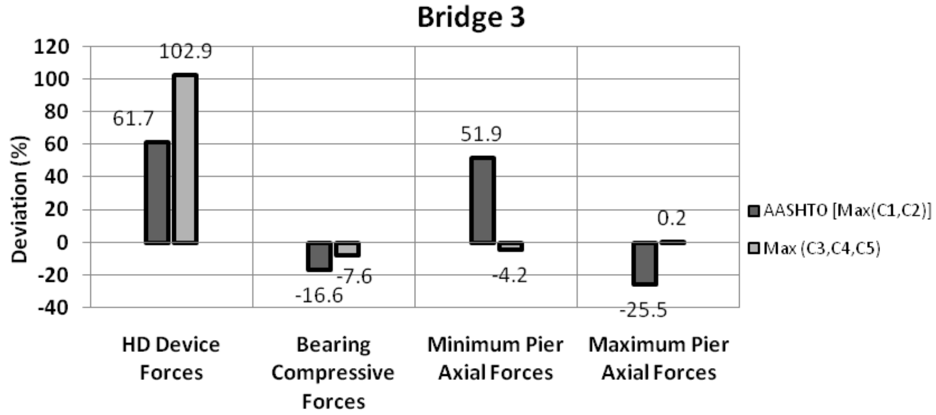

Figure 5.3: Average deviations for case study 3

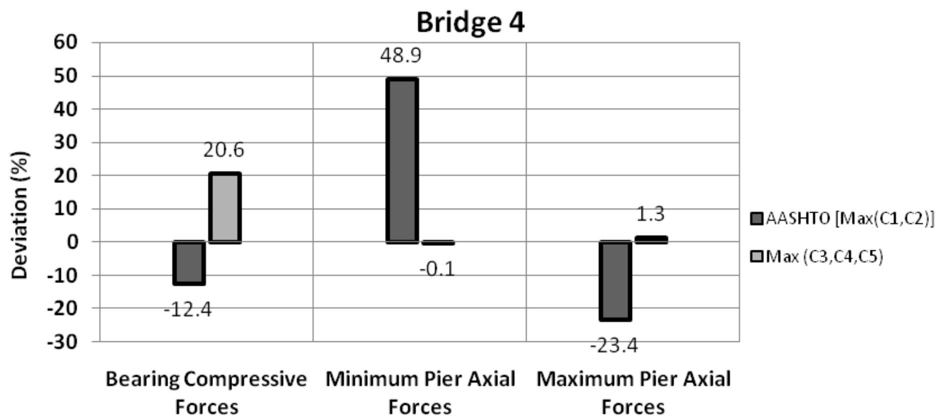

Figure 5.4: Average deviations for case study 4

Uplift forces in bearings due to vertical excitations were in average 51.1%, 29.5%, 38.6% and 36.1% of the compressive forces under dead loads for those case studies. Hence, it can be concluded that exceedance limit of 50% of forces under dead loads supplied in AASHTO to necessitate hold-down device design conservatively compensates effects of vertical excitation for these case studies. This requirement was also verified by LTH and NLTH cases. Absence of devices did not result in exceedance of support lengths for both Bridge 1 and Bridge 2. However, longitudinal displacements of bearings significantly increased for precast pre-stressed I-girder bridge (up to 2.6 times at abutments, and 5.7 times at piers). This increase was 42.7% in average for all bearings of Bridge 3.

Alteration of pier axial forces in bearings due to vertical excitations were in average 41.5%, 27.7%, 38.1% and 33.2% of the compressive forces under dead loads for those case studies. Thus, AASHTO Load combinations underestimated maximum forces and overestimated minimum of those in conformity with the findings of [34], as these combinations do not take into account the effects of vertical excitation.

On the other hand, AASHTO suggest a decrease of 0.25 times the actual load to check minimum axial load with maximum moment for column design in bridges of SPC A [2]. Even this approach were checked for all case studies, results showed that it can still yield an underestimation of axial force decrease due to vertical excitation especially for precast pre-stressed I-girder and composite steel I-girder bridges. Such an unexpected decrease of axial forces can lead to insufficient moment and shear capacity under strong ground motion.

An additional remark was that, bearings on the long piers of Bridge 1 possessed approximately two times greater uplift forces than those on short ones.

CHAPTER 6

CONCLUSIONS

Evaluation of hold-down device requirement per AASHTO Bridge Specifications has been made by time history analysis. Discussions are extended to cover variations of substructure responses due to vertical excitation, using six response spectrum compatible earthquake records, each having three orthogonal components (two horizontal and one vertical). An open-source freeware program, "RSCA" was debugged and improved for this research.

Using results of nonlinear and linear time-history analyses as reference, those obtained from AASHTO load combinations were compared for the investigated bridges of four different types.

The following conclusions based on the results of investigated bridges are:

1) The hold-down device requirements for uplift per AASHTO were satisfactory to identify the bearings that are vulnerable to uplift. However, the associated design forces could be underestimated by 10% for precast pre-stressed I-girder bridge or overestimated up to 60% for the case of post-tensioned concrete box section.

2) Similar to uplift forces, bearing compressive forces were also underestimated (5.8% - 16.6%). Inclusion of vertical excitation in AASHTO load combinations supplied more accurate design forces except for composite steel box section superstructure, in which forces were overestimated by 20%.

3) Even though AASHTO does not suggest considering vertical excitation in related load combinations for standard highway bridges, the cap beam moments for pre-stressed I-girder bridge were underestimated by 25%. Inclusion of vertical excitation to the load combinations was observed to eliminate these deviations in analysis results.

Moreover, AASHTO load combinations overestimated minimum pier axial forces by 35-60%, under dead loads and strong ground motion. These combinations also underestimated maximum axial forces by approximately 25% for all bridges. Reduced AASHTO load combinations (0.75D+EQ) decreased the deviations of minimum axial forces (2% to 21%). However, differences were still significant in especially precast pre-stressed I-girder bridge (17% in average). On the other hand, consideration of vertical responses in AASHTO load combinations provided quite accurate results.

4) Stability due to unseating of girders was not observed in the absence of hold-down devices. Stability was typically evaluated by checking the exceedance of minimum support length requirements per AASHTO. However, longitudinal bearing displacement could increase up to a ratio between 1.4 and 5.7, being especially large for precast pre-stressed I-girder bridges (increased by a ratio of 5.7 at piers).

5) Longitudinal excitations are likely to develop more vulnerability to the bearing locations of bridges with discontinuous girders over piers.

6) Transverse excitations were observed to induce more risk to bridges with bearings fewer in number and closer in spacing.

For future investigations, number of case studies including different superstructure types may be considered in the research. Different bridge configurations having discontinuous superstructures with expansion joints, various span lengths and pier heights may be helpful to achieve parametric results.

Also, increased number of strong ground motion records may be applied to improve the reliability of the results. As a final remark, additional nonlinear details to observe pounding effects and etc. may be introduced in future analyses.

REFERENCES

1. AASHTO (2000), “Guide Specifications for Seismic Isolation Design”, American Association of State Highway and Transportation Officials

2. AASHTO (2002), “Standard Specifications for Highway Bridges, 17th Edition”, American Association of State Highway and Transportation Officials

3. AASHTO (2007), “LRFD Bridge Design Specifications”, American Association of State Highway and Transportation Officials

4. API (1993), “Recommended Practice for Planning, Designing and Constructing Fixed Offshore Platforms - Working Stress Design”, American Petroleum Institute

5. ASCE-TCLEE (1999), “Lifelines Performance, Kocaeli, Turkey Earthquake, August 17, 1999”, American Society of Civil Engineering, Technical Council on Lifeline Earthquake Engineering

6. ATC (1986), “ATC 6, Seismic Design Guidelines for Highway Bridges”, Applied Technology Council

7. ATC (1996), “ATC 32, Improved Seismic Design Criteria for California Bridges: Provisional Recommendations”, Applied Technology Council

8. Bozorgnia, Y., Niazi, M. and Campbell, K. W. (1996), “Relationship Between Vertical and Horizontal Response Spectra for The Northridge Earthquake”, Proceedings, 11. World Conference of Earthquake Engineering, Acapulco, Mexico, 1996

9. Bozorgnia, Yousef, Mahin, Stephen A. and Brady, A. Gerald (1998), “Vertical Response of Twelve Structures Recorded During the Northridge Earthquake”, Earthquake Spectra, Vol.14, No.3, 411-431

10. Broekhuizen, Daniel Scott (1996), “Effects of Vertical Acceleration on Prestressed Concrete Bridges”, MS Thesis, University of Texas Austin

11. Button, Martin R., Cronin, Colman J. and Mayes, Ronald L (2002), “Effect of Vertical Motions on Seismic Response of Highway Bridges”, Journal of Structural Engineering, Vol.128, 1551-1564

12. CALTRANS (2006), “Seismic Design Criteria”, California Department of Transportation

13. Chang, K.C. (2003), “Damage Simulation of Yen-Feng Bridge under Chi-Chi Earthquake”, Presentation, Taiwan-Japan Workshop on Seismic Disaster Simulation and Loss Estimation, Taipei, Taiwan, 24-25.11.2003

14. Chopra, Anil K. (2000)., “Dynamics of Structures, Second Edition”, Prentice Hall, 843 pages

15. Clough, Ray W. and Penzien, Joseph (1975), “Dynamics of Structures International Second Edition”, McGraw-Hill Inc., 648 pages

16. Collier, C. J. and Elnashai, A. S. (2001), “A Procedure for Combining Vertical and Horizontal Seismic Action Effects”, Journal of Earthquake Engineering, Vol.5, No.4, 521-539

17. Cooper, James D., Friedland, Ian M., Buckle, Ian G., Nimis, Roland B. and Bobb, Nancy McMullin (1994), “The Northridge Earthquake Progress Made, Lessons learned in Seismic-Resistant bridge Design”, Public Roads On-line, Vol.58, No.1

18. Erduran, Emrah, Yilmaz, Zeynep, Kunnath, Sashi K., Abrahamson, Norman, Chai, Y H, Yashinsky, Mark, Sheng, Li-Hong (2006), “Effects of Near-Fault Vertical Ground Motions on Seismic Response of Highway Bridges”, Fifth National Seismic Conference on Bridges & Highways, San Francisco, California, 18.9.2006

19. General Directorate of Disaster Affairs Earthquake Research Department, Republic of Turkey (7.1.2008), “Deprem Bölgeleri Haritası”, www.deprem.gov.tr, last visited: 7.1.2008

20. Gillies, Antony G., Anderson, Donald L., Mitchell, Denis (2001), Tinawi, Rene, Saatcioglu, Murat, Gardner, N. John and Ghoborah, Ahmed “The August 17, 1999, Kocaeli (Turkey) earthquake - lifelines and preparedness”, Canadian Journal Of Civil Engineering, Vol.28, 881-890

21. Hadjian, Asadour H. (1972), “Scaling of Earthquake Accelerograms-A Simplified Approach”, Journal of the Structural Division, Vol.98, 547-551

22. Hibbeler, R.C. (2002), “Structural Analysis, Fifth Edition”, Prentice Hall, New Jersey

23. Hsu, Yao T. and Fu, Chung C. (2004), “Seismic Effect on Highway Bridges in Chi Chi Earthquake”, Journal of Performance of Constructed Facilities, Vol.18, No.1, 47-53

24. Kim, Sang-Hyo, Mha, Ho-Seong and Lee, Sang-Woo (2005), “Effects of bearing damage upon seismic behaviors of a multi-span girder bridge”, Engineering Structures, Vol.28, 1071-1080

25. Middle East Technical University, M.E.T.U. (1.12.2006), “Earthquake Engineering Research Center: Strong Ground Motion Data”, eerc.ce.metu.edu.tr, last visited: 7.1.2008

26. Ministry of Public Works and Settlement, Republic of Turkey (2007), “Afet Bölgelerinde Yapılacak Yapılar Hakkında Yönetmelik”

27. NYCDOT (2002), “Standart Specifications for Highway Bridges”, New York State Department of Transportation

28. Pamuk A., Kalkan E., H.I. Ling (2005), “Structural and geotechnical impacts of surface rupture on highway structures during recent earthquakes in Turkey”, Soil Dynamics and Earthquake Engineering, Vol.25, 581-589

29. Papageorgiou, Apostolos (1999), “Preliminary Reports From The Kocaeli (Izmit) Earthquake Of August 17, 1999”, MCEER

30. Papazoglu, A. J., Elnashai, A. S. (1996), “Analytical and Field Evidence of The Damaging Effect of Vertical Earthquake Ground Motion”, Earthquake Engineering & Structural Dynamics, Vol.25, No.10, 1109-1137

31. Theryo, Teddy S. (2004), “Precast Balanced Cantilever Bridge Design Using AASHTO LRFD Design Specifications”, Parsons Brinckerhoff

32. Thiele, Marko (2002), “Spectrum Compatible Accelerograms in Earthquake Engineering”, Universidad de La Serena, Chile, code.google.com/resca, last visited: 14.2.2008

33. U.S. Department of Transportation (1995) “Seismic Retrofitting Manual for Highway Bridges”, Federal Highway Administration

34. Wu, Haiyong and Najjar, Walid S. (2007), “Parametric Seismic Analysis of Curved Steel Box-girder Bridges with Two Continuous Spans”, Bridge Structures, Vol.3, No.3-4, 205-213

35. Yen, W. Phillip, Ghasemi, Hamid, and Cooper, James D., “Lessons Learned from Bridge Performance of the 1999 Turkish & Taiwan Earthquakes”

APPENDIX A

MODAL RESULTS FOR BRIDGE 1

Table A.1: Results of modal analysis (Bridge 1)

Mode #	Period (s)	Mass X (%)	Mass Y (%)	Mass Z (%)	Cumulative Mass X (%)	Cumulative Mass Y (%)	Cumulative Mass Z (%)
1	1.635	88.4	0.0	0.0	88.4	0.0	0.0
2	0.956	0.0	72.7	0.0	88.4	72.7	0.0
3	0.459	0.0	2.9	0.0	88.4	75.6	0.0
4	0.419	0.0	0.0	0.0	88.4	75.6	0.0
5	0.412	0.0	0.0	0.0	88.4	75.6	0.0
6	0.399	1.2	0.0	0.1	89.6	75.6	0.1
7	0.389	0.0	0.0	3.0	89.6	75.6	3.1
8	0.386	0.0	0.0	15.6	89.6	75.6	18.6
9	0.384	0.0	0.0	47.1	89.7	75.6	65.7
10	0.375	1.6	0.0	0.3	91.3	75.6	66.0
11	0.368	0.0	0.0	0.0	91.3	75.6	66.0
12	0.362	0.1	0.0	0.0	91.4	75.6	66.0
13	0.250	0.0	9.3	0.0	91.4	84.9	66.0
14	0.192	3.2	0.0	0.0	94.6	84.9	66.0
15	0.190	0.0	0.0	0.0	94.6	84.9	66.0
16	0.149	0.0	0.0	0.0	94.6	84.9	66.0
17	0.129	0.0	0.0	0.0	94.6	84.9	66.0
18	0.110	0.0	0.0	0.0	94.6	84.9	66.0
19	0.109	0.1	0.0	0.0	94.7	84.9	66.0
20	0.107	0.1	0.0	0.0	94.8	84.9	66.0
21	0.106	0.0	2.0	0.0	94.8	86.9	66.0
22	0.106	0.1	0.0	0.1	94.9	86.9	66.1
23	0.104	0.1	0.0	0.0	95.0	86.9	66.1
24	0.103	0.1	0.0	0.0	95.1	86.9	66.1
25	0.100	0.0	2.3	0.0	95.1	89.2	66.1
26	0.099	0.0	0.0	0.0	95.1	89.2	66.1
27	0.093	0.0	0.7	0.0	95.1	90.0	66.1
28	0.087	0.0	0.0	0.0	95.1	90.0	66.1
29	0.086	0.0	0.0	0.0	95.1	90.0	66.1
30	0.085	1.7	0.0	0.0	96.7	90.0	66.1
31	0.069	0.0	0.0	0.0	96.7	90.0	66.1
32	0.065	0.0	0.0	0.0	96.7	90.0	66.1
33	0.062	0.0	0.0	15.5	96.7	90.0	81.7
34	0.059	0.0	0.0	0.0	96.8	90.0	81.7

Table A.1 (continued)

Mode #	Period (s)	Mass X (%)	Mass Y (%)	Mass Z (%)	Cumulative Mass X (%)	Cumulative Mass Y (%)	Cumulative Mass Z (%)
35	0.055	0.0	1.8	0.0	96.8	91.8	81.7
36	0.055	0.0	0.0	4.5	96.8	91.8	86.2
37	0.053	0.0	0.0	1.2	96.8	91.8	87.4
38	0.050	0.0	0.0	0.4	96.8	91.8	87.8
39	0.049	0.0	0.0	0.0	96.8	91.8	87.8
40	0.045	0.0	0.0	0.0	96.8	91.8	87.8
41	0.045	0.0	0.0	0.0	96.8	91.8	87.8
42	0.044	0.0	1.0	0.0	96.8	92.8	87.8
43	0.044	0.0	0.0	0.0	96.8	92.8	87.8
44	0.043	0.0	0.0	0.0	96.8	92.8	87.8
45	0.041	0.0	0.0	0.0	96.8	92.8	87.8
46	0.039	0.0	0.6	0.0	96.8	93.4	87.8
47	0.038	0.0	0.9	0.0	96.8	94.3	87.8
48	0.038	0.0	0.1	0.0	96.8	94.3	87.8
49	0.038	0.0	0.0	0.0	96.8	94.3	87.8
50	0.038	0.0	0.0	0.5	96.8	94.3	88.3
51	0.036	0.0	0.1	0.0	96.8	94.4	88.3
52	0.036	0.0	0.0	0.7	96.8	94.4	89.0
53	0.035	0.0	0.2	0.0	96.8	94.6	89.0
54	0.034	0.0	0.3	0.0	96.8	94.9	89.0
55	0.034	0.0	0.0	0.0	96.8	94.9	89.0
56	0.034	0.3	0.0	1.1	97.1	94.9	90.1
57	0.033	0.2	0.0	1.0	97.3	94.9	91.1
58	0.032	0.0	0.0	0.0	97.3	94.9	91.1
59	0.032	0.0	0.0	0.0	97.3	94.9	91.1
60	0.032	0.0	0.0	0.0	97.3	94.9	91.1
61	0.032	0.0	0.2	0.0	97.3	95.1	91.1
62	0.031	0.5	0.0	0.9	97.8	95.1	92.0
63	0.030	0.0	0.0	0.0	97.8	95.1	92.0
64	0.029	0.0	0.0	1.1	97.9	95.1	93.2
65	0.028	0.0	0.0	0.3	97.9	95.1	93.4
66	0.027	0.0	0.0	0.1	97.9	95.1	93.5
67	0.027	0.4	0.0	0.5	98.3	95.1	94.0
68	0.027	0.0	0.3	0.0	98.3	95.4	94.0
69	0.026	0.0	0.0	0.0	98.3	95.4	94.0
70	0.026	0.0	0.0	0.5	98.3	95.4	94.5
71	0.025	0.0	0.0	0.1	98.4	95.4	94.6
72	0.023	0.0	0.0	0.1	98.4	95.4	94.6
73	0.022	0.0	0.0	0.0	98.4	95.4	94.6
74	0.021	0.0	0.0	0.0	98.4	95.4	94.6
75	0.021	0.0	0.0	0.0	98.4	95.4	94.6
76	0.021	0.0	0.1	0.0	98.4	95.5	94.6
77	0.021	0.0	0.0	0.0	98.4	95.5	94.6
78	0.021	0.0	0.0	0.0	98.4	95.5	94.6
79	0.021	0.0	0.0	0.0	98.4	95.5	94.6
80	0.021	0.0	0.0	0.0	98.4	95.5	94.6

Table A.1 (continued)

Mode #	Period (s)	Mass X (%)	Mass Y (%)	Mass Z (%)	Cumulative Mass X (%)	Cumulative Mass Y (%)	Cumulative Mass Z (%)
81	0.020	0.0	1.2	0.0	98.4	96.7	94.6
82	0.020	0.0	0.0	0.7	98.4	96.7	95.4
83	0.019	0.0	0.0	0.1	98.4	96.7	95.5
84	0.019	0.0	0.0	0.0	98.4	96.7	95.5
85	0.018	0.0	0.0	0.0	98.4	96.7	95.5
86	0.018	0.0	0.0	0.6	98.4	96.7	96.1
87	0.017	0.3	0.0	0.0	98.7	96.7	96.1
88	0.017	0.0	0.0	0.0	98.7	96.7	96.1
89	0.017	0.0	0.4	0.0	98.7	97.2	96.1
90	0.017	0.0	0.0	0.1	98.7	97.2	96.2
91	0.017	0.0	0.0	0.0	98.7	97.2	96.2
92	0.017	0.0	0.0	0.1	98.7	97.2	96.3
93	0.016	0.0	0.0	0.0	98.7	97.2	96.3
94	0.016	0.0	0.0	0.0	98.7	97.2	96.3
95	0.016	0.0	0.0	0.3	98.7	97.2	96.7
96	0.016	0.0	0.2	0.0	98.7	97.4	96.7
97	0.016	0.0	0.0	0.2	98.7	97.4	96.8
98	0.016	0.0	0.0	0.0	98.7	97.4	96.8
99	0.016	0.1	0.0	0.2	98.8	97.4	97.0
100	0.015	0.0	0.0	0.0	98.8	97.4	97.0

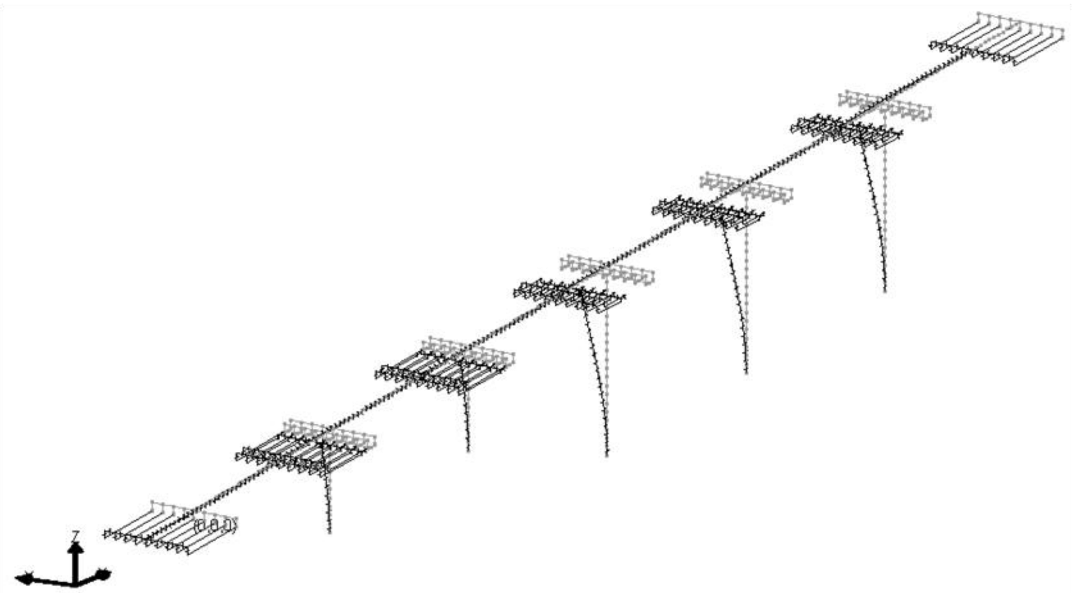

Mode 1: $T = 1.635\ sec, Mass\ Participation = 88.4\%$

Figure A.1: Shape of fundamental mode in X direction (Bridge 1)

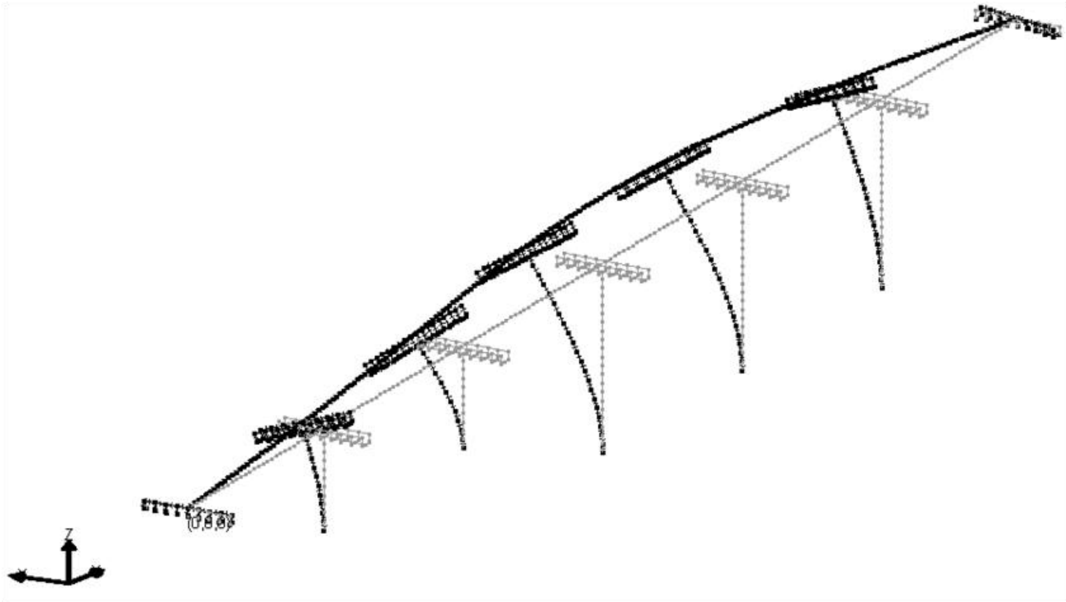

Mode 2: $T = 0.956\ sec$, $Mass\ Participation = 72.7\%$

Figure A.2: Shape of fundamental mode in Y direction (Bridge 1)

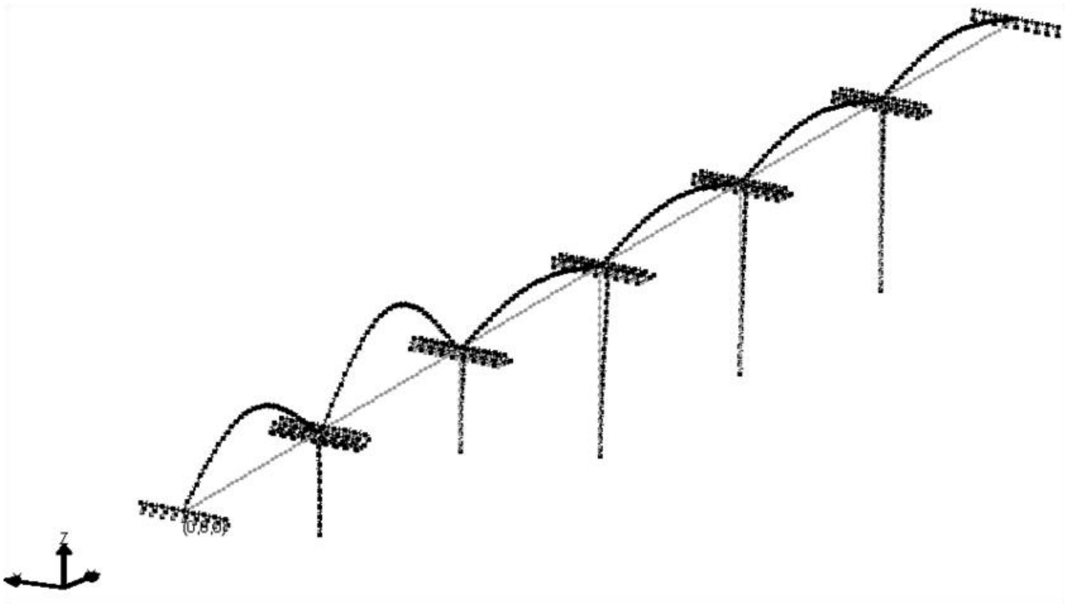

Mode 9: $T = 0.384\ sec$, $Mass\ Participation = 47.1\%$

Figure A.3: Shape of fundamental mode in Z direction (Bridge 1)

APPENDIX B

MODAL RESULTS FOR BRIDGE 2

Table B.1: Results of modal analysis (Bridge 2)

Mode #	Period (s)	Mass X (%)	Mass Y (%)	Mass Z (%)	Cumulative Mass X (%)	Cumulative Mass Y (%)	Cumulative Mass Z (%)
1	1.653	90.9	0.0	0.0	90.9	0.0	0.0
2	1.120	0.0	0.0	7.3	90.9	0.0	7.3
3	0.898	0.0	0.0	0.0	90.9	0.0	7.3
4	0.704	0.0	67.6	0.0	90.9	67.6	7.3
5	0.637	0.0	0.0	55.0	90.9	67.6	62.3
6	0.379	0.0	11.0	0.0	90.9	78.5	62.3
7	0.377	1.9	0.0	0.0	92.8	78.5	62.3
8	0.293	0.0	0.0	0.0	92.8	78.5	62.3
9	0.260	0.0	0.0	1.0	92.8	78.5	63.3
10	0.227	0.0	7.9	0.0	92.8	86.4	63.3
11	0.218	0.0	0.0	0.0	92.8	86.4	63.3
12	0.181	3.0	0.0	0.0	95.8	86.4	63.3
13	0.135	0.0	0.0	0.0	95.8	86.4	63.3
14	0.132	0.0	0.0	0.6	95.8	86.4	63.8
15	0.126	0.0	0.0	0.0	95.8	86.4	63.8
16	0.123	0.0	0.0	0.1	95.8	86.4	63.9
17	0.111	0.0	0.0	12.7	95.8	86.4	76.6
18	0.092	0.0	0.9	0.0	95.8	87.3	76.6
19	0.087	1.5	0.0	0.0	97.3	87.3	76.6
20	0.078	0.0	0.0	0.0	97.3	87.3	76.6
21	0.076	0.0	0.0	0.0	97.3	87.3	76.6
22	0.073	0.0	0.0	1.0	97.3	87.3	77.7
23	0.071	0.0	3.4	0.0	97.3	90.7	77.7
24	0.069	0.0	0.0	0.0	97.3	90.7	77.7
25	0.064	0.0	0.0	0.0	97.3	90.7	77.7
26	0.063	0.0	0.0	0.0	97.3	90.7	77.7
27	0.056	0.0	0.0	0.0	97.3	90.7	77.7
28	0.052	0.0	0.0	7.3	97.3	90.7	85.0
29	0.050	0.0	1.5	0.0	97.3	92.2	85.0
30	0.049	0.0	0.0	0.4	97.3	92.2	85.3
31	0.048	0.0	0.0	3.5	97.3	92.2	88.9
32	0.042	0.0	0.0	0.0	97.3	92.2	88.9
33	0.041	0.0	0.1	0.0	97.3	92.3	88.9
34	0.040	0.0	0.0	0.2	97.3	92.3	89.0

Table B.1 (continued)

Mode #	Period (s)	Mass X (%)	Mass Y (%)	Mass Z (%)	Cumulative Mass X (%)	Cumulative Mass Y (%)	Cumulative Mass Z (%)
35	0.035	0.0	0.0	1.0	97.3	92.3	90.1
36	0.035	0.0	0.0	0.0	97.3	92.3	90.1
37	0.033	0.0	1.0	0.0	97.3	93.3	90.1
38	0.032	0.5	0.0	0.0	97.9	93.3	90.1
39	0.032	0.0	1.0	0.0	97.9	94.3	90.1
40	0.032	0.0	0.0	0.0	97.9	94.3	90.1
41	0.031	0.0	0.0	3.3	97.9	94.3	93.4
42	0.029	0.0	0.0	0.0	97.9	94.3	93.4
43	0.028	0.9	0.0	0.0	98.8	94.3	93.4
44	0.028	0.0	0.0	1.0	98.8	94.3	94.4
45	0.027	0.0	1.1	0.0	98.8	95.3	94.4
46	0.026	0.0	0.0	0.3	98.8	95.3	94.7
47	0.025	0.0	0.0	0.0	98.8	95.3	94.7
48	0.025	0.0	0.4	0.0	98.8	95.7	94.7
49	0.024	0.0	0.0	0.0	98.8	95.7	94.7
50	0.022	0.0	0.0	0.4	98.8	95.7	95.1
51	0.021	0.0	0.0	0.0	98.8	95.7	95.1
52	0.021	0.0	0.0	0.0	98.8	95.7	95.1
53	0.020	0.0	0.0	0.0	98.8	95.7	95.1
54	0.020	0.0	0.5	0.0	98.8	96.3	95.1
55	0.020	0.0	0.0	1.0	98.8	96.3	96.1
56	0.018	0.0	0.0	0.1	98.8	96.3	96.2
57	0.018	0.0	0.0	0.0	98.8	96.3	96.2
58	0.018	0.0	0.0	0.0	98.8	96.3	96.2
59	0.017	0.3	0.0	0.0	99.0	96.3	96.2
60	0.017	0.0	0.0	0.1	99.0	96.3	96.3
61	0.016	0.0	0.0	0.0	99.0	96.3	96.4
62	0.016	0.0	0.4	0.0	99.0	96.7	96.4
63	0.016	0.0	0.0	0.0	99.0	96.7	96.4
64	0.015	0.0	0.0	0.1	99.0	96.7	96.5
65	0.015	0.0	0.3	0.0	99.0	97.0	96.5
66	0.015	0.0	0.0	0.0	99.0	97.0	96.5
67	0.014	0.0	0.2	0.0	99.0	97.2	96.5
68	0.014	0.0	0.0	0.0	99.0	97.2	96.5
69	0.014	0.0	0.0	0.1	99.0	97.2	96.5
70	0.014	0.0	0.0	0.6	99.0	97.2	97.1
71	0.013	0.0	0.0	0.1	99.0	97.2	97.2
72	0.013	0.0	0.0	0.0	99.0	97.2	97.2
73	0.013	0.0	0.0	0.0	99.0	97.2	97.2
74	0.012	0.0	0.7	0.0	99.0	97.8	97.2
75	0.012	0.0	0.1	0.0	99.0	97.9	97.2
76	0.012	0.0	0.0	0.2	99.0	97.9	97.4
77	0.012	0.0	0.0	0.1	99.0	97.9	97.5
78	0.012	0.0	0.0	0.0	99.0	97.9	97.5
79	0.011	0.0	0.0	0.0	99.0	97.9	97.5
80	0.011	0.0	0.0	0.2	99.0	97.9	97.6

Table B.1 (continued)

Mode #	Period (s)	Mass X (%)	Mass Y (%)	Mass Z (%)	Cumulative Mass X (%)	Cumulative Mass Y (%)	Cumulative Mass Z (%)
81	0.011	0.2	0.0	0.0	99.2	97.9	97.6
82	0.011	0.3	0.0	0.0	99.5	97.9	97.6
83	0.011	0.0	0.0	0.3	99.5	97.9	97.9
84	0.011	0.0	0.0	0.0	99.5	97.9	97.9
85	0.010	0.0	0.2	0.0	99.5	98.1	97.9
86	0.010	0.0	0.0	0.0	99.5	98.1	97.9
87	0.010	0.0	0.0	0.1	99.5	98.1	97.9
88	0.010	0.0	0.0	0.1	99.5	98.1	98.1
89	0.010	0.0	0.0	0.0	99.5	98.2	98.1
90	0.010	0.0	0.3	0.0	99.5	98.4	98.1
91	0.010	0.0	0.0	0.0	99.5	98.4	98.1
92	0.010	0.0	0.0	0.1	99.5	98.4	98.2
93	0.009	0.0	0.0	0.0	99.5	98.4	98.2
94	0.009	0.0	0.0	0.0	99.5	98.4	98.2
95	0.009	0.0	0.0	0.0	99.5	98.4	98.2
96	0.009	0.0	0.0	0.1	99.5	98.4	98.3
97	0.009	0.0	0.1	0.0	99.5	98.5	98.3
98	0.009	0.0	0.0	0.0	99.5	98.5	98.3
99	0.009	0.0	0.0	0.0	99.5	98.5	98.3
100	0.008	0.0	0.0	0.0	99.5	98.5	98.3

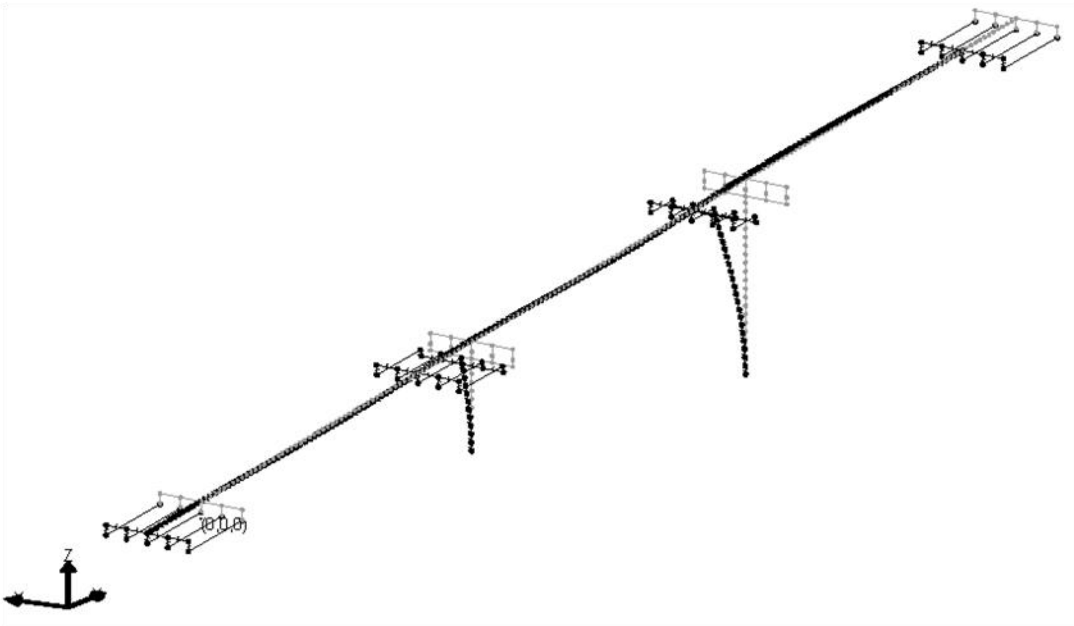

Mode 1: $T = 1.653\ sec, Mass\ Participation = 90.9\%$

Figure B.1: Shape of fundamental mode in X direction (Bridge 2)

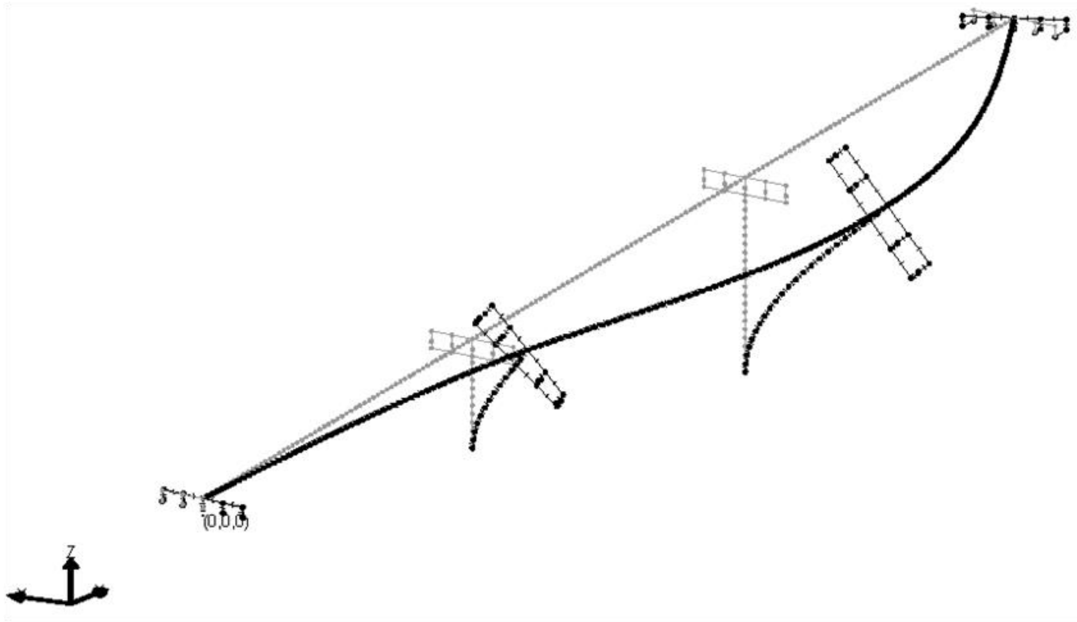

Mode 4: $T = 0.704\ sec,\ Mass\ Participation = 67.6\%$

Figure B.2: Shape of fundamental mode in Y direction (Bridge 2)

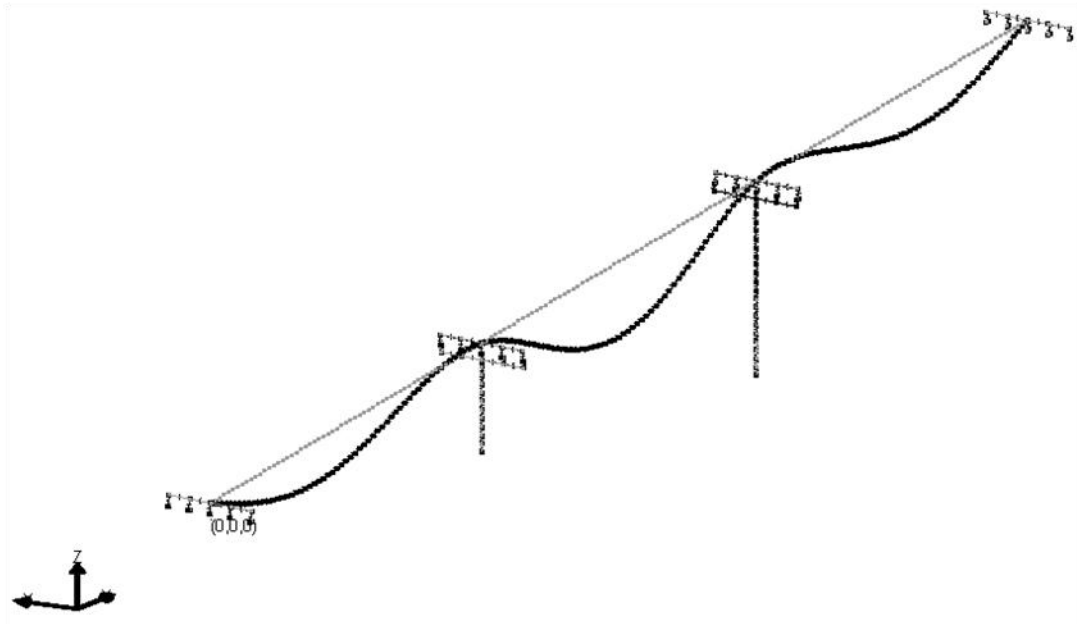

Mode 5: $T = 0.637\ sec,\ Mass\ Participation = 55.0\%$

Figure B.3: Shape of fundamental mode in Z direction (Bridge 2)

APPENDIX C

MODAL RESULTS FOR BRIDGE 3

Table C.1: Results of modal analysis (Bridge 3)

Mode #	Period (s)	Mass X (%)	Mass Y (%)	Mass Z (%)	Cumulative Mass X (%)	Cumulative Mass Y (%)	Cumulative Mass Z (%)
1	1.583	93.0	0.0	0.0	93.0	0.0	0.0
2	1.323	0.0	74.8	0.0	93.0	74.8	0.0
3	0.699	0.0	0.0	7.1	93.0	74.8	7.1
4	0.559	0.0	0.0	0.0	93.0	74.8	7.1
5	0.539	0.0	0.0	0.0	93.0	74.9	7.1
6	0.399	0.0	0.0	56.9	93.0	74.9	64.1
7	0.262	2.1	0.0	0.0	95.1	74.9	64.1
8	0.254	0.0	8.0	0.0	95.1	82.9	64.1
9	0.193	0.0	2.5	0.0	95.1	85.3	64.1
10	0.189	0.0	0.0	0.0	95.1	85.3	64.1
11	0.168	0.0	0.0	1.4	95.1	85.3	65.5
12	0.148	0.0	0.0	0.0	95.1	85.3	65.5
13	0.144	0.0	0.0	0.0	95.1	85.3	65.5
14	0.123	0.0	0.0	0.0	95.2	85.3	65.5
15	0.106	2.1	0.0	0.0	97.2	85.3	65.5
16	0.098	0.0	2.9	0.0	97.2	88.2	65.5
17	0.086	0.0	0.0	0.5	97.2	88.2	66.0
18	0.083	0.0	0.0	3.1	97.3	88.2	69.2
19	0.077	0.0	0.0	15.2	97.3	88.2	84.4
20	0.077	0.0	2.0	0.0	97.3	90.2	84.4
21	0.070	0.0	0.0	0.0	97.3	90.2	84.4
22	0.065	0.9	0.0	0.0	98.1	90.2	84.4
23	0.061	0.0	0.0	0.0	98.1	90.2	84.4
24	0.055	0.0	0.0	0.6	98.1	90.2	85.0
25	0.054	0.0	1.6	0.0	98.1	91.8	85.0
26	0.049	0.0	0.0	0.1	98.1	91.8	85.1
27	0.049	0.0	0.0	0.7	98.2	91.8	85.8
28	0.045	0.0	1.3	0.0	98.2	93.1	85.8
29	0.043	0.0	0.0	0.0	98.2	93.1	85.8
30	0.043	0.0	0.0	0.0	98.2	93.1	85.8
31	0.039	0.0	0.0	5.8	98.2	93.1	91.7
32	0.035	0.0	1.1	0.0	98.2	94.2	91.7
33	0.035	0.0	0.0	1.4	98.2	94.2	93.1
34	0.033	0.0	0.0	0.6	98.2	94.2	93.7

Table C.1 (continued)

Mode #	Period (s)	Mass X (%)	Mass Y (%)	Mass Z (%)	Cumulative Mass X (%)	Cumulative Mass Y (%)	Cumulative Mass Z (%)
35	0.031	0.0	0.0	0.0	98.2	94.2	93.7
36	0.030	0.0	0.0	0.0	98.2	94.2	93.7
37	0.029	0.0	0.0	0.1	98.2	94.2	93.7
38	0.028	0.3	0.0	0.0	98.5	94.2	93.7
39	0.026	0.0	0.7	0.0	98.5	94.9	93.7
40	0.026	0.0	0.0	0.3	98.5	94.9	94.0
41	0.026	0.0	0.0	0.0	98.5	94.9	94.0
42	0.025	0.0	0.0	0.0	98.5	94.9	94.0
43	0.024	0.1	0.0	0.0	98.7	94.9	94.0
44	0.023	0.4	0.0	0.0	99.1	94.9	94.0
45	0.023	0.0	0.0	0.0	99.1	94.9	94.0
46	0.022	0.0	0.0	1.3	99.1	94.9	95.3
47	0.021	0.0	0.0	0.0	99.1	94.9	95.3
48	0.020	0.0	0.6	0.0	99.1	95.5	95.3
49	0.020	0.0	0.0	0.1	99.1	95.5	95.4
50	0.019	0.0	0.2	0.0	99.1	95.7	95.4
51	0.018	0.0	0.0	0.0	99.1	95.7	95.4
52	0.018	0.0	0.0	0.0	99.1	95.8	95.4
53	0.018	0.0	0.0	0.3	99.1	95.8	95.7
54	0.018	0.0	0.8	0.0	99.1	96.6	95.7
55	0.018	0.0	0.0	0.0	99.1	96.6	95.7
56	0.017	0.0	0.0	0.0	99.1	96.6	95.7
57	0.016	0.0	0.5	0.0	99.1	97.0	95.7
58	0.016	0.2	0.0	0.0	99.3	97.0	95.7
59	0.016	0.0	0.0	0.0	99.3	97.0	95.7
60	0.015	0.0	0.0	0.0	99.3	97.0	95.7
61	0.015	0.0	0.0	0.0	99.3	97.0	95.7
62	0.014	0.0	0.0	0.0	99.3	97.0	95.7
63	0.014	0.0	0.4	0.0	99.3	97.4	95.7
64	0.014	0.0	0.0	0.9	99.3	97.4	96.6
65	0.014	0.0	0.0	0.0	99.3	97.4	96.6
66	0.013	0.0	0.0	0.0	99.3	97.4	96.6
67	0.013	0.0	0.0	0.0	99.3	97.4	96.6
68	0.012	0.0	0.0	0.0	99.3	97.4	96.6
69	0.012	0.0	0.4	0.0	99.3	97.8	96.6
70	0.012	0.0	0.0	0.3	99.3	97.8	96.8
71	0.012	0.0	0.0	0.2	99.3	97.8	97.0
72	0.012	0.0	0.2	0.0	99.3	98.0	97.0
73	0.011	0.0	0.0	0.0	99.3	98.0	97.0
74	0.011	0.0	0.0	0.1	99.3	98.0	97.1
75	0.011	0.0	0.0	0.0	99.3	98.0	97.1
76	0.011	0.1	0.0	0.0	99.4	98.0	97.1
77	0.011	0.0	0.0	0.3	99.4	98.0	97.4
78	0.011	0.0	0.3	0.0	99.4	98.3	97.4
79	0.010	0.2	0.0	0.0	99.6	98.3	97.4
80	0.010	0.0	0.0	0.0	99.6	98.3	97.4

Table C.1 (continued)

Mode #	Period (s)	Mass X (%)	Mass Y (%)	Mass Z (%)	Cumulative Mass X (%)	Cumulative Mass Y (%)	Cumulative Mass Z (%)
81	0.010	0.0	0.0	0.0	99.6	98.3	97.4
82	0.010	0.0	0.0	0.0	99.6	98.3	97.4
83	0.010	0.0	0.0	0.2	99.6	98.3	97.6
84	0.010	0.0	0.2	0.0	99.6	98.5	97.6
85	0.009	0.0	0.0	0.0	99.6	98.5	97.6
86	0.009	0.0	0.0	0.1	99.6	98.5	97.6
87	0.009	0.0	0.0	0.0	99.6	98.5	97.6
88	0.009	0.0	0.0	0.0	99.6	98.5	97.6
89	0.009	0.0	0.2	0.0	99.6	98.7	97.6
90	0.009	0.0	0.0	0.2	99.6	98.7	97.8
91	0.008	0.0	0.0	0.0	99.6	98.7	97.8
92	0.008	0.0	0.2	0.0	99.6	98.9	97.8
93	0.008	0.0	0.0	0.0	99.6	98.9	97.8
94	0.008	0.0	0.0	0.0	99.6	98.9	97.8
95	0.008	0.0	0.0	0.1	99.6	98.9	97.9
96	0.008	0.1	0.0	0.0	99.7	98.9	97.9
97	0.008	0.0	0.1	0.0	99.7	99.0	97.9
98	0.008	0.0	0.1	0.0	99.7	99.1	97.9
99	0.008	0.0	0.0	0.0	99.7	99.1	97.9
100	0.008	0.0	0.0	0.0	99.7	99.1	97.9

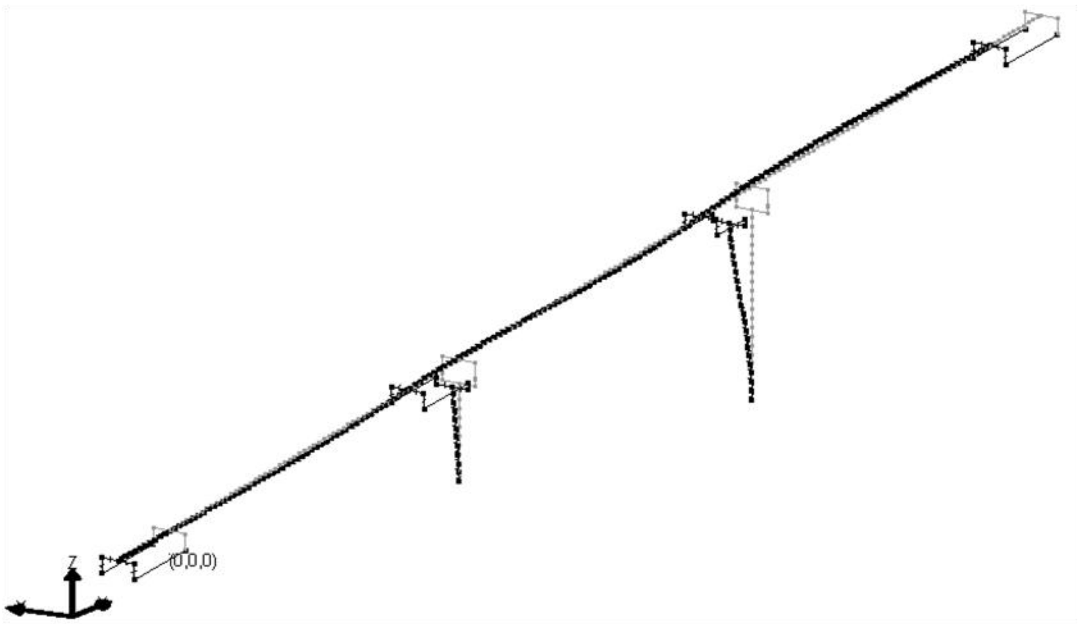

Mode 1, $T = 1.583\ sec, Mass\ Participation = 93.0\%$

Figure C.1: Shape of fundamental mode in X direction (Bridge 3)

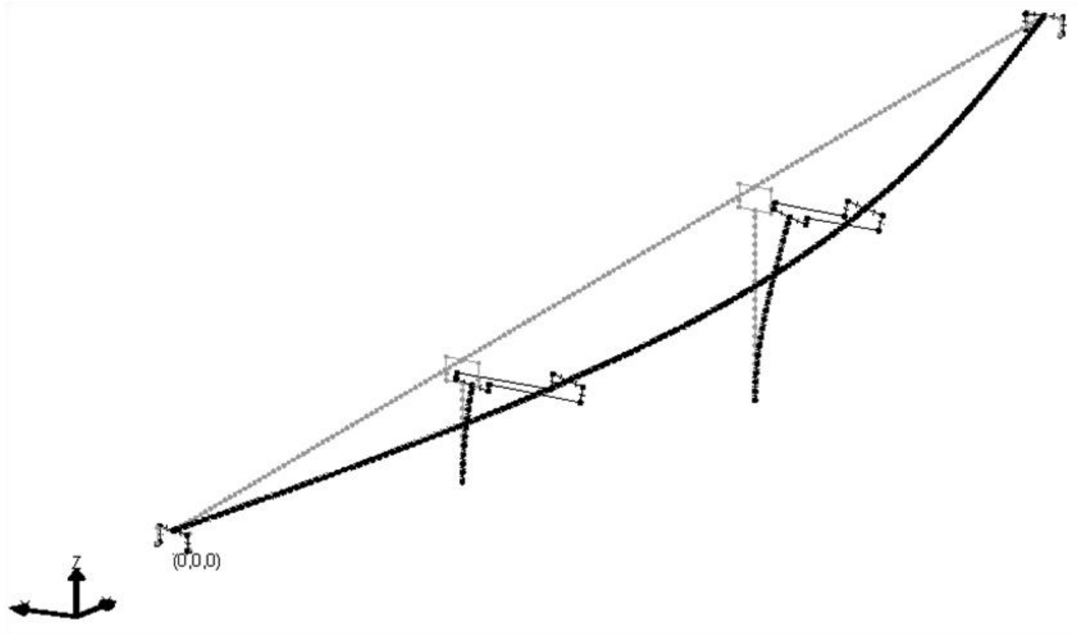

Mode 2: $T = 1.323\ sec, Mass\ Participation = 74.8\%$

Figure C.2: Shape of fundamental mode in Y direction (Bridge 3)

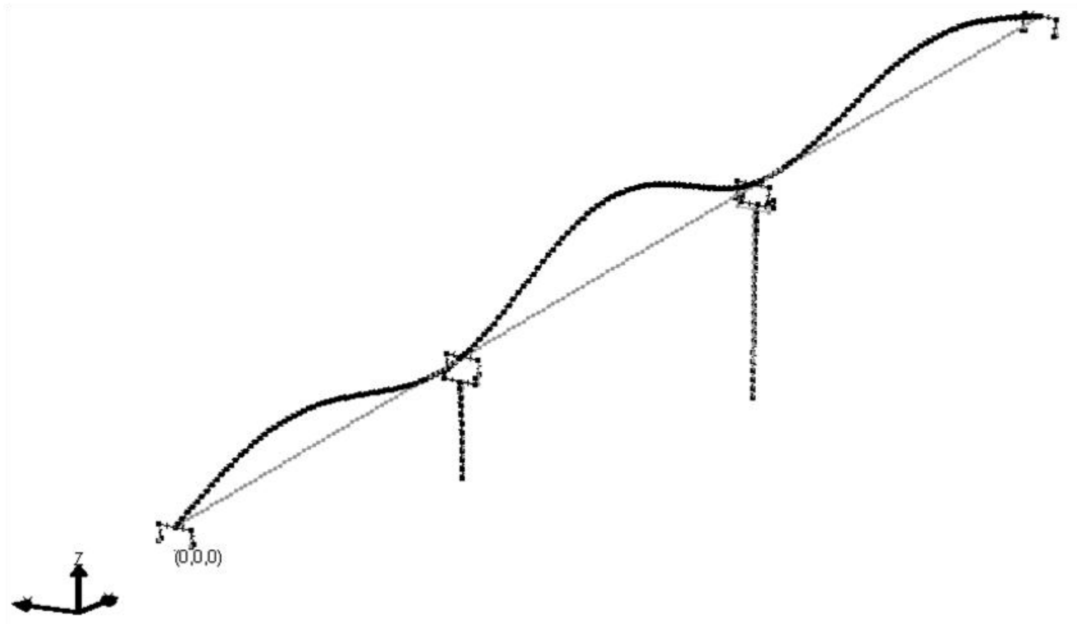

Mode 6: $T = 0.399\ sec, Mass\ Participation = 56.9\%$

Figure C.3: Shape of fundamental mode in Z direction (Bridge 3)

APPENDIX D

MODAL RESULTS FOR BRIDGE 4

Table D.1: Modal analysis results

Mode #	Period (s)	Mass X (%)	Mass Y (%)	Mass Z (%)	Cumulative Mass X (%)	Cumulative Mass Y (%)	Cumulative Mass Z (%)
1	1.552	89.7	0.0	0.0	89.7	0.0	0.0
2	1.253	0.0	72.0	0.0	89.7	72.0	0.0
3	0.807	0.0	0.0	7.1	89.7	72.0	7.1
4	0.646	0.0	0.0	0.0	89.7	72.0	7.1
5	0.512	0.0	0.0	0.0	89.7	72.0	7.1
6	0.459	0.0	0.0	54.9	89.7	72.0	62.0
7	0.345	2.4	0.0	0.0	92.1	72.0	62.0
8	0.249	0.0	3.8	0.0	92.1	75.8	62.0
9	0.246	0.0	7.2	0.0	92.1	83.1	62.0
10	0.211	0.0	0.0	0.0	92.1	83.1	62.0
11	0.188	0.0	0.0	1.1	92.1	83.1	63.1
12	0.160	0.5	0.0	0.0	92.6	83.1	63.1
13	0.158	2.7	0.0	0.0	95.2	83.1	63.1
14	0.142	0.0	0.0	0.0	95.2	83.1	63.1
15	0.129	0.0	0.0	0.0	95.2	83.1	63.1
16	0.101	0.0	2.7	0.0	95.2	85.8	63.1
17	0.096	0.0	0.0	0.5	95.2	85.8	63.7
18	0.094	0.0	3.5	0.0	95.2	89.3	63.7
19	0.090	0.0	0.0	0.4	95.3	89.3	64.1
20	0.083	0.6	0.0	9.4	95.8	89.3	73.5
21	0.083	1.1	0.0	4.9	96.9	89.3	78.4
22	0.068	0.0	0.0	0.0	96.9	89.3	78.4
23	0.065	0.0	0.0	0.0	96.9	89.3	78.4
24	0.056	0.0	0.0	1.4	96.9	89.3	79.8
25	0.055	0.0	0.0	0.2	96.9	89.3	80.1
26	0.053	0.0	0.0	0.1	96.9	89.3	80.1
27	0.053	0.0	0.1	0.0	96.9	89.5	80.1
28	0.052	0.0	3.2	0.0	96.9	92.6	80.1
29	0.048	0.0	0.0	0.0	96.9	92.6	80.1
30	0.043	0.0	0.0	0.0	96.9	92.6	80.1
31	0.042	0.0	0.0	0.0	96.9	92.6	80.1
32	0.041	0.0	0.0	8.0	96.9	92.6	88.1
33	0.037	0.0	0.0	1.4	96.9	92.6	89.5
34	0.036	0.0	0.0	1.4	96.9	92.6	90.9

Table D.1 (continued)

Mode #	Period (s)	Mass X (%)	Mass Y (%)	Mass Z (%)	Cumulative Mass X (%)	Cumulative Mass Y (%)	Cumulative Mass Z (%)
35	0.035	0.0	1.0	0.0	96.9	93.6	90.9
36	0.034	0.0	0.0	0.0	96.9	93.6	90.9
37	0.032	0.0	0.0	0.0	96.9	93.6	90.9
38	0.032	0.6	0.0	0.0	97.5	93.6	90.9
39	0.031	0.0	0.0	0.0	97.5	93.6	90.9
40	0.030	0.0	0.0	0.0	97.5	93.6	90.9
41	0.028	0.0	0.0	1.0	97.6	93.6	91.9
42	0.027	1.0	0.0	0.0	98.6	93.6	91.9
43	0.026	0.0	0.0	0.0	98.6	93.6	91.9
44	0.026	0.0	0.0	0.0	98.6	93.6	91.9
45	0.026	0.0	0.7	0.0	98.6	94.3	91.9
46	0.024	0.0	0.0	2.4	98.6	94.3	94.3
47	0.023	0.0	0.0	0.0	98.6	94.3	94.3
48	0.022	0.0	1.1	0.0	98.6	95.4	94.3
49	0.022	0.0	0.6	0.0	98.6	96.0	94.3
50	0.022	0.0	0.0	0.5	98.6	96.0	94.8
51	0.022	0.0	0.0	0.0	98.6	96.0	94.8
52	0.020	0.0	0.5	0.0	98.6	96.5	94.8
53	0.020	0.0	0.0	0.2	98.6	96.5	95.0
54	0.019	0.0	0.0	0.0	98.6	96.5	95.0
55	0.019	0.0	0.0	0.0	98.6	96.5	95.0
56	0.018	0.0	0.0	0.0	98.6	96.5	95.0
57	0.018	0.0	0.0	0.3	98.6	96.5	95.3
58	0.017	0.3	0.0	0.0	98.9	96.5	95.3
59	0.017	0.0	0.4	0.0	98.9	96.9	95.3
60	0.016	0.0	0.0	0.0	98.9	96.9	95.3
61	0.016	0.0	0.0	0.0	98.9	96.9	95.3
62	0.016	0.0	0.0	1.0	98.9	96.9	96.2
63	0.015	0.0	0.0	0.0	98.9	96.9	96.2
64	0.015	0.0	0.0	0.1	98.9	96.9	96.3
65	0.014	0.0	0.0	0.0	98.9	96.9	96.3
66	0.014	0.0	0.3	0.0	98.9	97.2	96.3
67	0.013	0.0	0.3	0.0	98.9	97.5	96.3
68	0.013	0.0	0.0	0.0	98.9	97.5	96.3
69	0.013	0.0	0.0	0.0	98.9	97.5	96.3
70	0.013	0.0	0.0	0.2	98.9	97.5	96.6
71	0.013	0.0	0.0	0.0	98.9	97.5	96.6
72	0.012	0.0	0.0	0.2	98.9	97.5	96.8
73	0.012	0.0	0.2	0.0	98.9	97.8	96.8
74	0.012	0.0	0.0	0.0	98.9	97.8	96.8
75	0.012	0.0	0.0	0.0	98.9	97.8	96.8
76	0.012	0.0	0.0	0.5	98.9	97.8	97.3
77	0.011	0.2	0.0	0.0	99.1	97.8	97.3
78	0.011	0.0	0.0	0.0	99.1	97.8	97.3
79	0.011	0.3	0.0	0.0	99.4	97.8	97.3
80	0.011	0.0	0.2	0.0	99.4	98.0	97.3

Table D.1 (continued)

Mode #	Period (s)	Mass X (%)	Mass Y (%)	Mass Z (%)	Cumulative Mass X (%)	Cumulative Mass Y (%)	Cumulative Mass Z (%)
81	0.011	0.0	0.0	0.0	99.4	98.0	97.3
82	0.011	0.0	0.0	0.1	99.4	98.0	97.5
83	0.011	0.0	0.3	0.0	99.4	98.3	97.5
84	0.010	0.0	0.0	0.0	99.4	98.3	97.5
85	0.010	0.0	0.0	0.2	99.4	98.3	97.6
86	0.010	0.0	0.0	0.0	99.4	98.3	97.6
87	0.010	0.0	0.1	0.0	99.4	98.4	97.6
88	0.010	0.0	0.0	0.1	99.4	98.4	97.7
89	0.010	0.0	0.0	0.2	99.4	98.4	97.9
90	0.009	0.0	0.0	0.0	99.4	98.4	97.9
91	0.009	0.0	0.2	0.0	99.4	98.6	97.9
92	0.009	0.0	0.0	0.0	99.4	98.6	97.9
93	0.009	0.0	0.0	0.1	99.4	98.6	97.9
94	0.009	0.0	0.1	0.0	99.4	98.7	97.9
95	0.009	0.0	0.0	0.0	99.4	98.7	97.9
96	0.009	0.0	0.0	0.0	99.4	98.7	97.9
97	0.008	0.0	0.0	0.2	99.4	98.7	98.1
98	0.008	0.0	0.0	0.0	99.4	98.7	98.1
99	0.008	0.1	0.0	0.0	99.5	98.7	98.1
100	0.008	0.0	0.1	0.0	99.5	98.8	98.1

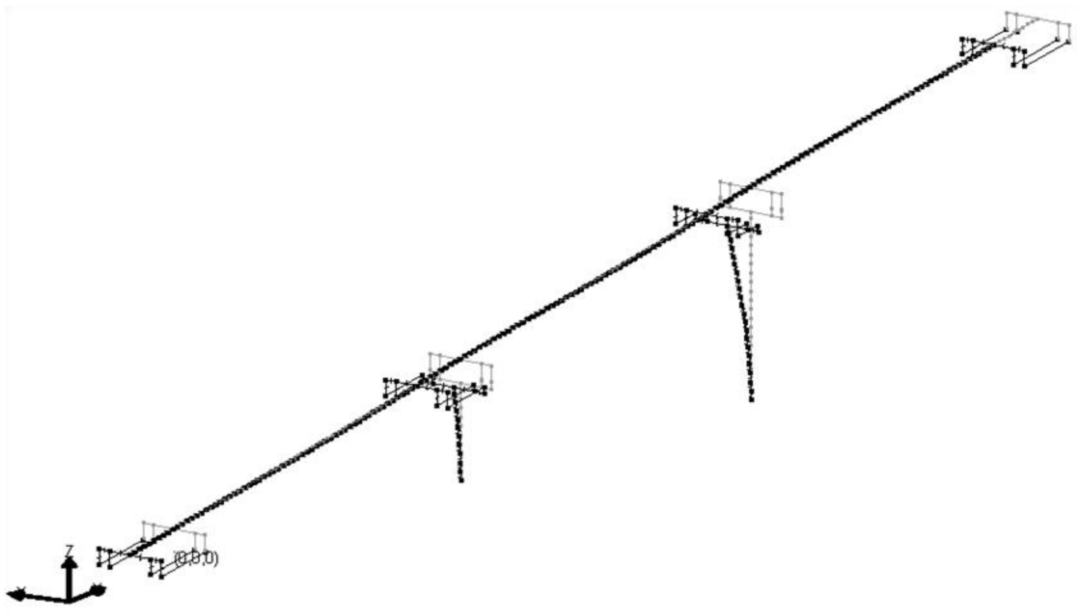

Mode 1: $T = 1.552\ sec, Mass\ Participation = 89.7\%$

Figure D.1: Shape of fundamental mode in X direction (Bridge 4)

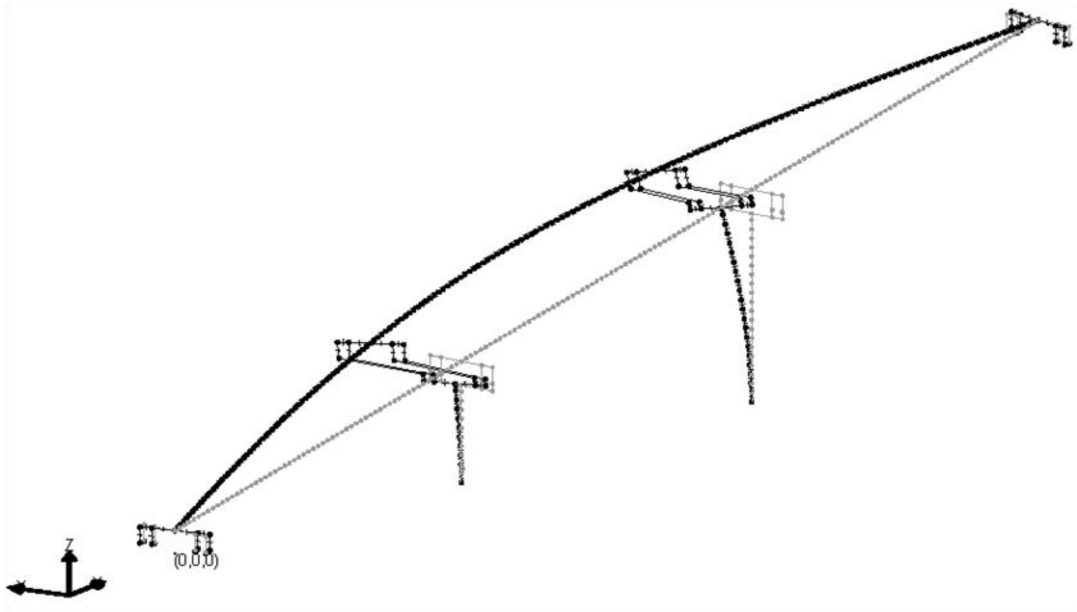

Mode 2: $T = 1.253\ sec, Mass\ Participation = 72.0\%$

Figure D.2: Shape of fundamental mode in Y direction (Bridge 4)

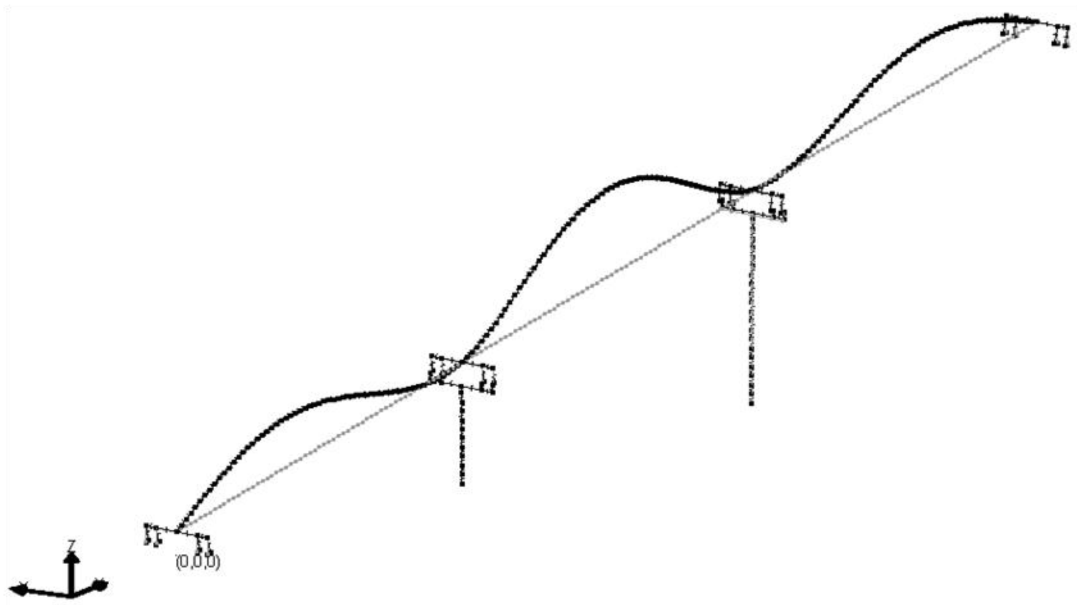

Mode 6: $T = 0.459\ sec, Mass\ Participation = 54.6\%$

Figure D.3: Shape of fundamental mode in Z direction (Bridge 4)

APPENDIX E

RESPONSE SPECTRA OF EARTHQUAKE RECORDS

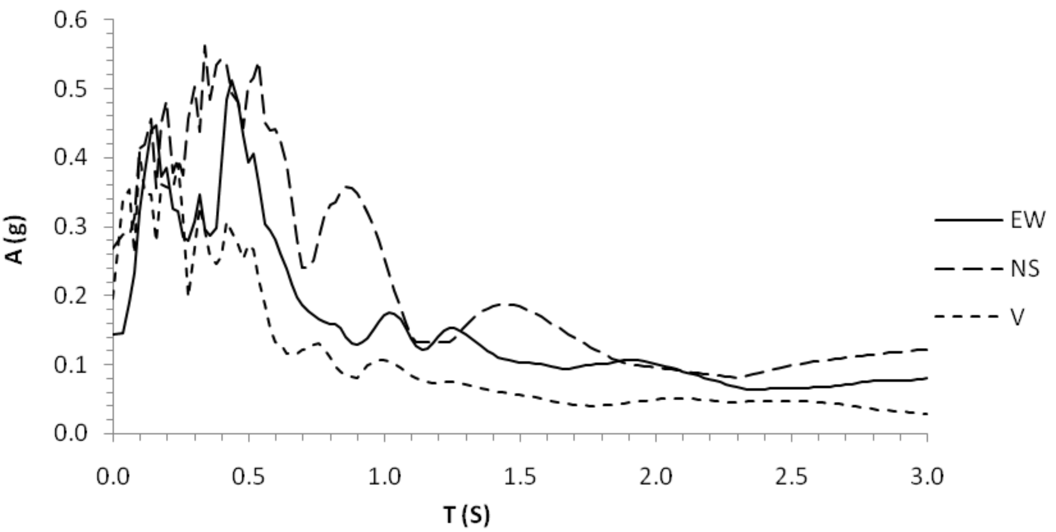

(a) Original components

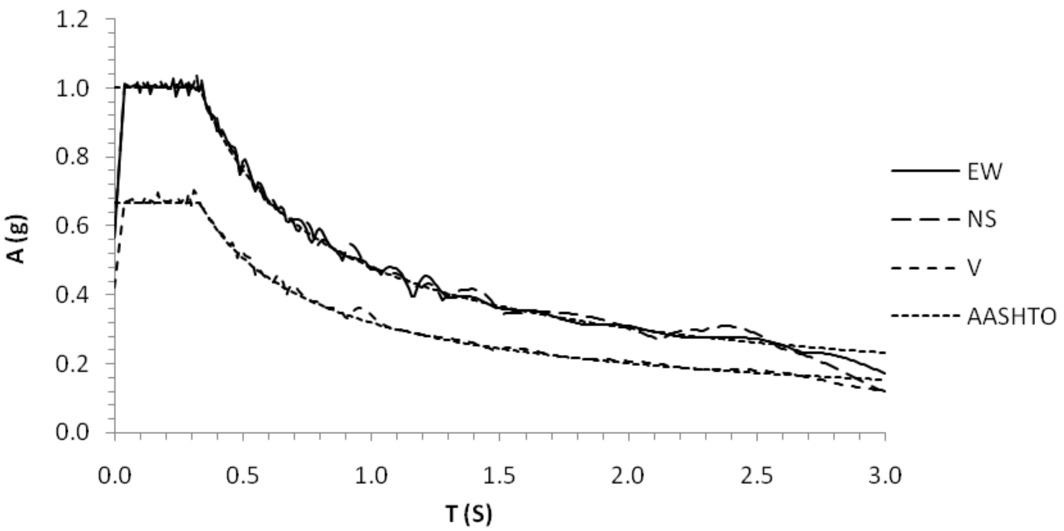

(b) Modified components

Figure E.1: Pseudo acceleration response spectra of original and modified components of record 1

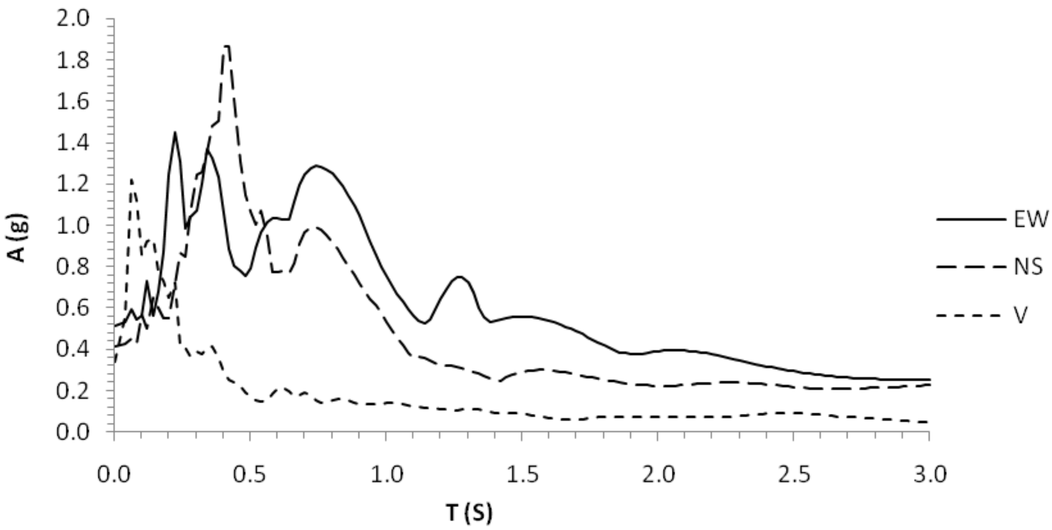

(a) Original components

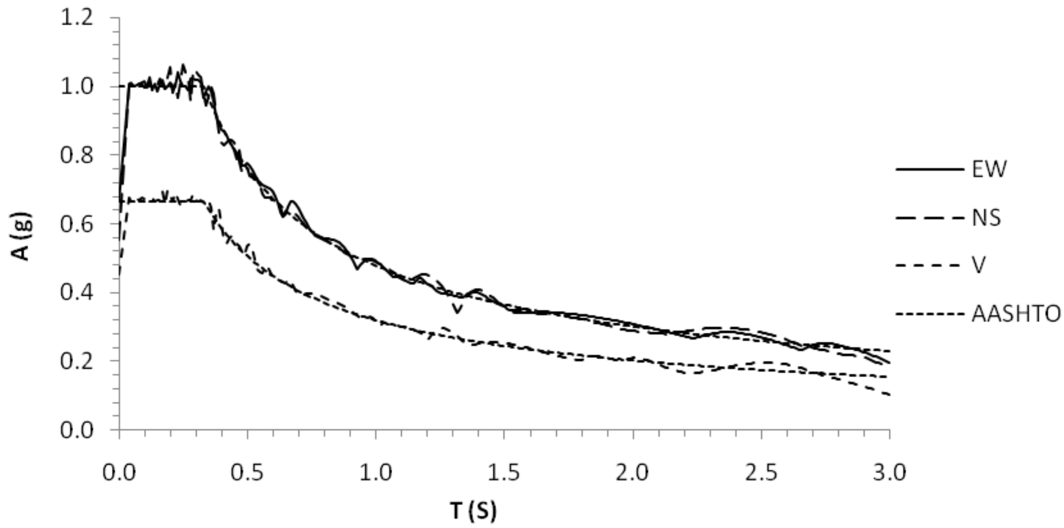

(b) Modified components

Figure E.2: Pseudo acceleration response spectra of original and modified components of record 2

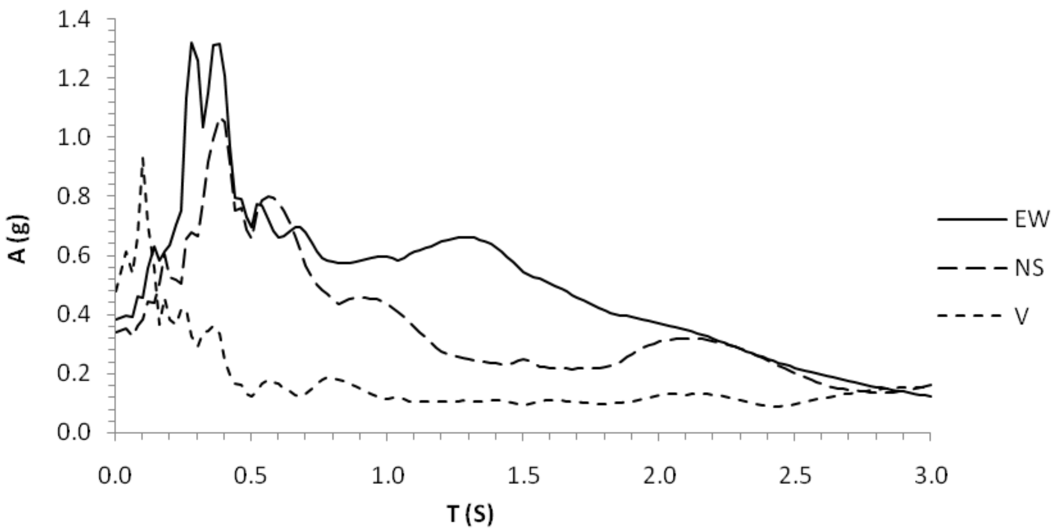

(a) Original components

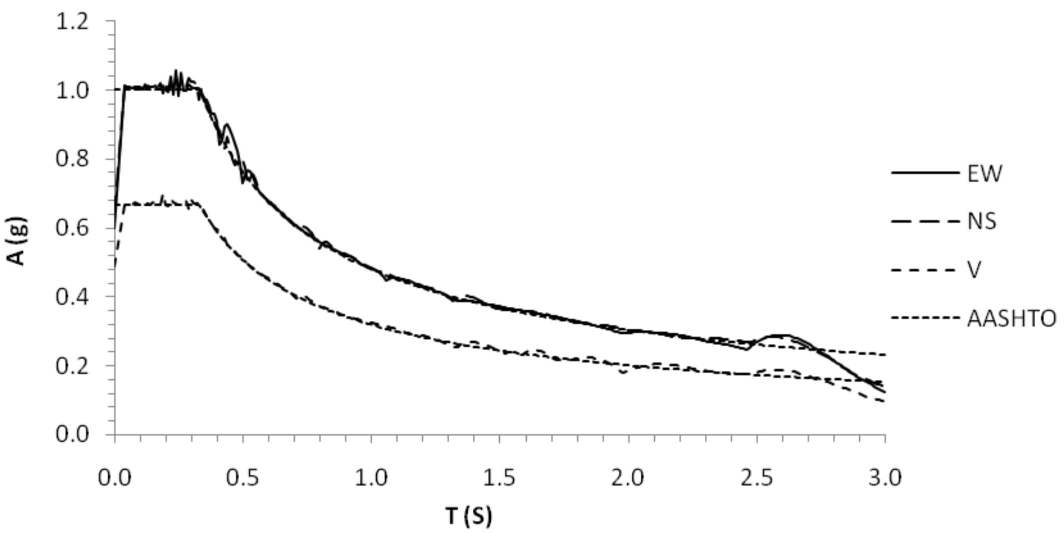

(b) Modified components

Figure E.3: Pseudo acceleration response spectra of original and modified components of record 3

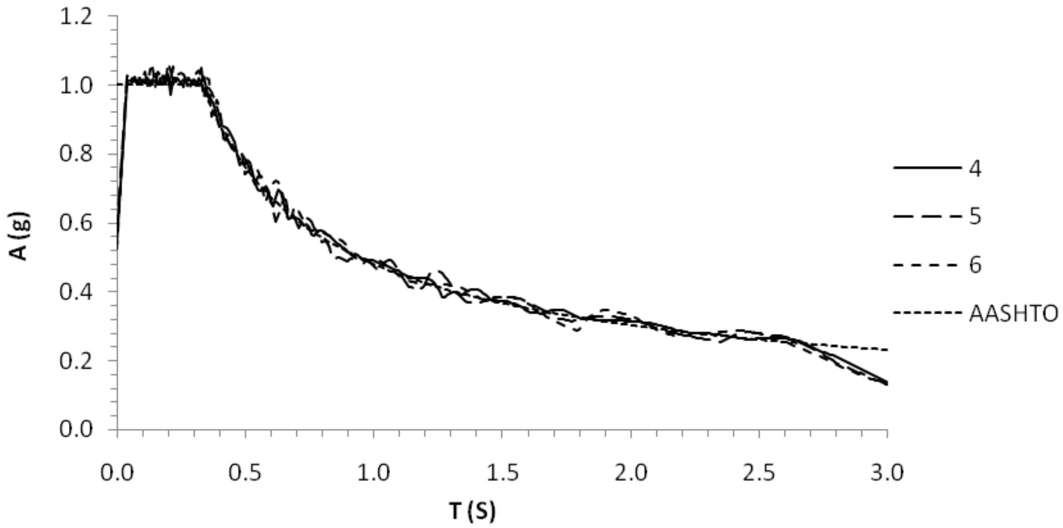

Figure E.4: Pseudo acceleration response spectra of synthetic records 4, 5 and 6

APPENDIX F

VERIFICATION OF UPLIFT FORCES FOR BRIDGE 1

For Bridge 1, the uplift forces in bearings due to longitudinal excitations originated from upper pier moments, which tended to create axial force couples in bearings along opposing sides of the cap beam. As a foresight, this superstructure type may be deemed to suffer from the discontinuity of I-girders and resulting bearing layout. Deformation of fundamental mode of vibration in longitudinal direction and moment diagram of a pier under longitudinal excitation are shown in Figure F.1.

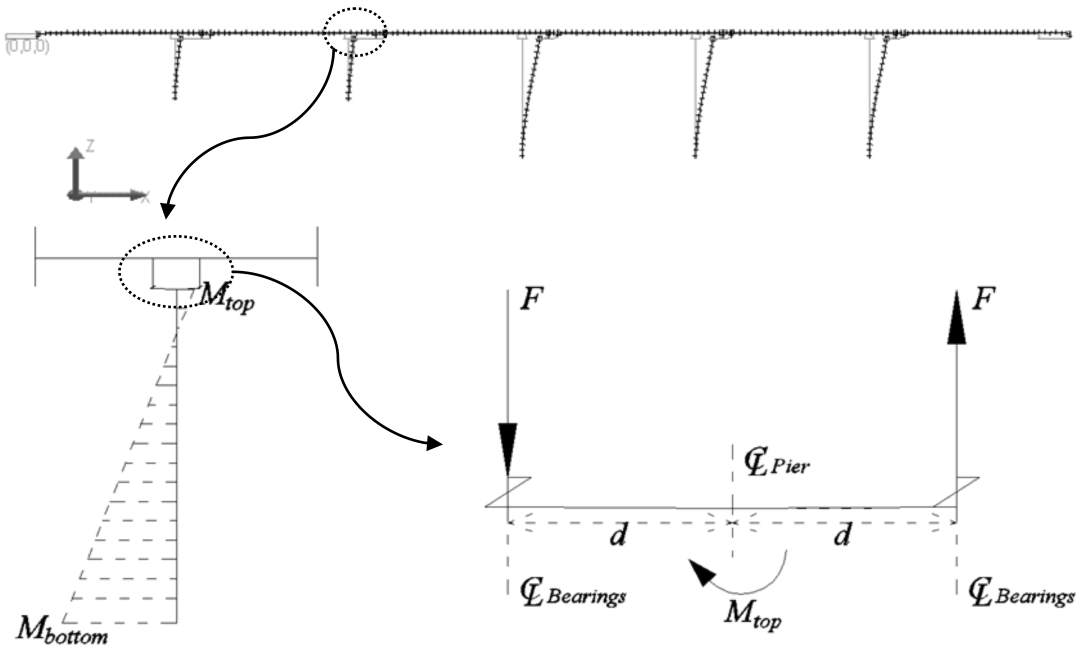

Figure F.1: Axial force in bearings couple resulting from longitudinal earthquake excitation (Bridge 1)

Axial force couple in bearings can be expressed as;

$$F = M_{top} / d \tag{F.1}$$

And total tensile and compressive axial forces in bearings become;

$$\begin{aligned} F_c &= F + F_{dead} \\ F_t &= F - F_{dead} \end{aligned} \tag{F.2}$$

It shall be noticed that bearing forces denoted by F_t need not to be in tensile direction at every time instant or for every bearing, if F resulting due to longitudinal excitation does not exceed forces under dead loads, F_{dead} . In that case, it will be equal to the lesser of two compressions forces in the bearings on opposing sides. A pier, including bearings and superstructure connection can be idealized as a single degree of freedom system as shown in Figure F.2.

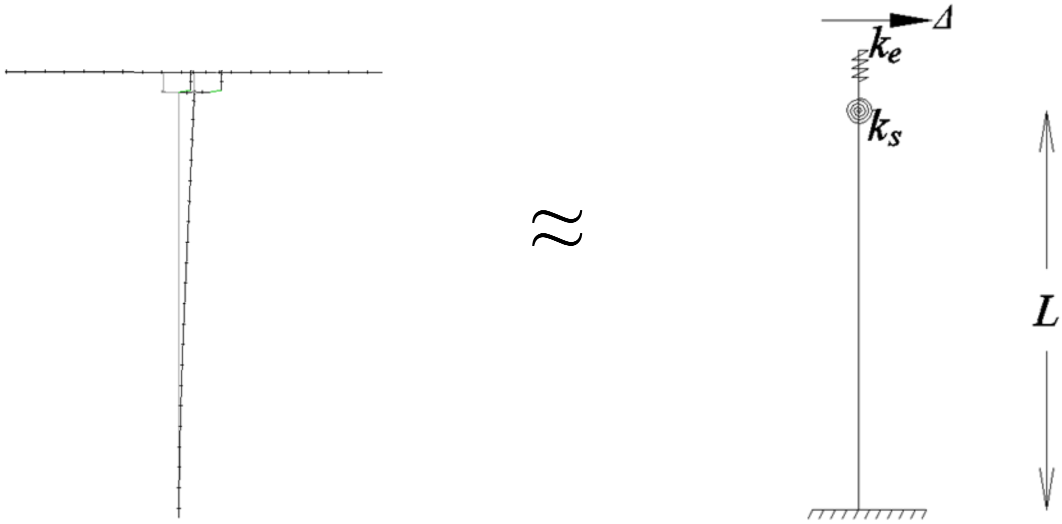

Figure F.2: Idealization of a pier with bearings and superstructure connection (Bridge 1)

Here k_e and k_s represent the translational stiffness of bearings and rotational stiffness contribution coming from superstructure to the top of pier, respectively. Degree of freedom Δ denotes the tip displacement of the compound element. This assembly consists of a cantilever beam fixed at the bottom and connected to a rotational spring at the top, and a two-node translational spring connected to this beam in series.

From now on, translational stiffness of that compound element, which will be denoted by k_p, will be obtained step by step. The 2x2 stiffness matrix of a beam element having degree of freedoms Δ_{top} and θ_{top} at an end can be written as [22];

$$k_b = \begin{bmatrix} 12EI/L^3 & -6EI/L^2 \\ -6EI/L^2 & 4EI/L \end{bmatrix} \tag{F.3}$$

First, inserting term k_s gives us;

$$k_{bs} = \begin{bmatrix} 12EI/L^3 & -6EI/L^2 \\ -6EI/L^2 & 4EI/L + k_s \end{bmatrix} \tag{F.4}$$

During longitudinal excitation, external forces that are transmitted from superstructure to the pier are in the same direction, since load vector of whole structure contains only translational terms under idealized ground motion, represented by the $-\mathbf{m}\ddot{u}_g(t)$ recalling Equation (3.4). Thus degree of freedom θ_{top} in the stiffness matrix of Equation (F.4) can be condensed as;

$$\begin{Bmatrix} F \\ M = 0 \end{Bmatrix} = \begin{bmatrix} 12EI/L^3 & -6EI/L^2 \\ -6EI/L^2 & 4EI/L + k_s \end{bmatrix} . \begin{Bmatrix} \Delta_{top} \\ \theta_{top} \end{Bmatrix}$$

$F = 12EI/L^3 . \Delta_{top} - 6EI/L^2 . \theta_{top}$ (Multiplication of 1. row)

$M = 0 = -6EI/L^2 . \Delta_{top} + (4EI/L + k_s) . \theta_{top}$ (Multiplication of 2. row)

Which gives;

$$\theta_{top} = \Delta_{top} . (6EI/L^2)/(4EI/L + k_s) \tag{F.5}$$

Substituting Equation (F.5) into the multiplication of first row gives;

$$F = \Delta_{top} . k_{bc} = \Delta_{top} . [12EI/L^3 - 36(EI/L^2)^2/(k_s + 4EI/L)] \tag{F.6}$$

The term k_{bc} is the stiffness of the cantilever beam assembled to a rotational spring, k_s at top. This obtained formula can be easily verified as follows; if the rotational stiffness of the spring k_s approaches zero, Equation (F.6) becomes;

$F = \Delta_{top} \,.\, 3EI/L^3$

which is the case of a cantilever beam, and if rotational stiffness of the spring k_s approaches to infinity, Equation (F.6) again becomes;

$F = \Delta_{top} \,.\, 12EI/L^3$

which is the case of a beam having rotational fixity at both ends.

Finally, k_{bc} and k_e are to be combined in order to obtain the translational stiffness k_p of the top of the assembly shown in Figure F.2. This can be easily done by recognizing that the combined system is nothing more than two translational springs connected in series.

Hence;

$k_p = 1/(1/k_{bc} + 1/k_e)$

$k_p = k_e/(k_e/k_{bc} + 1)$

$$k_p = k_e/(k_e/[12EI/L^3 - 36(EI/L^2)^2/(k_s + 4EI/L)] + 1) \tag{F.7}$$

and recalling Equation (F.5), the top moment in beam member of Figure F.2 is;

$$M_{top} = k_s.\theta_{top} = k_s.\Delta_{op}.(6EI/L^2)/(4EI/L + k_s) \tag{F.8}$$

Now, notice two single degree of freedom systems shown in Figure F.3, representing short and long piers of Bridge 1 respectively.

Since the superstructure is continuous and relatively short in length, axial elongation across the whole length of bridge will be negligible and top of bearings can be assumed to displace same under longitudinal excitation ($\Delta_1 = \Delta_2$).

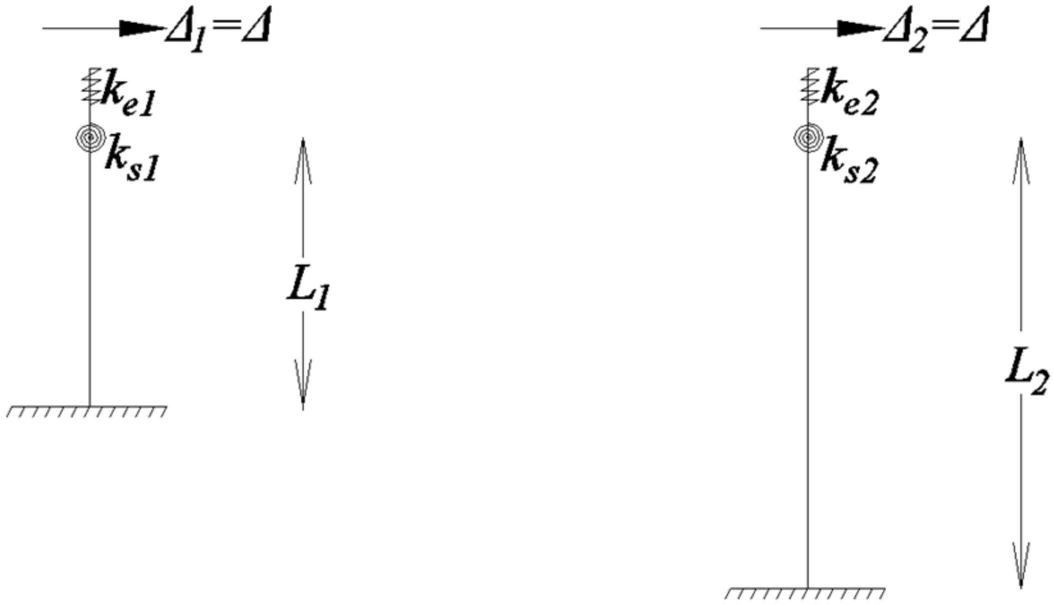

Figure F.3: SDOF systems representing short and long columns (Bridge 1)

Translational stiffness of bearings on all columns are equal also for Bridge 1. To reduce the unknowns in the problem, rotational stiffness contribution of superstructure to top of all columns will be assumed to be the same, which is reasonable since span lengths are equal between each axis. Under these simplifications, and recalling $L_2 = 2.L_1$ from Figure 4.14, ratios of top moments of short piers over those of long piers will become;

$$\frac{M_{top\ 1}}{M_{top\ 2}} = \frac{\Delta_{top\ 1}.(6EI/{L_1}^2)/(4EI/L_1 + k_s)}{\Delta_{top\ 2}.(3EI/2.{L_1}^2)/(2EI/L_1 + k_s)} = \frac{4.\Delta_{top\ 1}.(2EI/L_1 + k_s)}{\Delta_{top\ 2}.(4EI/L_1 + k_s)} \qquad \text{(F.9)}$$

Now it is necessary to obtain the ratio of pier top displacements, $\Delta_{top\,1}/\Delta_{top\,2}$. Substituting $\Delta_1 = \Delta_2$, ratio shear forces in the same columns becomes;

$$F_1/F_2 = k_{p1}/k_{p2} \qquad \text{(F.10)}$$

Same ratio can be written in terms of pier top displacements as;

$$F_1/F_2 = (k_{bc1}.\Delta_{top\,1})/(k_{bc2}.\Delta_{top\,2}) \qquad \text{(F.11)}$$

Thus;

$$\Delta_{top\,1}/\Delta_{top\,2} = (k_{p1}/k_{p2}).(k_{bc2}/k_{bc1}) \tag{F.12}$$

Substituting this equation into (F.9) gives the ratio of top pier moments, thus bearing axial forces of both columns;

$$\frac{M_{top\ 1}}{M_{top\ 2}} = \frac{4.(k_s+2EI/L_1).(k_e+3EI/2{L_1}^3)-9/4.(EI/{L_1}^2)^2}{(k_s+4EI/L_1).(k_e+12EI/{L_1}^3)-36(EI/{L_1}^2)^2} \tag{F.13}$$

Recalling Equation (F.1) and considering that cap beam sections are identical for all piers, this ratio will also be equal to uplift forces in bearings. The stiffness coefficients k_s and k_e were normalized dividing by EI/L_1 and $EI/{L_1}^3$ respectively, and moment ratio obtained from Equation (F.13) versus $k_s.L_1/EI$ is plotted on Figure F.4, for $k_e.{L_1}^3/EI = 0.605$. Recalling that eighteen bearings exist on a pier, this value of k_e was calculated as;

$$k_e.{L_1}^3/EI = 18 * k_{bearing}\ /(EI/{L_1}^3)$$
$$k_e.{L_1}^3/EI = 18 * 977/(23650000 * 1.2285/10^3) \cong 0.605$$

Observing Figure F.4, it is seen that the values of $M_{top\,1}/M_{top\,2}$ are in the range of 0.544 and 0.667. This result verifies the ratios of bearing axial force couple at pier axis P3 to those at P4, which range between 0.629-0.639 (Table 4.5, RSP case 1).

Additionally, Figure F.4 indicates that the rotational stiffness contribution of superstructure at the top of piers does not have a significant effect on the trend discussed up to here, that is; bearings on the long columns possess greater bearing forces than the ones on short columns in Bridge 1, under longitudinal excitation. As a minor remark, it is seen that the initial value representing the case of two cantilevers is indeterminate since both moments are zero in this case.

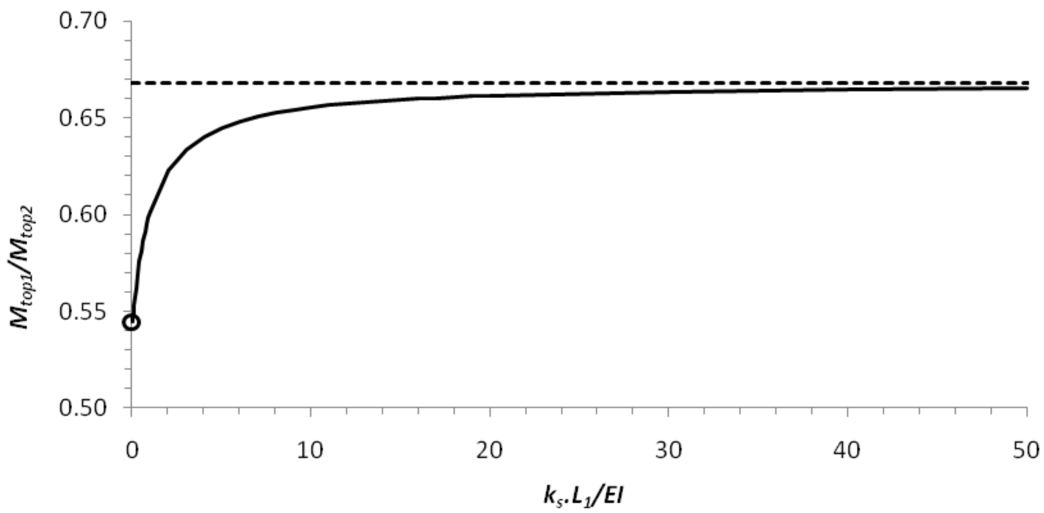

Figure F.4: Ratio of for $M_{top\,1}/M_{top\,2}$, versus k_s (Bridge 1)

Again a simple approach can be developed to reveal the answer of the question why do axial bearing forces develop under transverse excitation? The bearing layout of a bridge having an odd number of bearings on pier ($2n+1$) is shown on the cross section in Figure F.5. Top moment in the pier will be compensated by total moment originating due to compressive and tensile bearing forces shown in same figure, which is equal to;

$$M_{top} = 2.(F_1.d + F_2.d + \cdots + F_n.d) \tag{F.14}$$

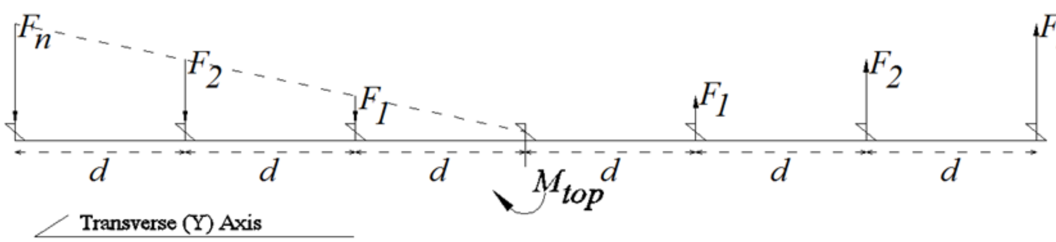

Figure F.5: Bearing layout on a fictitious cross section

Superstructure and cap beam can be assumed as rigid members in bending about longitudinal axis, to simplify the problem. This is indeed the case in the analysis model.

Under these conditions, bearing forces exhibit triangular similarity and Equation (F.14) reduces to;

$$M_{top} = 2.F_1.d.\sum_{i=1}^{i=n} i^2 \tag{F.15}$$

and the axial force in the bearing number n can be calculated as;

$$F_n = n.F_1 = n.M_{top}/(2.d.\sum_{i=1}^{i=n} i^2) \tag{F.16}$$

As explained earlier, one important property of Bridge 1 is that, there are two transverse lines of bearings on a pier, placed on the opposing sides of cap-beam. Superstructure is continuous via slab section over the cap beam only.

As slab section is relatively much flexible than compound superstructure section in terms of torsional stiffness, it is quite possible for opposing sides of superstructures to make different rotations, which will cause the bearings in the opposing sides to be exposed to different axial forces, even in different directions at the same time instant. Thus Equation (F.16) will only approximate to the summation of axial forces on opposing bearings. This concept is illustrated on Figure F.6.

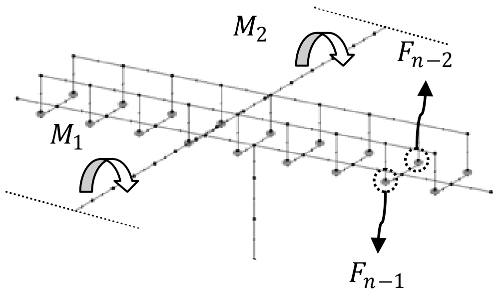

M_1 $need\ not\ to\ be\ equal\ to\ M_2; thus$

F_{n-1} $also\ need\ not\ to\ be\ equal\ to\ F_{n-2}$

$F_n = F_{n-1} + F_{n-2}$

Figure F.6: Validity of Equation (F.16) for Bridge 1

To verify the approach developed so far, total axial forces of edge bearings (ID’s 37 and 28) on P3 axis will be checked for LTH analysis case 5 for ground motion record 1, of which whole results are not presented here to avoid number mess;

$M_{top} = 6507\ kN.m$ (Maximum at t = 11.27 s)

$F_4 = 4 * 6507/(2 * 1.3 * 30) \cong 334\ kN$ (From Equation (F.16))

$F_{27} = -115\ kN$ (t = 11.27 s)

$F_{38} = 424\ kN$ (t = 11.27 s)

$F_{27+38} = 424 - 115 = 309\ kN$ (t = 11.27 s)

This 8.1% difference ([334-309]/309) is primarily due to the fact that Equation (F.16) ignores the mass of the cap beam, which will also create moments at pier top due to developing accelerations during transverse excitation. But this simplified approach describes the occurrence of axial forces in bearings under transverse excitation.